國立臺灣大學工學院土木工程學系

碩士論文

Department of Civil Engineering

College of Engineering

National Taiwan University

Master Thesis

局部沖刷對沖積河川影響之研究

Investigation of Local Scour Effects in Alluvial Rivers

陳峰琨

Chen, Feng-kun

指導教授：楊德良 教授

Advisor: Young, Der-Liang

中華民國 100 年 7 月

July, 2011

國立臺灣大學碩士學位論文
口試委員會審定書

局部沖刷對沖積河川影響之研究
Investigation of Local Scour Effects in Alluvial Rivers

本論文係陳峰琨君（R98521321）在國立臺灣大學土木工程學系碩士班完成之碩士學位論文，於民國 100 年 7 月 25 日承下列考試委員審查通過及口試及格，特此證明

口試委員：

楊德良	
（指導教授）	
吳祥生任	謝慶壽
張順益	林昊傑
系主任 呂良正	

（簽名）

致謝

能夠完成這一本論文，要感謝的人太多人。首先我要感謝收留我的楊德良老師，記得當初在找指導老師之前，對於楊老師在學術界給人的印象就是嚴厲、認真，但是等到真的跟老師接觸之後，發現並不是這麼一回事，老師對學生其實是相當親切、風趣的，但是不變的就是老師對研究的嚴謹的態度以及課業上的要求，在這兩年中，讓我獲益良多，也學會如何更謹慎地去處理我所需要面對的問題。這段時間的學習經歷會是人生中寶貴的資產。

也感謝指導的口試委員，吳祚任教授、羅慶瑞教授、欉順忠博士以及林英傑博士對於我整篇論文的方向、架構、以及內容需要改進的缺失都給予許多的建議，讓這本論文內容可以更加完善。

也要感謝楊門的這些學長，在林英傑學長的指導下，我學會如何操作 Flow-3D 這個軟體，不只讓我可以順利從事我的研究工作也在以後找尋工作上比別人多了一份優勢，也感謝吳清森學長的幫忙，沒有你的幫忙，我不可能完成這本論文，每次寫完還要你耐著性子看完我寫的英文去改正錯誤，我知道這對你來說是件痛苦的事情，也要常常被我問一大堆問題，也是學長讓我了解到，做研究不是件簡單的事情。沈立軒學長和嘉蓬學長，在我們煩悶時會帶我們出去走走，或是在我們研究遇到瓶頸時會跟我們閒聊開導，讓我們有更多的精神去投入下一次的工作。還有身邊的同學，宗毅、姿帆、宜玲，多虧這些夥伴，讓我在學習的路上並不孤單，在那段每次只要趕工的艱困時段就在研究室叫麥當勞當晚餐的日子我會懷念的。

感謝卡艾瑋老師團隊的謝欣霓同學以及欉順忠博士的實驗的數據以及資料照片提供，讓我可以順利完成論文。

最後是我最要感謝的人就是爸爸、媽媽，沒有你們一路辛苦的養育，我沒辦法順利完成各個階段的學業，更不可能有機會來台大念研究所，現在我也順利完成碩士這個階段的學業了，很開心可以跟你們分享這份喜悅，謝謝你們。也感謝哥哥，在當初準備研究所考試煩躁時會給予我鼓勵，也時時擔心生活上有沒有什麼問題，讓我可以更專心的去念書。也感謝瑜斐這一路來的陪伴，尤其是在準備研究所期間比較沒辦法一直陪在妳身邊，感謝妳的體諒讓我可以專心去準備考試，在最後寫論文這段期間聽我抱怨，或是跟你分享快樂的事情都讓我輕鬆不少，你們都是我最愛的家人，謝謝你們。

摘要

本論文主要以數值模擬來探討局部沖刷於橋墩附近的流況變化及其物理機制，使用了兩個不同的現場案例，分別爲后豐大橋的橋樑沖刷以及大甲溪實施固床工保護的間隙沖刷。數值模擬應用於此問題一直以來都是相當困難的課題，因此，於本論文中藉由商業軟體 Flow-3D 做分析及討論，其分析內容同時包含了定床跟動床兩種數值模型設置，並藉由實驗結果輔助之。於橋樑沖刷部分，定床的模擬中，分析第一根橋柱前的水深比較，其數值結果實驗結果相當吻合；於動床模擬中，在實驗設置裡加入了超音波儀器，從模擬結果可以清楚發現其存在位置會影響到底床的沖刷深度以及整個流場的變化，因此移除了該裝置之後，試著去探討在橋墩前所產生的跌水現象所引起的沖刷所帶來的影響。由模擬結果發現，有跌水沖刷的部分，主要沖刷位置會集中在橋柱前方形成一個沖刷坑，同時底床被掏刷過程中，橋柱迎水面會受到強勁的水流的流速衝擊，橋柱靠近底床部分最大，往上遞減。然而沒有跌水沖刷的部分，主要沖刷位置落在第一根橋柱周圍，其因素歸因於向下射流以及馬蹄型渦流。再者，固床工的間隙沖刷模擬，當底床設置爲固床時，可以發現不論在何種大小流量下都會在第三階部分產生一個明顯的 Z 方向流速，並於固床工邊緣產生明顯的渦流。由於此間隙沖刷案例的模擬，其物理問題設置屬不連續體排列，因此在數值模擬過程中，不易觀察其確切的物理現象，因此，此部分的數值模擬尚待開發。

關鍵詞：局部沖刷，后豐大橋，固床工，間隙沖刷，數值模擬，Flow-3D，跌水沖刷，

Abstract

In this thesis, the flow field and physical mechanism of local scour problem around the bridge piers is mainly used by numerical simulation. Two different field cases are studied: they are the bridge scour effects surrounding the Hou-Feng Bridge and the gap scour effects about the stepped concrete block grade control structure in Ta-Jia river, respectively. It is an extremely difficult problem by using the numerical programming to solve these problems. Hence we seek the help from the commercial software, Flow-3D, to analyze the problem. The problem setting includes the rigid-bed and mobile-bed simulation and the laboratory experiments are aided in the meantime. The numerical results of the rigid-bed simulation are compared with the laboratory results in terms of the fluid depth in front of the first pier. The results from numerical studies and laboratory experiments match very well. In the mobile-bed simulation, the ultrasound device is added in the experiment and the scour depth and the variation of the whole flow field are interfered with the sensor. Hence after the ultrasound device is removed, the influence of the overfall flow in the bridge scour simulation can be clearly classified. The mainly scour hole is concentrated in front of the first pier in the numerical simulation with the overfall flow. In the meantime, the upstream of the first pier is borne by the current flow and the maximum flow velocity is measured close the bottom of the first pier. If the overfall flow is not considered in the simulation, the mainly scour hole is concentrated around the first pier. The reasons are attributed to the down flow and the horseshoe vortex. As for the rigid-bed simulation of the gap scour, the third step of the stepped concrete block grade control structure always existed the obvious velocity on the Z-axis and the strong vortex near the edge of the stepped concrete block grade control structure in the numerical simulation no matter how strength of the flow. In the gap scour simulation, it is difficult to observe the accurate physical phenomenon during the numerical simulation in light of its physical problem setting belongs to the discontinuous arrangement. Hence the numerical simulation still needs to improve regarding this part.

Keywords: local scour, Hou-Feng bridge, stepped concrete block grade control structure, gap scour, numerical simulation, Flow-3D, overfall scour,

Content

Figure Lists

Table Lists

Chapter 1 Introduction

In recent years, the sediment scouring problem is one of the most significant current discussions in Taiwan. In this island, the rivers and creeks are mostly the east west dirctions but our transportation and pipeline system is northwestward. Hence inevitably there are a lot of artificial buildings, structures, oil trachea bridges and water supply pipes have to cross the rivers and creeks. When the flood comes, the river bed around the bridge piers or other structures, which can cause significant amounts of erosion, this situation can make the bridge topple over and cause the traffic to cut off. In order to prevent this kind of accidents, people try to build stepped concrete block grade control structures. They are widely used in Taiwan to protect riverbeds from degradation and to dissipate the associated high energy of flow over weirs. Unfortunately not all of them can work very well so this study focuses on the two events. One is about Hou-Feng Bridge failure case, and another is the collapse of the stepped concrete block grade control structure downstream of Highway No.1 in Ta-Jia River.

1.1 Descriptions of the damage near Hou-Feng Bridge

The Hou-Feng Bridge is located at the downstream of Ta-Jia River in the central Taiwan. It is the main traffic artery in Taichung (see Figure 1.1) which connects the Houli township and the Fengyun city. In October 2008, Typhoon Sinlaku induced the failure of two spans of the Hou-Feng Bridge, across the Ta-Jia River. The failure caused fatalities, and was extensively covered in the news. It located only three kilometers downstream of the Shih-Kang Dam, the bridge is located in a river segment that appears to have been steadily degrading over the years. Due to this degradation, a water supply pipe (which was made by Taiwan Water Corporation and they built a concrete structure to cover the pipeline) located immediately upstream of the bridge and originally buried beneath the river bed became exposed to the river flow (see Figure 1.2). Upon further degradation, a drop of up to 6m arose between the river bed elevation upstream and downstream of the pipe, which acted as a rigid sill controlling the upstream river bed. The downrush of flood waters past this drop is likely to have aggravated the local scour around the bridge piles, contributing to their undermining and the collapse of the corresponding spans of the bridge deck (see Figure 1.3). To better understand the mechanisms of this bridge failure, we collect and analyze a set of structural, hydrological, and topographical data, and conducted our own survey of the

corresponding valley segment and bridge scour. Based on these field survey data, we are able to formulate specific hypotheses regarding the sequence of events which lead to the failure of Hou-Feng Bridge. The first specific application domain selected to test our modeling is the issue of bridge scour, and its possible enhancement by structural obstacles across rivers. This represents a complex problem in which water flow, engineered structures, and the granular river bed respond to each other, sometimes with catastrophic results. For this case, we are able to demonstrate the potential of novel modeling in predicting and monitoring the bridge scour process.

Figure 1.1 The location of Hou-Feng Bridge (from Google earth)

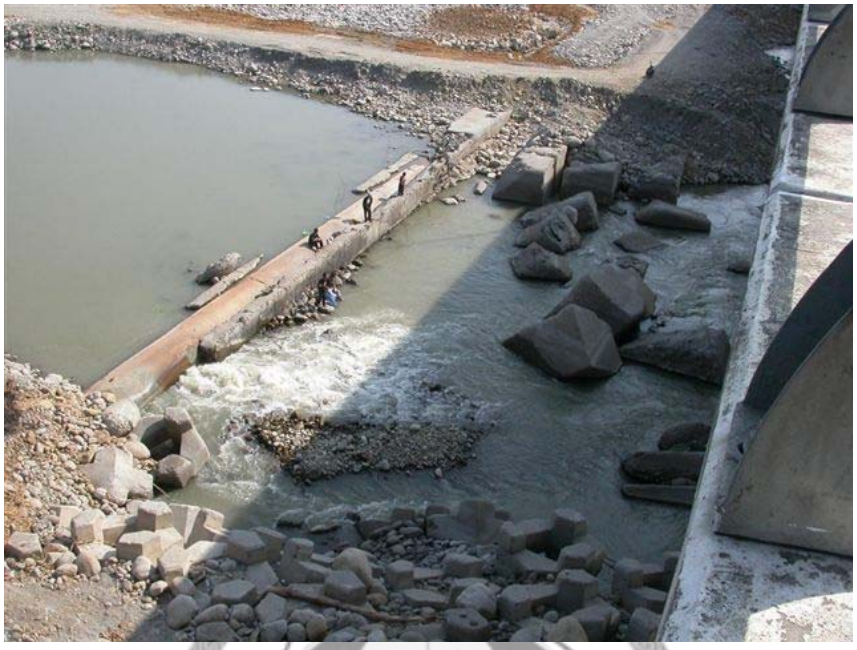

Figure 1.2 View of the exposed water main during low flow prior to the bridge failure. (photo courtesy of Zoe Lin, TBS)

Figure 1.3 Failure of Hou-Feng Bridge connecting Houli and Fengyuan in Taichung due to Typhoon Sinlaku in October 2008. This view of the failed bridge a few days after failure. (photo by H.Capart)

1.2 Review of previous investigations

As we mentioned in chapter 1.1, the event of Hou-Feng Bridge includes the sequence of complex factors, for example, the strong current, the overfall flow, the sediment scour, the local scour and the multiple bridge piers. Hence we want to study the interaction mechanism between the overfall scour and local scour near the bridge.

It has several names in terms of the near-vertical changes in channel bed surface elevations, including headcut, overfall, and waterfall and this field has been studied for a long time. Rouse [2] has applied the vertical jet flow to study the sediment scour in 1940. Beltaos [3] and Beltaos and Rajaratnum [4] determined stress distributions for planar and circular submerged jets. Robinson [5] measured stress and pressure distributions for the impinging jet zone in a free overfall and developed the dimensionless equations to illustrate the maximum stress and pressure which are based on the overfall height, backwater depth, approach flow depth, and unit discharge. Fogle [6] et al. developed stress distributions for the impinging jet zone which is based on the research of Beltaos and Rajaratnum [4] and Robinson [5]. Stein et al [7]. developed an excess stress relationship for a free overfall jet based on jet diffusion principles. Jia et al. [8] developed a dynamic stress and pressure method to estimate plunge pool scour about

the loose bed materials. Hanson et al. [9] developed a similar excess stress parameter approach for the submerged circular which is similar to Stein did before.

Earlier researchers studied the relative scour depth to the Froude number regarding the local scour. Most of the conclusions mentioned that the scour depth increases indefinitely with increasing velocities when we obtain the given fluid depth. Later researchers, e.g. Chabert and Engeldinger [10], Laursen [11] etc. illustrated that when the approach velocity exceeds the critical velocity for, the scour depth decreases to about 10% less than the maximum scour depth at critical velocity and the scour depth keeps constant irrespective of the further increases in velocity. More recently, Jain and Fischer [12] indicated that the scour depth decreases slightly at velocity just exceeding threshold but increases again with further increase in velocity. Chee [13] also found the initial decrease and subsequent increase in scour depth with increasing velocity. Early researchers generally indicated that the influence of sediment size in the depth of scour around bridge piers is negligible. Ettema [14], however, showed that clear-water scour depth can be significantly reduced if the relative size of the pier to sediment is less than 50. In addition, the effect of fluid depth on the depth of local scour around bridge piers in both clear-water and live-bed phases is studied quite extensively by early researchers. They agreed that the scour depths increase as the ratio of the flow depth to the width of

pier increases until a certain limiting value after which scour depths become independent of the ratio of the flow depth to the bridge width. Ettema [14] concluded, based on results from an extensive clear-water experimental program, that the influence of flow depth is affected by the size of the pier and sediment. At the same time, the flow depth can be neglected when the ratio of the flow depth to the bridge width is greater than 3. Chiew [15] investigated the relationship between local scour depth and mean approach velocity to determine the relation between the flow depth and the sediment size on the equilibrium scour depth in live-bed phase.

1.3 The gap scour at stepped concrete block grade control structure

Weirs for water intake and check dams for bridge protection are structures built across rivers. These structures raise the level of water, which increases the scour potential to the downstream riverbed. Engineers use stepped concrete block grade control structures to protect the riverbed from degradation and dissipate high flow energy. The structures normally are constructed using concrete blocks arranged in a stagger and descending manner (see Figure 1.4). Specific gap width and drop height between blocks are used and large-size stones are placed in the gaps as lateral support.

The gaps aligned in the streamwise and transverse directions are called longitudinal and lateral gaps.

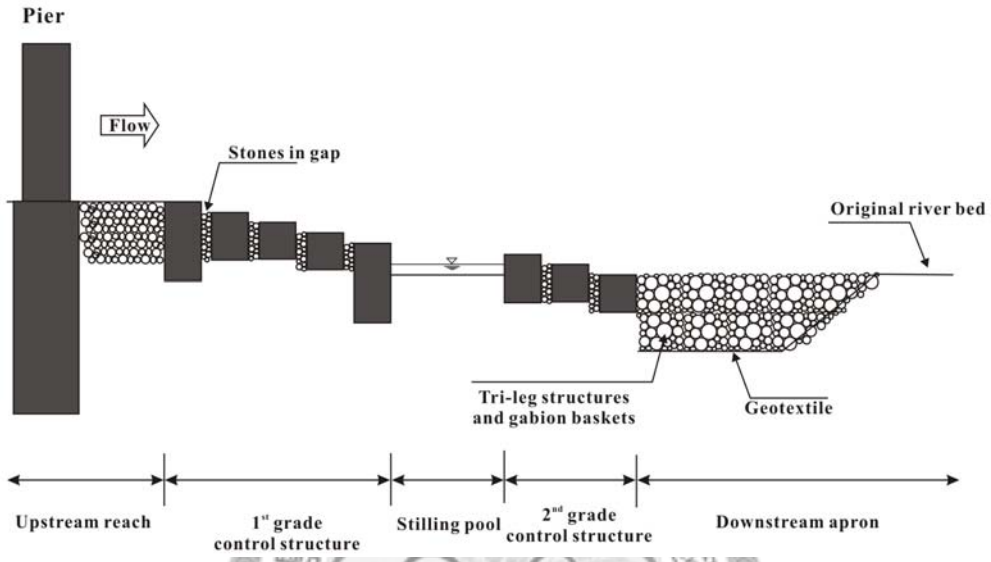

Figure 1.4 Sketch of protection structures in a river

Research on gap scour is few compared to the studies on edge scour. Armoring effects with reference to the relationship between sediment transport and approach flow conditions are widely studied. Raudkivi and Ettema [30] studied the stability of an armor layer before extending it to include scour protection around piers (Raudkivi and Ettema [31]).Worman ([32], [33]) studied the transport of fine sediment with an armor layer. Sumer et al. [34] applied flow visualization techniques to examine the suction mechanism of fine sediment under an armor layer. They found that vortices that formed in the gap sucked out fine sediment particles between the gravels. They published a

regression equation to estimate bed degradation due to the erosion of the fine sediment. The results of the Sumer et al. [34] study explains the physics government sediment entrainment and mobility associated with the gap scour of stepped concrete block grade control structures. Researchers must keep in mind the significant difference in the geometrical layout and compositions of both structures in order to apply their findings.

1.4 Flow 3D

In 1980, Dr. C.W.Hirt founded Flow Science Company. They tried to develop a set of accurate CFD software and hope to simulate the behavior among gas, liquid and solid with this software for users. Finally flow 3D commercial edition was released formally in 1985. Its intact theoretical foundations and basic numerical method were depended on continuity equation, momentum equation preface and Navier-Stokes Equations, etc. Nowadays it is used extensively at many different fields such as aerospace, casting, coating, consumer products, inkjets, micro fluidics and water & environmental engineerings, etc.

The spirits of this software that we employed is introduced but why we choose this software for simulating. Then we will show some of its advantage. First of all, it

includes the techniques of fraction area/volume obstacle representation (FAVOR) and multi-blocks of mesh generation.

(1) The FAVOR is a technique that it can define the obstacle in the numerical model. Its original theory is the control volume conception. Briefly speaking, the FAVOR can provide the method to validate the crossing area of control volume between fluid and obstacles. In our numerical model, we should ensure that our cylinder piers would have complete shape. Hence the FAVOR plays an important rule for our numerical modeling.

(2) FLOW-3D offers multi-block meshing (see Figure 1.5), which is designed to add even more flexibility and efficiency to the finite difference meshing technique. In a standard finite difference mesh, local refinements may lead to a substantial increase in the total number of cells since mesh lines extend all the way to domain boundaries in all three directions. Use of multiple blocks allows such refinements to be more localized, and therefore requires fewer computer resources. The multi-block feature is especially useful in so-called "rangy" problems, where features exist that are small compared to the overall domain size, like small obstacles and thin channels. Using multiple mesh blocks, a user can "link" individual blocks to mesh a "rangy" domain and mesh only the areas of interest and limit the total number of

computational cells. Using a "nested" block, a user can enhance the resolution around an area of interest.

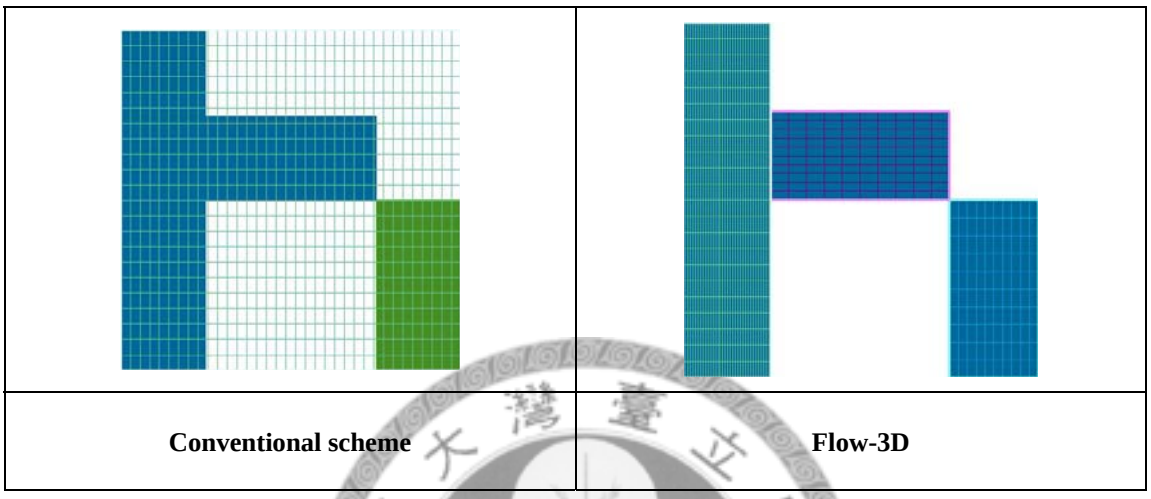

Figure 1.5 Mesh generations for conventional scheme and numerical scheme

The fully 3D computational fluid dynamics (CFD) model, Flow-3D, is used for simulating the above-mentioned problems and the 3D simulation is necessary because of the complicated flow field. It is difficult to ignore the structure neighboring affect. Furthermore the 3D simulation can easily compare the numerical result to laboratory experiment.

1.5 Structure of this thesis

In this context, it is pertinent to mention that none of the aforementioned studies

focus on the effects of various factors on local scour no matter in laboratory experiments or numerical simulations. It is particularly difficult to study the sediment scour problem by means of the numerical methods. Hence the present study aims at the investigation of 3D numerical simulation on bridge local scour which is included the complex material parameters. At the same time, the numerical results are compared to the small scale of laboratory experiments which is set by H.N. Hsieh [1] about the bridge local scour. On the other hand, the experiment of gap scour is set by Dr. S.C. Tsung.

The structure of this thesis is divided into six chapters:

Chapter 1: Introduce the motivation of this thesis and review the previous investigation.

Chapter 2: Some basic theory about the local scour and illustration of the experimental setting.

Chapter 3: Introduce the numerical setting in the Flow-3D.

Chapter 4: Results and discussions

Chapter 5: Experimental setting of gap scour and discussions

Chapter 6: Conclusions

Chapter 2 Basic theory for local scour and the experimental setting

2.1 The classification of erosion type

The advanced investigations of scouring phenomena with respect to the collapse of the bridge structure can roughly be divided into four general categories in micromechanic views [17] (see Figure 2.1):

(1). The general long-term type of erosion: We use the long time to observe the phenomenon between flow and the sediment on the channel.

(2). The general short-term type of erosion: We use the short time to observe the phenomenon between flow and the sediment on the channel.

(3). Contraction scour: The flow strength reduces in light of the structural building or channel cross-section. This phenomenon will make the flow accelerate to cause the contraction area and produce the localized eroding.

(4). Local scouring: Because of the structural building the flow produces some interference phenomenon in the rivers and enhance the behavior of scouring near the structural building.

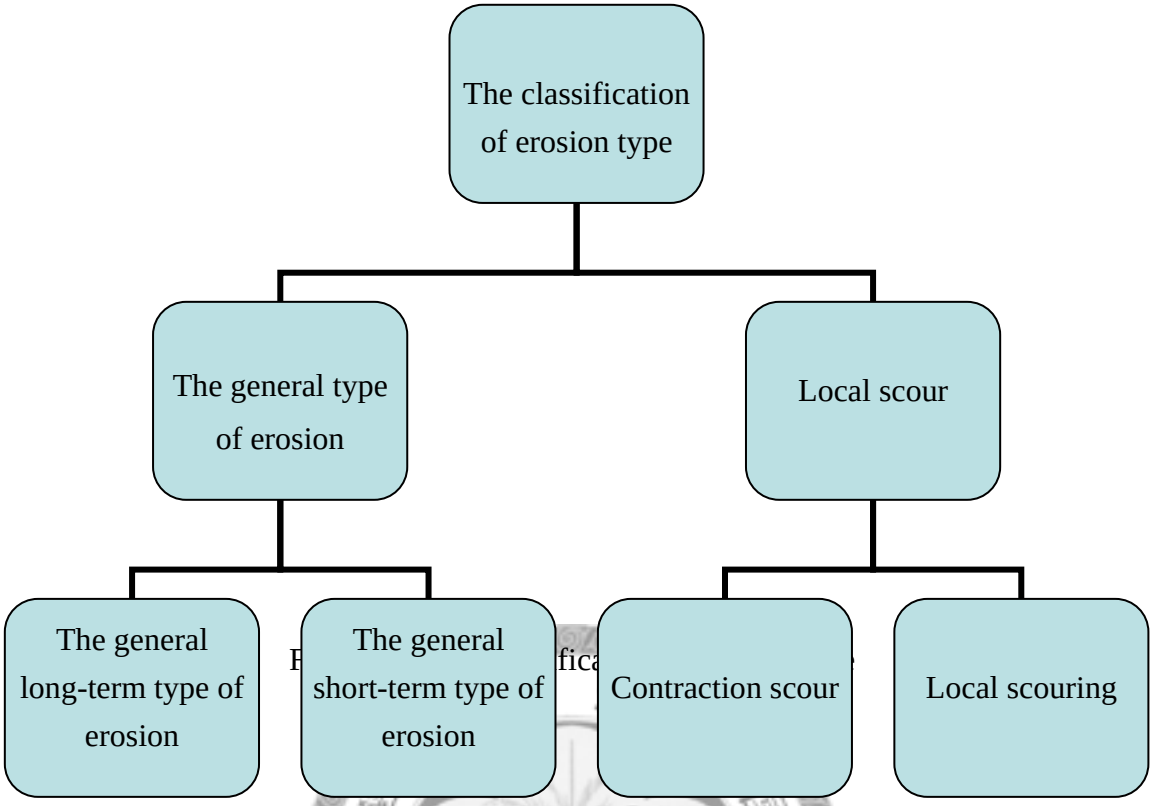

Figure 2.1 The classification of erosion type

On the other hand, in Laursen's opinion [18], it can be shown with sediment continuity equation regarding the local area of scouring status in the channel:

$$\frac{\partial \forall}{\partial t} = Q_{out} - Q_{in}$$

$\frac{\partial \forall}{\partial t}$: sediment volume dilation

Q_{out} : outflow of sediment

Q_{in} : inflow of sediment

According to the relationship between Q_{out} and Q_{in}, we can estimate the observation area is scouring or deposit. By this method, we can divide local scouring into three types:

(1). $Q_{out} = Q_{in} = 0$ …(no scouring)

(2). $Q_{out} > Q_{in} \cong 0$ …(clear water scouring)

(3). $Q_{out} > Q_{in} > 0$ …(live-bed scouring)

In this thesis, the occurring mechanism of the local scouring effect is the main target to discuss. There are a lot of parameters which can influence the behavior of bridge local scouring. Roughly speaking, it includes four major parts: flow condition, characteristic of river bed, shape of bridge piers & arrangement and time. In Melville's study [19], the influence factors of bridge local scouring can be shown as the following equation:

$$d_s = f[\text{Flow Condition}(V, \rho, \nu, y, g),\ \text{Characteristic of River Bed}(\sigma_g, d_{50}, \rho_s, V_c),$$
$$\text{Bridge Pier Geometry}(a_p, \text{Sh}, \text{Al}),\ \text{Time}(t, t_e)] \quad \ldots(2.1)$$

where ρ and ν are fluid density and kinematic viscosity coefficient, respectively; V is mean approach flow velocity; y is mean approach flow depth; **g** is acceleration of gravity; d_{50} and σ_g is median size and geometric standard deviation of the sediment particle size distribution; ρ_s is sediment density; V_c is critical mean approach flow velocity for entrainment of bed sediment; a_p is pier width; Sh and Al are the parameters describing the shape and alignment of the pier respectively; t is time; t_e is time for equilibrium depth of scour to develop. Assuming constant relative density of

sediment and the absence of viscous effects, according to the Buckingham Pi Theorem, we can transform the equation 2.1 into the dimensionless equation as follows:

$$\frac{d_s}{a_p} = f\left(\frac{V}{V_c}, \frac{\rho V a_p}{\nu}, \frac{y}{a_p}, \sigma_g, \frac{d_{50}}{a_p}, \rho_s, \text{Sh}, \text{Al}, \frac{t}{t_e}\right) \tag{2.2}$$

(1). Flow intensity $\frac{V}{V_c}$:

In Melville and Chiew study [19], the maximum scour depth is called the threshold peak. This value can clearly define the clear-water scour and live bed scour (see Figure 2.2). The local scour depth increases almost linearly with flow intensity to a maximum at the threshold velocity under clear-water conditions. When the velocity exceeds the threshold velocity, the local scour depth will decrease and then increase again to a second peak, but the second peak is not bigger than the first one. This is the reason why we usually use the clear-water scour in local bridge scour experiments. The scour depth changes with flow intensity are explained in terms of the balance between sediment input and output from the scour hole. These trends are evident in many data sets, including those of Chabert and Engeldinger [10], Shen et al. [20], Maza [21], Ettema [22], and Chiew [23].

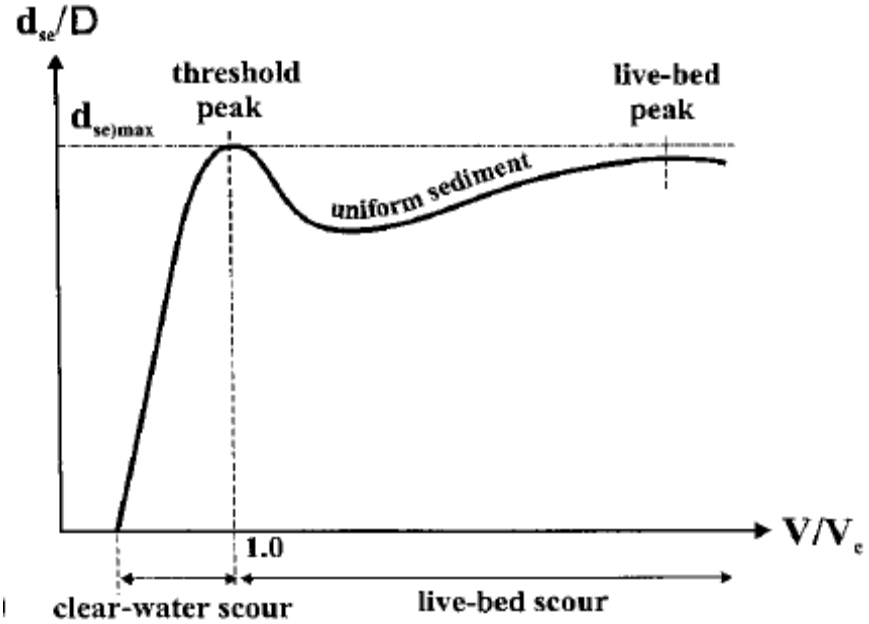

Figue2.2 Flow shallowness [19] (Melville and Chiew, 1999)

(2). Flow depth $\frac{y}{a_p}$:

$\frac{y}{a_p}$ is the ratio of fluid depth and width of the pier. When the value is smaller, the local scour depth is concerned about flow depth. On the contrary, the scour depth will be influenced by the width of the pier when $\frac{y}{a_p}$ is bigger. In Raudkivi and Ettema opinion [24], we can neglect the influence of variation of fluid depth in the local scouring experiments while $\frac{y}{a_p}$>3. Furthermore, in Melville and Chiew study, the bridge local scour depth only connects with the diameter of piers when $\frac{y}{a_p}$>1.43. The local bridge scour is influenced by the fluid depth when $\frac{y}{a_p}$<0.2.

(3). Sediment coarseness $\frac{d_{50}}{a_p}$:

When the sediment particle is coarse, the river bed is prevented to scour and the maximum scour depth decreases due to this reason. On the other hand, the finer particle sediment size makes the river bed be scoured easily. In Raudkivi and Ettema's opinion [25], the scour depth is not influenced by the sediment particle when $\frac{a_p}{d_{50}}$<50.

(4). Time:

In the clear-water scour, the scour depth increases as the time goes on. In live-bed scour, the scour depth easily approaches the equilibrium time. In Melville and Chiew experiments [19], the quilibrium time of scour depth can be written as:

$$\frac{d(d_{se})}{dt} \le \frac{0.05a_p}{24} \tag{2.3}$$

Where d_{se} is the quilibrium scour depth and from their experimental results, we can obtain the quilibrium time for scour depth as follows:

$$t_e(\text{days}) = 48.26\frac{a_p}{V}\left(\frac{V}{V_c}-0.4\right), \frac{y}{a_p}>6 \tag{2.4}$$

$$t_e(\text{days}) = 30.89\frac{a_p}{V}\left(\frac{V}{V_c}-0.4\right)\left(\frac{y}{a_p}\right)^{0.25}, \frac{y}{a_p} \le 6 \tag{2.5}$$

In Melvilleand Chiew study [19], the clear-water scour can produce the maximum scour depth. In this thesis, the clear water scoring condition is used because it can simplify our laboratory experimental setting and easy to observe the results. The

detailed data are collected by the field surveys regarding this collapse event. The key methods and results from these efforts are presented in the following subsections.

2.2 Physical behavior of the flow over the local scour region

The principal reason for generating local scour around the bridge piers is in light of the interaction between the flow condition and structural building under river. The flows are interfered with structural building. It makes the flow field to change and interrupt the balance for the original river bed. In addition, it may enhance the complexity for flow field. The flow condition around the structural building can be divided into four parts (see Figure 2.3):

(1). Surface roller

When the flows pass through structural building, the kinetic energy of flow transforms into potential energy on the upstream face along the structural building. From the longitudinal section; it will generate the bow wave phenomenon on the surface of upstream face.

(2). Down flow

The flow velocity decreases with vertical direction from upper to down and so

stagnation pressure does. In this reason, it generates the down flow. Generally speaking, this phenomenon is considered as the most important fact for bridge scouring.

(3). Horseshoe vortex

The down flow runs into the crosswise flow and it change to three dimension vortex. Because the shape likes the horseshoe, it calls Horseshoe vortex. This major reason causes the local scour around the structural building.

(4). Wake vortex

When the flows pass through the structural building, it generates the separation point on the downstream side of the structural building and makes the cross-section of flow velocity produce discontinuity face. Then the wake vortex generates by this procedure.

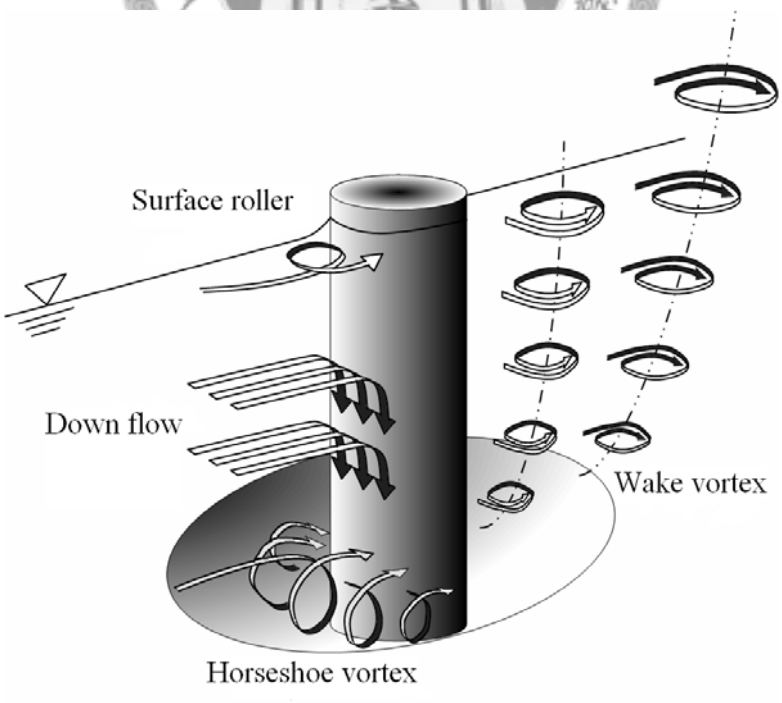

Figure 2.3 The flow condition around the structural building. (Chang [39])

2.3 Laboratory experiments

The Figure 2.4 shows the Hou-Feng Bridge under destruction after the Sinlaku typhoon. There are four piers to support the bridge floor and the current was swift at that time. Besides we can discover that there are a lot of armors around the piers because the engineers placed the armors there not only to prevent the strong current to scour the river bed but also to decrease the flow velocity. The prolonged scouring is the primary reason to make the Hou-Feng Bridge collapse. In this section, the laboratory experiment settings are respectively introduced. In order to simulate the Hou-Feng Bridge with simplification, we have to consider the whole circumstances in advance from experimental setting in lab scale.

Figure 2.4 Local scour around four bridge piles.

2.3.1 Transform field scale to laboratory scale

Before the laboratory experiments works, the scale of the setting needs to be defined. In the Hou-Feng Bridge case, experimental channel is planned 20 cm width and place four piers in the central area of the cannel. Hence the settings are designed to a scale of 1 to 200.

- Geometric similarity:

$$\frac{L_m}{L} = \lambda = \frac{1}{200}$$

- Kinematic similarity:

$$\frac{V_m}{\sqrt{g_m L_m}} = \frac{V}{\sqrt{gL}}$$

- The discharge:

$$\frac{Q_m}{Q} = \frac{V_m L^2{}_m}{VL^2} = \lambda^{5/2}$$

According to the filed information we have measured, the complete data in the experimental setting are shown in Table 2.1.

Table 2.1 Key dimensions used in experiment set up (layout by H.N. Hsieh)

Key dimensions	Field site information	Calculated model dimension
Channel slope	0.011	0.01
Main channel width	240 m	20 cm
Flow rate	4230.54 m^3s^{-1}	1246 cm^3s^{-1}
River bed material D50	80 mm	2.9 mm
Specific gravity	2.65	2.65
Pier diameters	Two for 2 m, two for 4 m	Two for 1 cm, two for 2 cm
Pier length	10 m	5 cm
Caisson diameters	Two for 4 m, two for 5 m	Two for 2 cm, two for 2.5 cm
Caisson length	14 m	7 cm
Distance among the piers	6.8 m, 8.8 m, 6.8 m	3.3 cm, 4.4 cm, 3.4 cm
Distance between pier to pier	20.7542 m	10 cm
Depth of the drop	5.025 m	2.25 cm

2.3.2 Laboratory experimental setting and equipments

The experimental arrangements are depicted in Figure 2.5. The dimensions of the experimental model are conducted in 180 cm long and 20 cm wide. The water supplier (see Figure 2.6) provides the discharge. The water box is designed to be a 50 cm width, 55 cm long and 60 cm height. As we open the outlets, the water flows into the channel and stays in the upper part of the channel till the tank is full. Then the water flows rapidly to the second river bed across the first one (see Figure 2.7).

The first river bed as depicted in Figure 2.6 is used to protect by a concrete structure to cover the water pipelines which were manufactured by Taiwan Water Corporation. The second river bed spreaded for 103 cm long and the sediment filled up to a thickness of 7 cm. There are four piers located above the second river bed. The four piers have the two kinds of size. One has the top of cylinder pier with 1 cm and bottom of cylinder pier is 2 cm. Another one has the top of cylinder pier with 2 cm and the bottom of cylinder pier is 2.5 cm. All the piers are needed to bury into the river bed (2 cm). The properties of the bed sediment selected for the experiments are that the mean particle diameter of the sediment is 0.1 cm and the specific weight of the sediment particle is 2.65. The slope of tank in our laboratory setting is equal to 0.01.

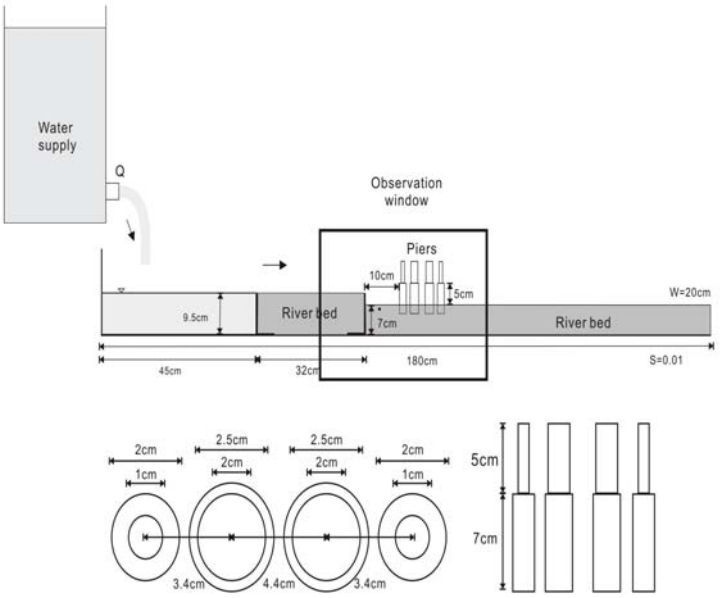

Figure 2.5 Experimental setting of Hou-Feng Bridge with scouring effect.
(designed by H.N. Hsieh)

Figure 2.6 The water supplier system. (photo by H.N. Hsieh)

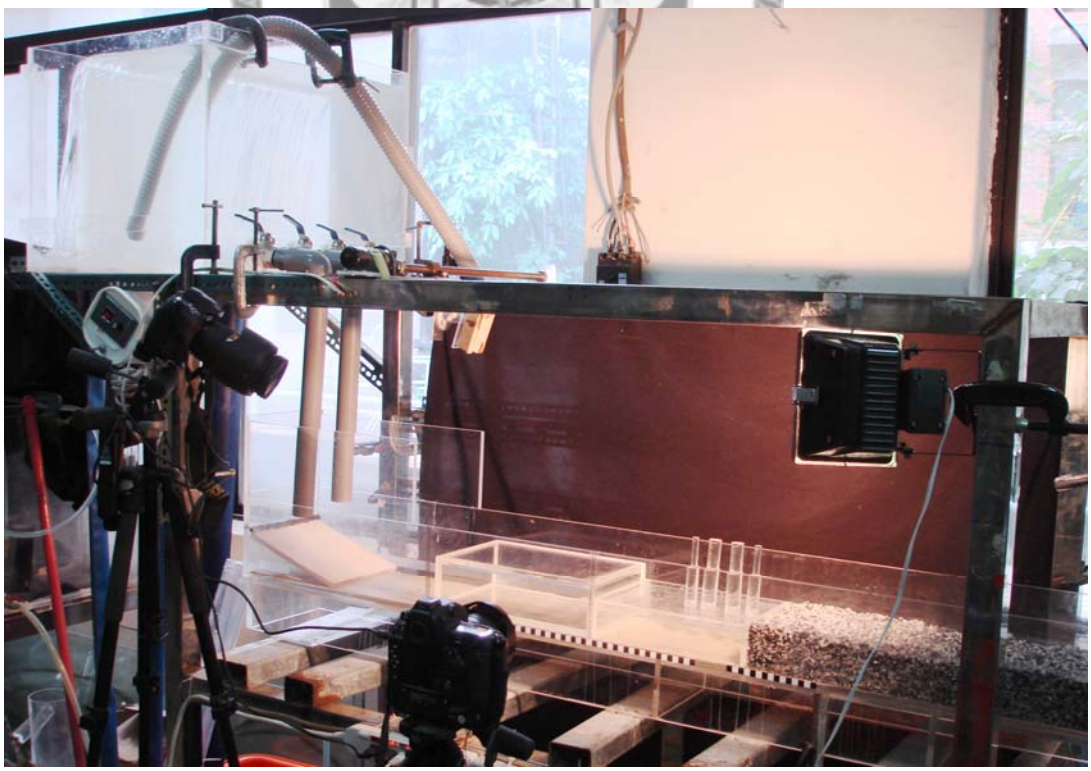

Figure 2.7 Laboratory experimental setting. (photo by H.N. Hsieh)

2.4 Procedure of laboratory experiments

Different material parameters depended on the catagories of the experimental setting. Every experiment all has its purpose: Experiment 1 is designed to compare results with numerical simulations. Experiment 2 is major parts of serious experiments. We execute this part for observing the bed erosion with clear water.

Table 2.2 Experiment parameters information

	Experiment 1	Experiment 2	Experiment 3
Discharge(cm^3s^{-1})	1370	1290	1350
material	Rigid bed	gravel	Gravel/fine sand
Time(min)	none	62	8
Instruments	camera	Ultrasound/camera	Ultrasound/camera

Table 2.3 The material information

	gravel	Fine sand
D_{50}(mm)	2.9	0.08
D_{60}(mm)	3.2	0.085
D_{10}(mm)	1.1	0.038
Coefficient of Uniformity $=D_{60}/ D_{10}$(mm)	2.9	2.25

We provide the properties of the materials for the experiments in Table 2.3. These data were measured by sand supplier. For gravels, it was measured in the geotechnical laboratory. The materials size used in experiment was bigger than the size calculated by dimension analysis. From pictures (see Figure 2.4) in Hou-Feng Bridge as typhoon comes, we can observe that were amors be washed away by flood. Hence our experiment was suffering the strong discharge. That means the size we used in experiment also can be washed. This reason is why we choose this size of gravels.

2.4.1 Experiment 1: rigid bed

We execute this experiment just to test the experiments and not only for laboratory

parts but also for numerical parts. It will be too complicated when we put the gravel in the channel. Hence we consider simplifying experiments first. The second river bed is removed and we used a box which size was 20 cm width, 32 cm long and 9.5 cm height replaced the second river bed (see Figure 2.8). Furthermore, the designed experiment 1 was not same as the setting we have shown before. The setting of rigid bed case is shown in Figure 2.9. We also use the digital camera to record flow condition. In the processing, the variation of topography was very quick. The timer connected with digital camera to take pictures per second.

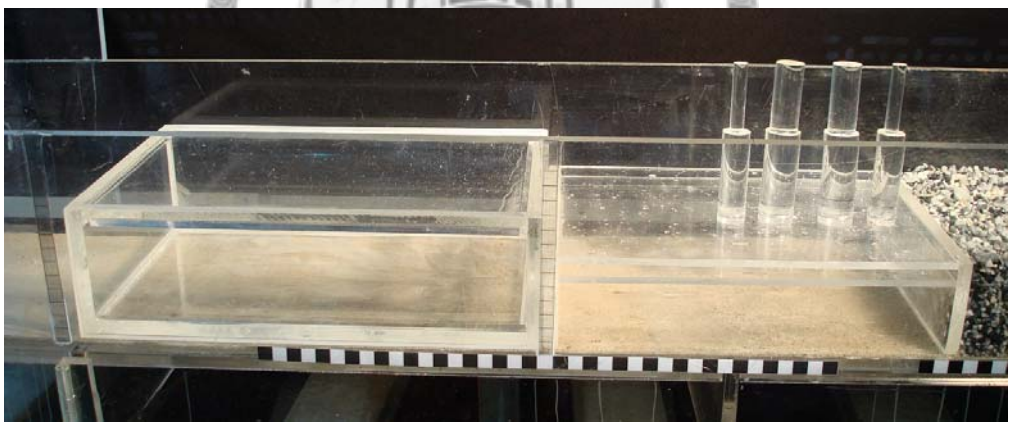

Figure 2.8 The experiment 1 (photo by H.N. Hsieh)

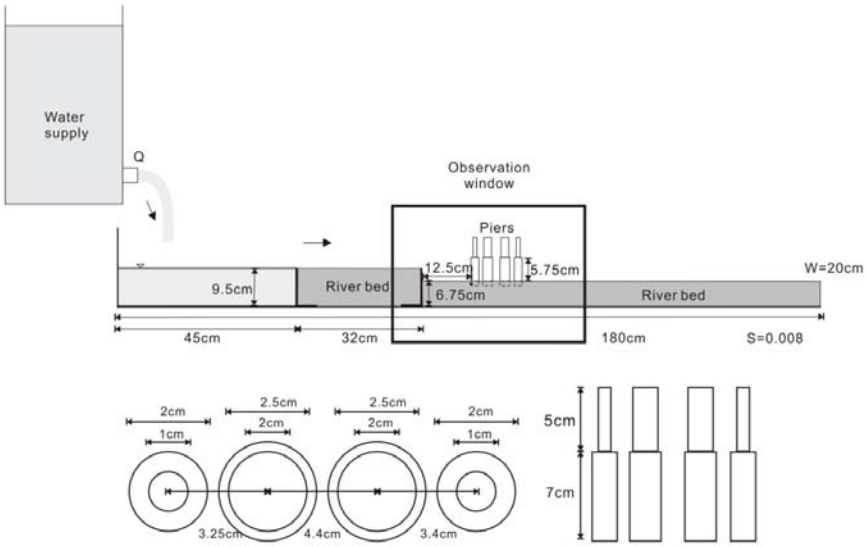

Figure 2.9 The setting of rigid bed case (layout by H.N. Hsieh)

2.4.2 Experiment 2: gravel and clear water

We change rigid bed to mobile bed in this experiment and put the gravel in the channel as we mentioned before. Besides in this case we use the ultrasound device to scan the topography (see Figure 2.10). The position of ultrasound device is in front of the piers (see Figure 2.11) and we hope that we can observe the scour which were caused by the overfall flow. One digital camera are used to record the procedure of scouring in the same way as experiment 1 and the experiment processing was also the same as before (see Figure 2.12).


(a)

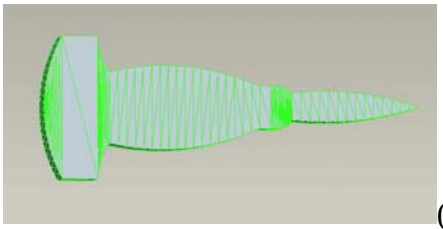
(b)


(c)

Figure 2.10 (a) the ultrasound device which we used in the experiment 2. (b) we make this model by pro/e and put this sensor into numerical simulation. (c) the ultrasound device

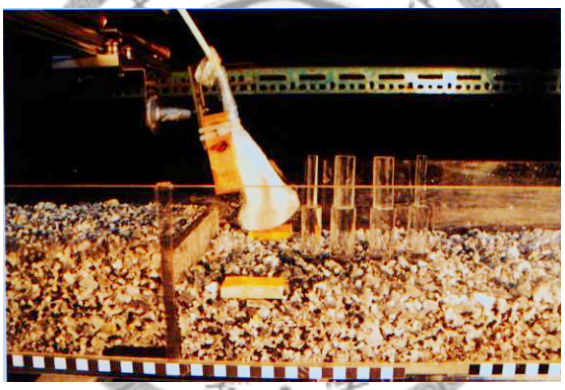

Figure 2.11 The end view from digital camera of experiment 2. (photo by H.N. Hsieh)

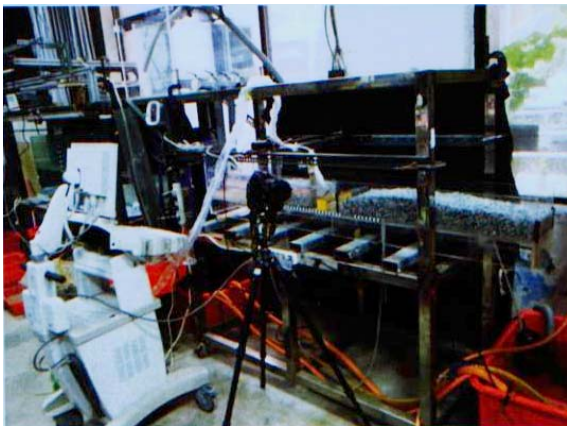

Figure 2.12 Work field of experiment 2(photo by H.N. Hsieh)

Chapter 3 Numerical experiments

In this thesis, the FLOW-3D commercial software is employed to simulate all the experimental cases which are set up in chapter 2. Why we choose this software and collect the 3D results? There have been a lot of researchers to study the sediment scour problem theoretically, it is still difficult to simulate by programming numerically. Hence we want to rely on this powerful software to simulate our problems.

The types of local bridge scour have been introduced in chapter 2. The phenomena of local scour surrounding the bridge have the horseshoe-shape scouring hole. Hence we can not use the 2D viewpoint to observe the procedure of generation mesh and associated numerical results. In other words, we can not focus on the sediment scour variation for the z-direction. In addition the flow conditions are complicate surrounding the bridge piers. The 3D simulations are necessary in our numerical studies. Finally, the procedure of setting is illustrated for the whole numerical simulation in this section. The numerical simulations are roughly divided into two parts. One is rigid bed simulation and other is mobile bed simulation. The rigid case is designed to simplify our numerical settings and to make sure the numerical setting can be executed in the initial stage. The

mobile cases are the mainly parts in our numerical simulation and they include three types: the mobile bed with or without ultrasound device, and we remove the first river bed case.

3.1 Procedure of numerical setting by Flow-3D

The FLOW-3D is not only powerful but also easy to operate and it has the humanization interface. We can use it intuitively. First of all, we have to build up a workspace and create a new simulation file. The next step is turned on from the user interface by selecting “General” and entering the simulation time we want. After entering the simulation time, we should select the suitable unit. Then we have to import all the parameters referenced from the experimental setting, which consists of fluid density, gravity and the turbulence model. After these two parts are done, we start to dispose the difficult parts of numerical setting, build geometry and mesh generation. In the meantime, we have to check if we need to use graphics software to build the complicated geometry. Because FLOW-3D can build the simple geometric shape only, however, the more complicated geometries need to depend on graphics software such as pro/e or AutoCAD. However, a significant note is that as finishing the geometry in the

graphics software, we have to save the file into STL file. Only STL file can be read in the FLOW-3D. The detailed procedure of numerical settings are described in the flow chart as shown in Figure 3.1.

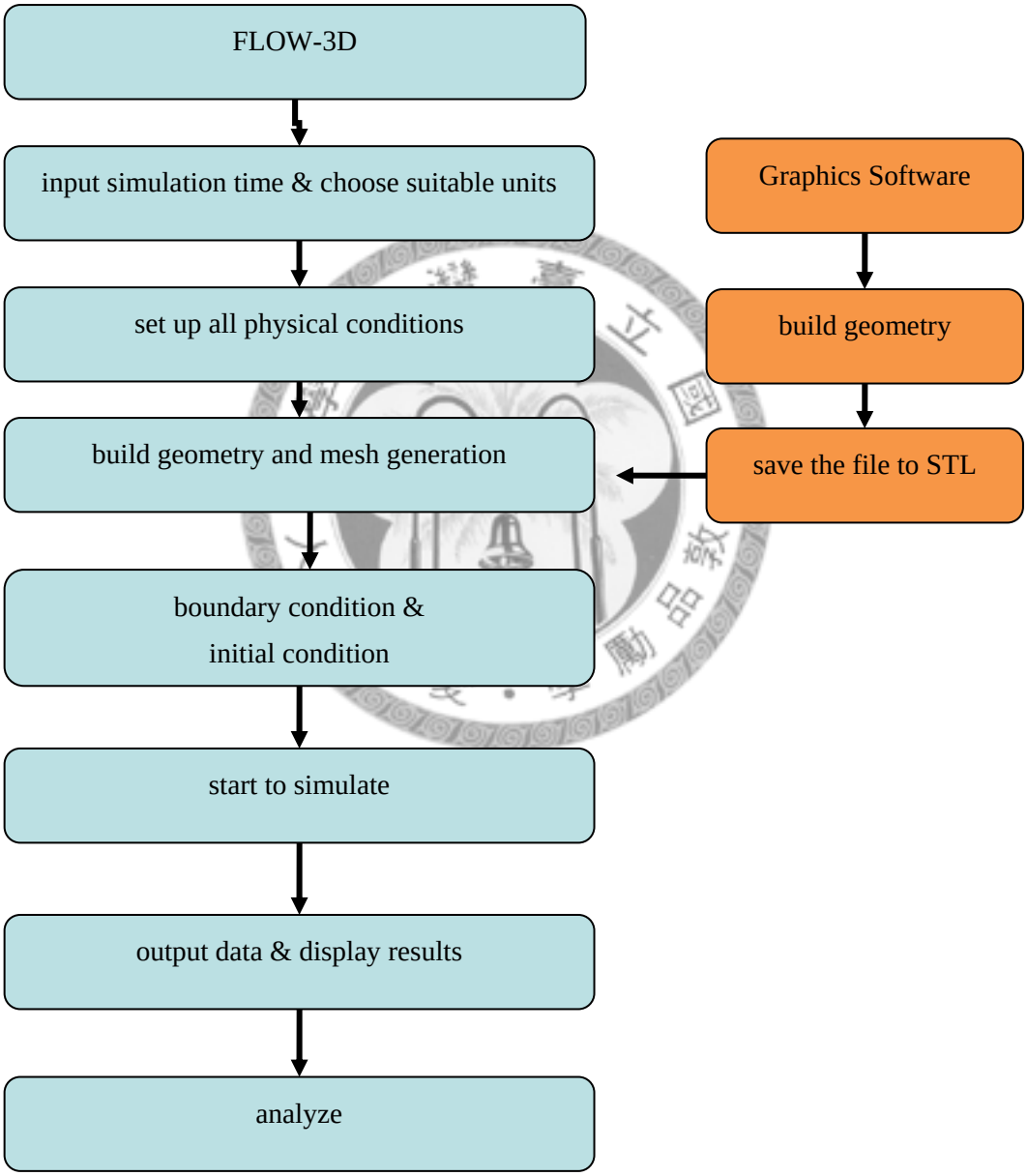

Figure 3.1 The flow chart of numerical simulation

3.2 Numerical simulation 1: rigid bed case

The flowchart of numerical setting has been explained in chapter 3.1. The laboratory experimental setting is shown in Figure 3.2(a) and we built the geometry from the design chart (see Figure 2.11). In Figure 3.2(b), the yellow part in left had side is designed as the water supplier system in our numerical simulation which supplies the constant discharge.

In Figure 3.3 (a), the mesh size is not uniform. It is the characteristic of FLOW-3D. We set up the fine mesh around piers because this part is the important observation region. Here we can observe the flow condition in front of piers. On the other hand, other areas use coarse mesh and the computation resource can be used more effectively. In addition the channel of the laboratory experiment has slope. However, it is difficult to dispose the slope from geometry in FLOW-3D. In addition, the gravity vector is defined in every direction in order to simulate the slope of channel. The parameter setting is exhibited in Table 3.1.

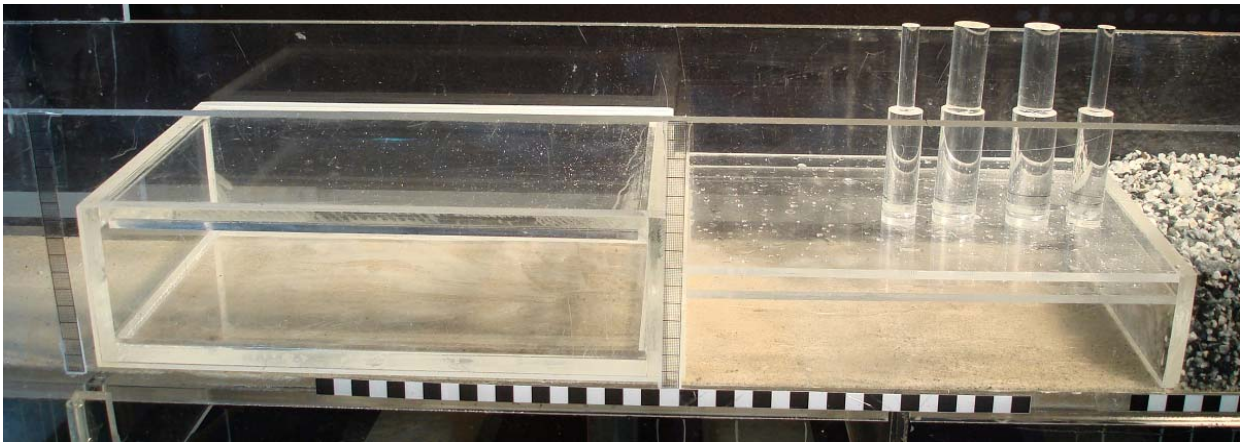

(a)

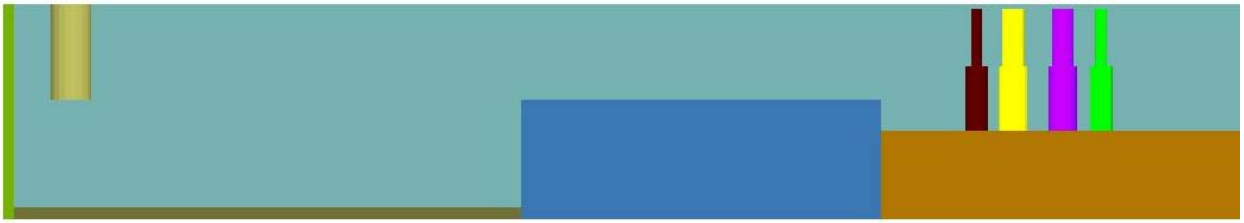

(b)

Figure 3.2 (a) rigid bed case of laboratory experiment (photo by H.N. Hsieh) (b) rigid bed case of numerical geometry

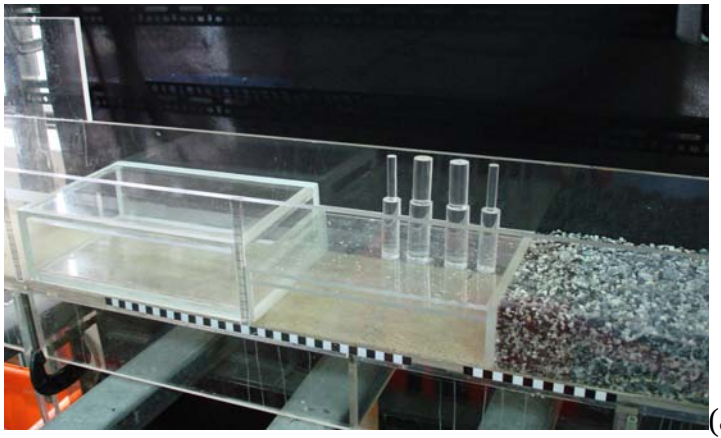

(a)

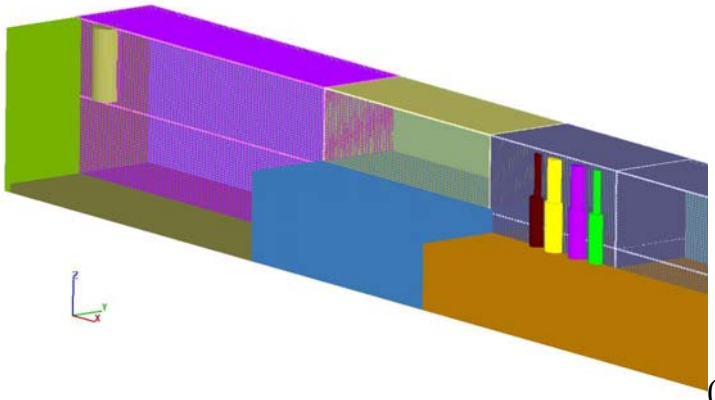

(b)

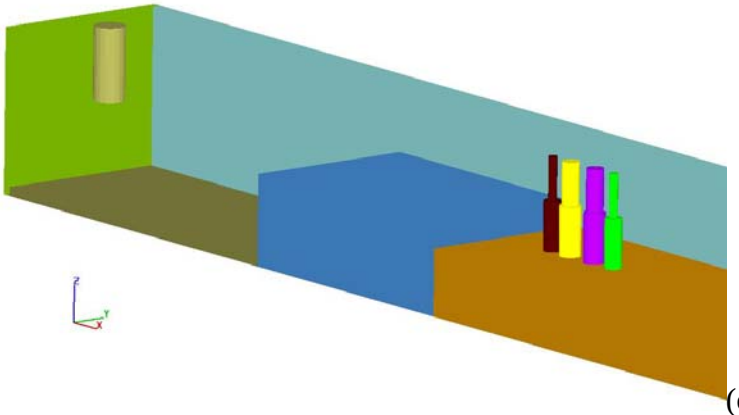

(c)

Figure 3.3 (a) the rigid bed case of laboratory experiment (photo by H.N. Hsieh) (b) numerical mesh we build (c) the different view of rigid bed case

Table 3.1 The condition and parameter setting of rigid bed case in FLOW-3D

simulation time	60 s
simulation units	CGS
gravity vector	X: 7.83981
	Y: 0
	Z: -979.9686
turbulent model	RNG model
total number of cells	about 3,210,000 points
boundary condition	x-min: wall
	x-max: out flow
	y-min: wall
	y-max: wall
	z-min: wall
	z-max: wall
pressure solver options	implicit
momentum advection	second order monotonicity preserving
Fluid flow solver options	Solve momentum and continuity equations

3.3 Use the small domain to simulate all the mobile bed cases

The numerical geometry for mobile bed cases are not like the rigid bed case that we build before. In the previous numerical setting, we build the whole channel but this method wastes the computation resources. We merely concern about the sediment scour in the live-bed simulations so the initial part is not the key point regarding our discussions. Hence we hope that we can define another boundary condition for our numerical simulation by ourselves. The water supplier system and the geometry of tank built in Flow-3D is shown in Figure 3.4. The original method is to set a tube in order to obtain the initial condition, and it provides the constant flow rate. It is shown in Figure 3.4 (the red circle part). However, we do not want to do the same thing in every numerical simulation. The cross-sections are set here due to this reason in the Flow-3D and we can obtain the flow rate and the fluid depth by means of the cross-section. The new boundary condition and initial condition are obtained by this way.

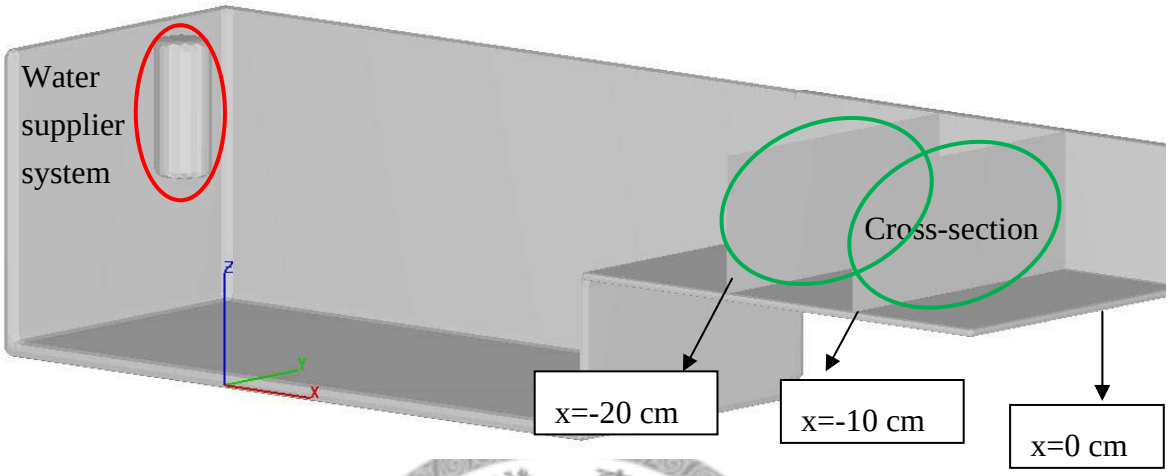

Figure 3.4 The water supplier system and the tank geometry in Flow-3D

Of course, the method should be verified first and then we can make sure that we can use these data as our new boundary condition. In Figure 3.4, two cross-sections are defined in the rigid bed simulation and the time history in this case is about 30 sec. After we obtain the flow rate and fluid depth for two cross-sections, we build the small domain for the rigid bed case (see Figure 3.5). Finally, the fluid depth of full domain is compared for two types of simulations in front of the first pier. The result is exhibited in Figure 3.6(a). The black line, the blue line and the red line are the full domain results, small domain(x=-20) and the other small domain(x=-10) respectively. The fluid depth and the flow rate on the boundary are also compared in the numerical simulations. The numerical results are shown in Figure 3.6. As can be seen, the numerical result which

we use the new boundary condition corresponds to the original numerical setting. The mesh points are decreased apparently by means of this method and we can retrench the computation resource.

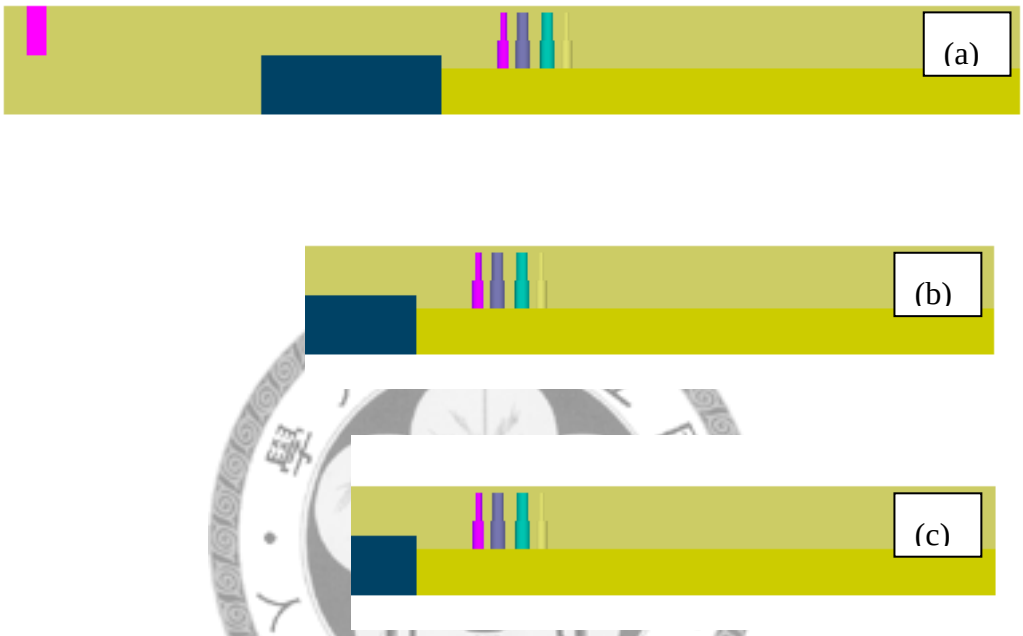

Figure 3.5 The numerical geometry of the full domain and the small domain (a) full domain for rigid bed simulation (b) small domain (x=-20) (c) small domain (x=-10)

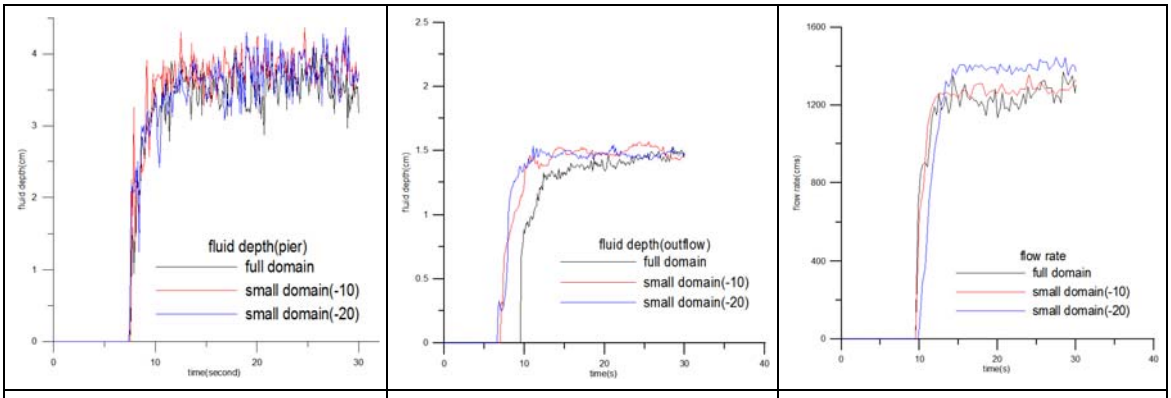

(a)	(b)	(c)

Figure 3.6 The numerical results for the different domain (a) fluid depth in front of the first pier (b) the fluid depth in the out flow (c) the flow rate in the out flow

3.4 Experiment 2: mobile bed with ultrasound device

In the laboratory experiments, the ultrasound device is used to scan the sediment height. This device is not adopted in initial stage because they usually use the infrared ray device to scan the topography. However, the infrared ray device is not suitable in the sediment experiments because the water is easily polluted in light of the sediment particle. The accuracy of infrared ray is perturbed due to the muddy water of the channel. Furthermore maybe the devices can not be employed in laboratory experiments. Hence they try to seek another tool and the ultrasound device is chosen to replace the infrared ray device in their experiments. The ultrasound device can be used extensively in a lot of complex entertainments. Of course, the ultrasound device can work normally in the muddy water condition. Nevertheless, it still has some disadvantage which the data is collected from the experiments needed to disposal by Matlab code.

The ultrasound device is built by graphics software in the numerical simulation (see Figure 3.7(b)). Furthermore, the experimental scale for the mobile bed case is different from rigid bed case. The detailed setting is shown in Figure 2.9 and 2.11. The slope of channel is changed so the gravity vectors have to be modified in the numerical setting. The most important setting in this simulation is that we have to define the

sediment condition. In Figure 3.7 (c), the yellow part stands for alluvial river bed, and it is the significant region which we want to observe. It is a tough work for us because not all the parameters are easy to define in numerical simulation. We have to do the trial and error to test some parameters that we need.

The first step is turned on from the user interface by selecting sediment scour in physics condition. We need to specify the number of sediment species and can decide the names of each sediment species. In our test case, we only use one kind of sediment species. The value of the maximum packing fraction can be entered as well. The density, critical Shields number, drag coefficient, entrainment coefficient, bed-load coefficient and angle of repose must be defined for each sediment species. Note that the only parameters required are the density and the diameter; all other specifications are optional and the defaults are shown except for the critical shields number and test the critical Shields number will be introduced in chapter 3.4.2.

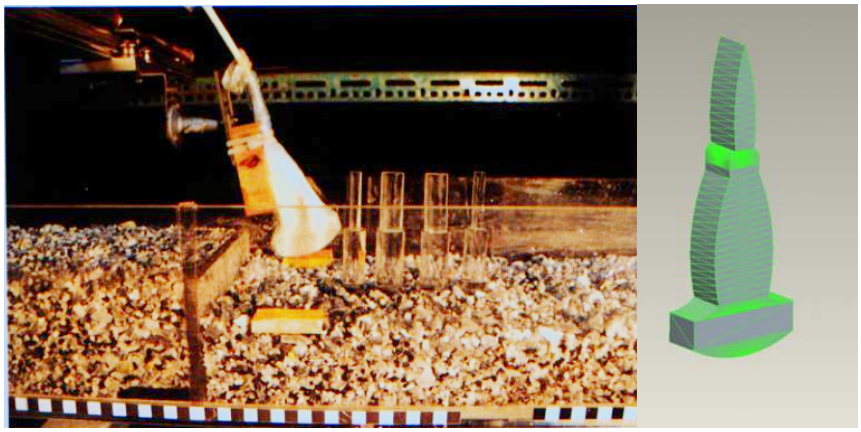

(a) (b)

(c)

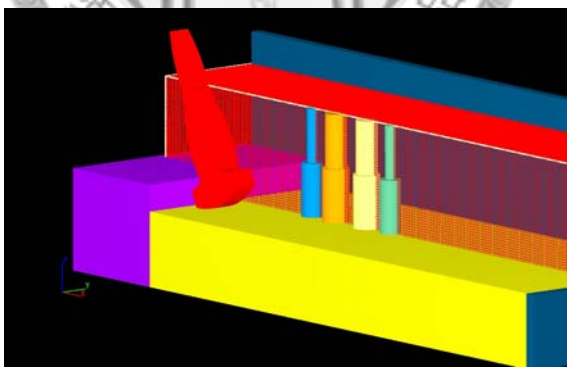

(d)

Figure 3.7 (a) setting of laboratory experiment (photo by H.N. Hsieh) (b) ultrasound device edited by graphics software (c) setting of numerical experiment (d) mesh of mobile bed case with ultrasound device

Table 3.2 The condition and parameter setting of mobile bed case with ultrasound device in FLOW-3D

simulation time	120 s
simulation units	CGS
gravity vector	X: 9.8088
	Y: 0
	Z: -980.581
turbulent model	RNG model
total number of cells	about 1500,000 points
boundary condition	x-min: volume flow rate
	x-max: out flow
	y-min: wall
	y-max: wall
	z-min: wall
	z-max: symmetry
pressure solver options	implicit
momentum advection	second order monotonicity preserving
Fluid flow solver options	Solve momentum and continuity equations

3.5 Experiment 3: mobile bed case

We remove the ultrasound device in this numerical experimental setting because we want to understand whether the sensor will affect the variation of sediment scour around the piers. The same physical setting is employed (see Table 3.2). By this step, we can more concentrate on the variation of sediment height near the piers. The laboratory experimental setting and numerical geometry are exhibited in Figure 3.8. The laboratory experimental results are only recorded by the digital camera, that is to say, there are no tools used to measure the scour elevation in the experiments. With the help of numerical simulation, we can find out more mechanism of sediment scour.


(a)


(b)

Figure 3.8 (a) numerical experiment for mobile bed (end view) (b) mobile bed case without ultrasound device (photo by H.N. Hsieh)

3.6 Experiment 4: remove the first river bed in mobile bed case

The first river bed stands for the water supplier system in our experiments. The overfall flow phenomenon is due to this artificial structure. Some one doubts that the collapse of Hou-Feng Bridge is attributed to this structure. In the laboratory experiments, they do not set up the experiments to test the first river bed but this numerical simulation is imperative in author's opinion. Hence we want to study the influence about the overfall flow effect. The mobile bed case is used here again but the first river bed is removed in our numerical setting (see Figure 3.9). The physical conditions are employed in Table 3.3.

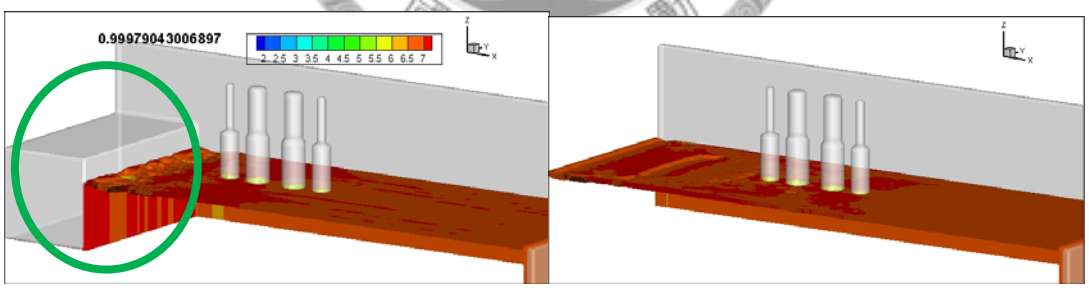

Figure 3.9 The mobile bed case (left hand side) and remove the first river bed (right hand side)

Table 3.3 The condition and parameter setting of mobile bed case in FLOW-3D

simulation time	60 s
simulation units	CGS
gravity vector	X: 9.8088
	Y: 0
	Z: -980.581
turbulent model	RNG model
total number of cells	about 1500,000 points
boundary condition	x-min: volume flow rate
	x-max: out flow
	y-min: wall
	y-max: wall
	z-min: wall
	z-max: symmetry
pressure solver options	implicit
momentum advection	second order monotonicity preserving
Fluid flow solver options	Solve momentum and continuity equations

Chapter 4 Results and discussions

In this section, the results of clear-water simulation with Flow-3D software would be compared to the small-scale experiments to validate the robustness of the numerical analysis. The discussions in this chapter are divided into four parts: (i) the variation of the local scour effect over the rigid-bed, (ii) over the mobile bed with ultrasound device, (iii) mobile bed and (iv) remove first river bed. For the rigid-bed, first of all we use the material parameters which are obtained from the experimental setting are served as the initial and boundary conditions animates by the Flow-3D. To the authors' knowledge, seldom references disposed such kind of problem which both have the swift current and the local scour problem simultaneously. For the change of mobile-bed of the scouring problem, we would put up the experimental analog of bedrock-alluvial transitions and local bridge scour configurations which is correspondent with the numerical setting.

4.1 Rigid-bed case

As mentioned before, our threshold is going to simplify local bridge scour problem. In this section, we focus on the dropping water and the water level would fluctuate due

to the flow ram into the obstruction. It would make the fluid depth to have the periodic oscillation. Before starting the animations, the fluid depth along the bridge have to initialize which corresponds to the experimental setting as shown in Figure 4.1.

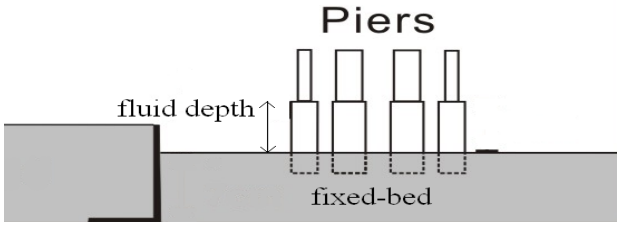

Figure 4.1 The sketch of the piers over the fixed bed and its fluid depth.

For the laboratory experiments, we have done them three times with the same manipulation and obtain three kinds of the statistics as shown in Figure 4.2. The three sings are symbol of the different group about laboratory experiments and the black line is the numerical result. After that, the numerical modeling is built by Flow-3D as shown in Figure 4.3. For the whole analysis, the results from Flow-3D exhibit good agreement with the small-scale laboratory experiment data. The fluid depth in front of the first pier shows periodic oscillation in height as shown in Figure 4.2. The predicted data is similar to the measured data, and it can be observed that three experiments had some variation in water surface height even if they had same configurations. The non-bed rock simulation plays an important role in validating the inflow and outflow boundary conditions by choosing an appropriate grid resolution for simulations, since this

problem is simple and easy to simulate.

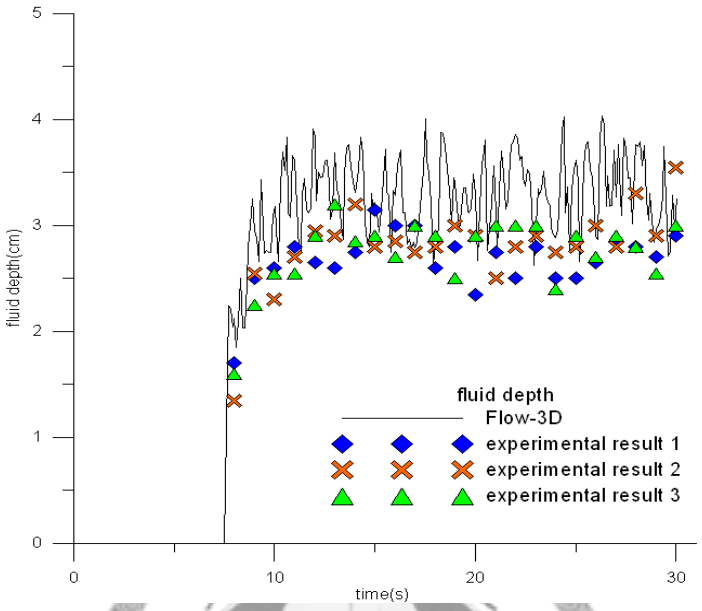

Figure 4.2 The fluid depth for numerical result and the experiment results.

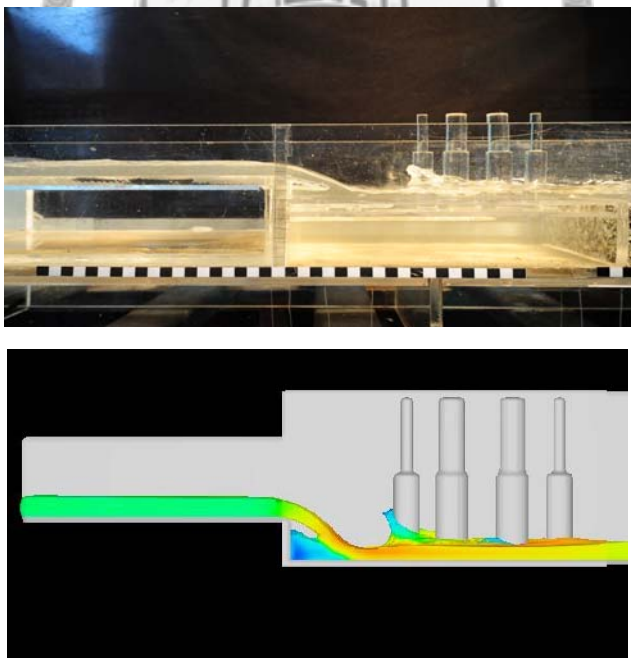

Figure 4.3 The laboratory experiment result and the numerical animate in Flow-3D (rigid-bed)

In order to distinguish from the numerical results conveniently, the three cross-sections are defined in Figure 4.4. The origin is defined among first river bed and the alluvial river bed and it is located at x=-10 cm. This cross-section is used to record the velocity. We want to compare the flow condition to the overfall flow. The second cross-section is located on x=7 cm and it is set in order to observe the major scour area in our numerical simulation. The third cross-section is located on 13.5cm and it is set for measuring the flow condition around the bridge piers.

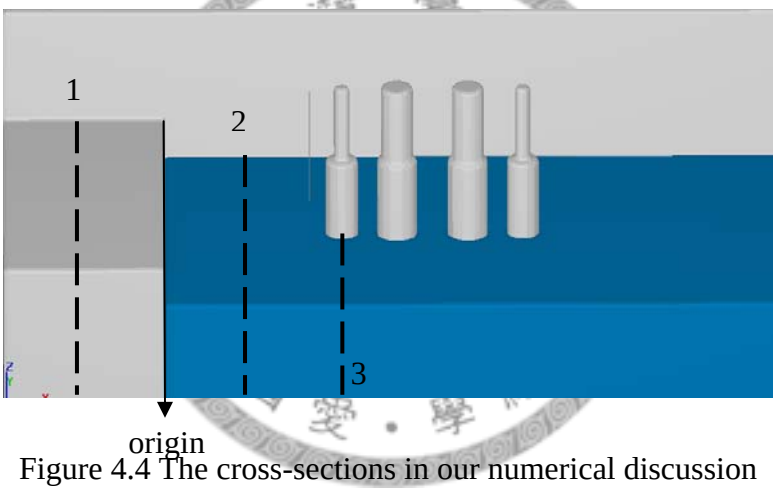

Figure 4.4 The cross-sections in our numerical discussion

The velocity field is shown in Figure 4.5 (a). The black dashed line is the origin which has been illustrated before. As seen, the x-velocity increases so quickly in light of the overfall flow. It is because that the potential energy from the first river bed transforms into the kinematic energy. In addition, the negative velocity occurs in front of the first piers because the strong current ran into it. Although the sediment is

influenced by the x-velocity, it is not the principle cause. It is particularly important for the z-velocity which is exhibited in Figure 4.5 (b). As seen, the minimum z-velocity occurs where the water drop, and we have illustrated the reason before. The z-velocity in front of the first pier is positive and it has the interesting numerical results. We find out the down flow is not conspicuous and the down flow is introduced in chapter 2.2 which is the key point about the bridge local scour. Naturally, the numerical result here is suitable for the rigid bed case only. We can not assume that the mobile bed simulation has the analogous trend as we simulate the rigid bed case. In this case, another interesting phenomenon is the variation of the fluid depth. We focus on the four bridge piers. Undoubtedly, the maximum fluid depth occurrs in the first pier; however the second fluid depth is found out in the third bridge piers. This is similar to the bow wave effect and it can perturb the sediment scour. Hence we can pay attention to the sediment scour for the third pier in mobile bed simulation, too.

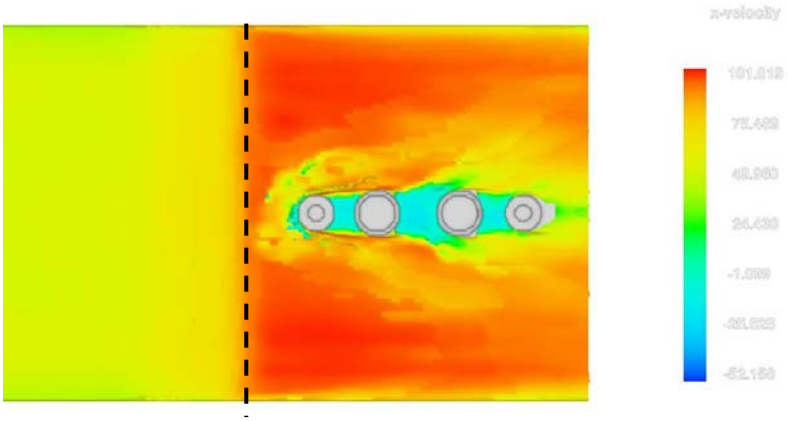

(a)

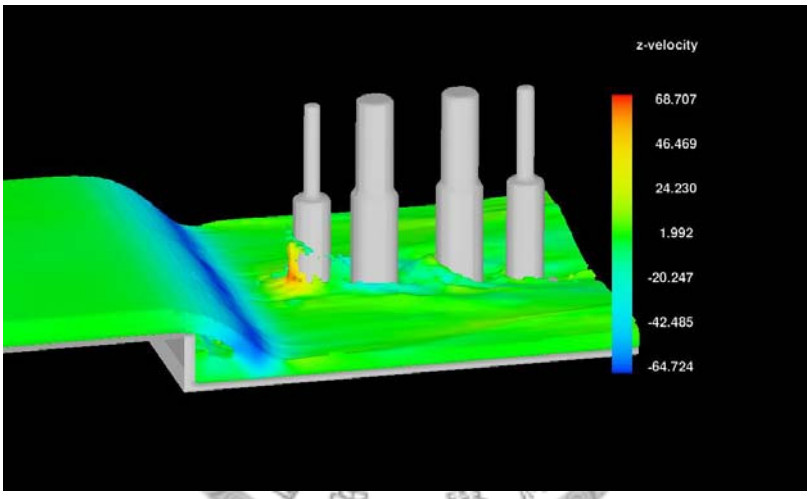

(b)

Figure 4.5 The velocity of rigid bed simulation (a) the x-velocity (vertical view) (b) the z-velocity

The vortices results are exhibited in Figure 4.6 and we can more realize the flow condition by means of the vortices. The y-vorticity is shown in Figure 4.6(a) and the maximum value occurs at the water drop. At the same time, the minimum value is measured in front of the bottom of the first pier. Hence we believe that this place is

scoured obviously in the mobile bed simulation. The z-vorticity is shown for vertical view in Figure 4.6(b). The major vorticity is generated on both sides of bridge piers so the sediment particle may be entrained in light of the vortex effect. Hence we can notice the variation of sediment scour among the bridge piers in our mobile bed simulation.

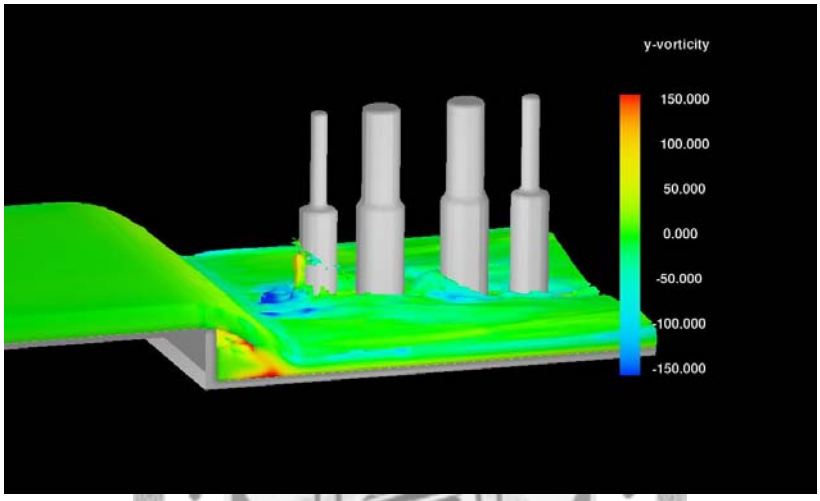

(a)

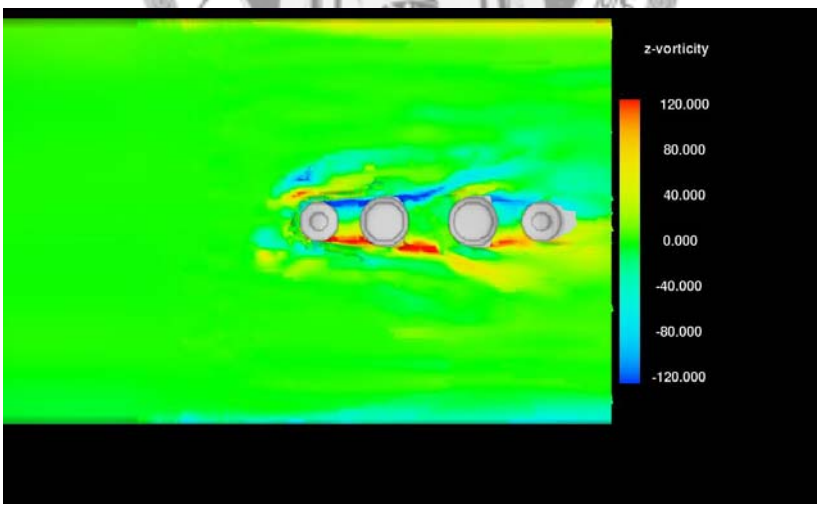

(b)

Figure 4.6 The vorticity of rigid bed simulation (a) the y-vorticity (b) the z-vorticity (vertical view)

(1) First cross-section :

The Figure 4.7(a) is the x-velocity in first cross-section. As can be seen, the x-velocity contours are symmetry and it means that the flow conditions are not turbulent before the water drop. The x-velocity increased from the bottom to top and the maximum x-velocity is located on both sides. On the other hand, the z-velocity contours are not symmetry in Figure 4.7(b). The simulation results are chosen at 27 sec because the flow conditions have been approached the quasi-steady in rigid bed simulation.

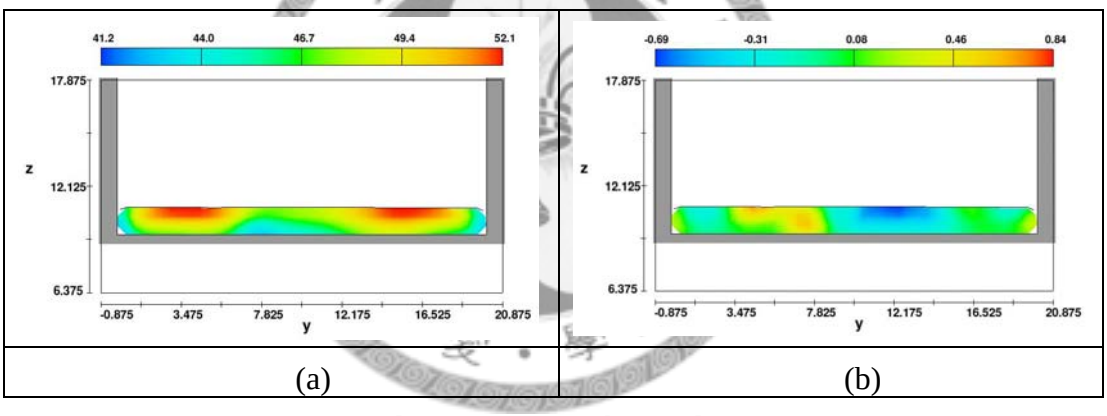

(a) (b)

Figure 4.7 (a) x-velocity contours (b) z-velocity contours

(2) The second cross-section:

In Figure 4.7(a) and 4.8(a), the x-velocity increased rapidly, and the higher x-velocity is speared on the fluid surface. Hence the noticeable phenomenon here is that the minimum x-velocity is bigger than the maximum x-velocity in the first cross-section. It implies that the sediment is entrained more easily in light of this

reason. In addition, the maximum value of x-velocity in second cross-section is about two times than the first cross-section because this cross-section is located on the place where the water drops. The z-velocity is similarly influenced due to the overfall flow. The fluid force is reflected when the flow rams into the rigid bed in this simulation. According to this behavior, the consequence of the minimum z-velocity is close to the water surface.

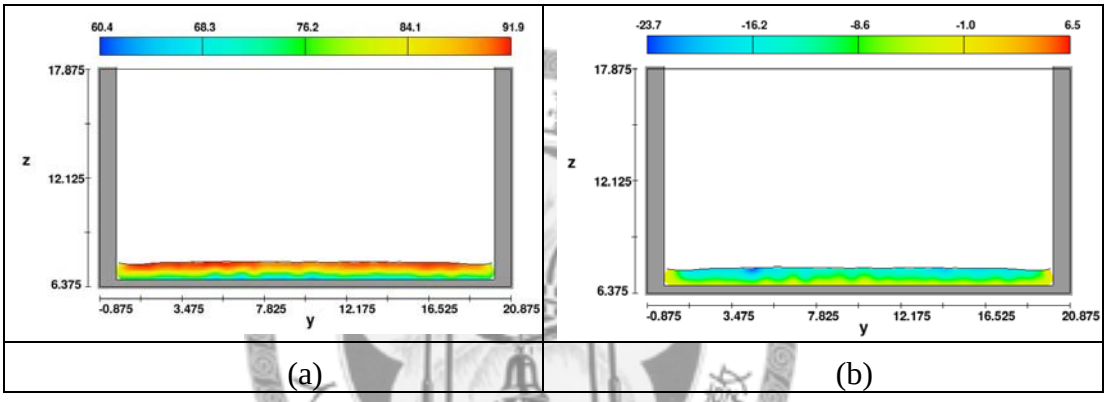

(a) (b)

Figure 4.8 (a) x-velocity contours (b) z-velocity contours

(3) the third cross-section:

In Figure 4.9(a), the black dashed line stands for the first pier and it can be seen that the x-velocity decreased gradually from the central line to the wall in the channel. At the same time, the down flow not occurred around the bridge pier. Hence it implies that the horseshoe vortex effect is insignificant here. Furthermore, while the flow across the structure such as the bridge piers, the angle of attack is generated in the meantime (see Figure 4.10). The z-velocity does not have the obvious variation in Figure 4.9(b) and the maximum z-velocity is close to the first pier and its direction is toward to the positive z-axis. The results tell us, that the sediment particles do not be entrained for both sides.

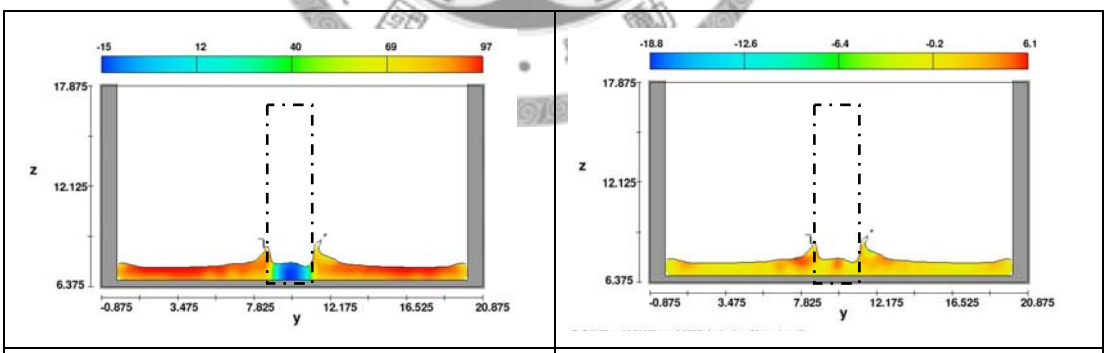

(a) (b)

Figure 4.9 (a) x-velocity contours (b) z-velocity contours

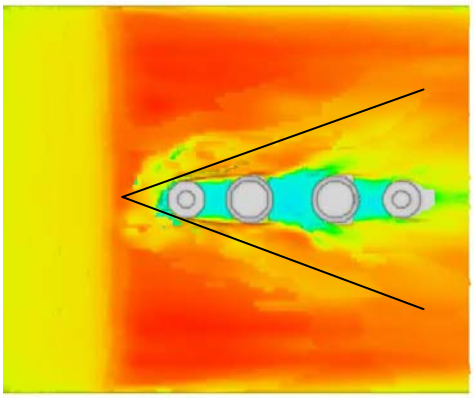

Figure 4.10 The angle of attack in the rigid bed simulation

4.2 Critical Shields number

Before the sediment simulations are discussed, we have to introduce the critical Shields number and define it. This parameter plays an important role in sediment scour simulation. It directly affects our numerical stability. In numerical setting, we can define the critical Shields number by ourselves or depend on the system automatically. The detail basic theory about critical Shields number can be found in Flow-3D users manual [16]. One part of users manual is chosen in next paragraph in order to illustrate the significance of the critical Shields number.

Sediment is entrained by the picking up and re-suspension of packed sediment in light of shearing and small eddies at the packed sediment interface. Because it is not possible to compute the flow dynamics about each individual grain of sediment and it is

oftentimes difficult to compute the boundary layer at the interface, an empirical model must be used. The model theory used here is based on Mastbergen and Von den Berg [29]. Furthermore, we can use the Shields-Rouse equation [26] to predict the critical Shields number, or define the value by ourselves.

The first step to computing the critical Shields number is to be calculate the dimensionless parameter R_i^*

$$R_i^* = d_{s,i}\frac{\sqrt{0.1(\rho_{s,i}-\rho_f)\rho_f \|g\| d_{s,i}}}{\mu_f} \tag{4.1}$$

Then R_i^* can be used to calculate the dimensionless critical Shields parameter by means of Shields-Rouse equation [26].

$$\theta_{cr,i} = \frac{0.1}{R_i^{*(2/3)}} + 0.054[1-\exp(-\frac{R_i^{*(0.52)}}{10})] \tag{4.2}$$

The effects of armoring are also included in the model, whereby coarse sediment particles protect finer particles from becoming entrained. The effect of armoring is important in sediment scouring. First of all, we have to calculate the local mean particle size in the computational cell:

$$d_{50} = \frac{1}{\sum_{i=1,ns} c_{s,i}} \sum_{i=1,ns} c_{s,i} d_{s,i} \tag{4.3}$$

Where $c_{s,i}$ is the mass concentration of sediment species i.

The critical Shields parameter is then modified by the Egiazaroff function [27]:

$$\theta'_{cr,i} = \theta_{cr,i} \frac{1.666667}{\log_{10}\left(19\frac{d_{s,i}}{d_{50}}\right)^2} \tag{4.4}$$

In addition, the critical Shields parameter is modified for sloping surfaces to include the angle of repose one step further. The conception here is that at sloping interfaces, the packed sediment is unstable and is more easily taken away by the moving fluid. The modification further alters $\theta'_{crit,i}$ [28]:

$$\theta''_{cr,i} = \theta'_{cr,i} \frac{\cos\psi \sin\beta + \sqrt{\cos^2\beta \tan^2\varphi_i - \sin^2\psi \sin^2\beta}}{\tan\varphi_i} \tag{4.5}$$

Where β is the computed angle of the packed interface normal relative to the gravitational vector **g;** φ_i is the user-defined angle of repose for sediment species i and ψ is the angle between the flow and the upslope direction.

After we know how adequate critical Shields number is suitable for the realistic filed, some tests are worked in our numerical simulation. In Figure 4.11, the scouring hole would shift gradually as the time went on in laboratory experiment. We use the mobile bed case with the ultrasound device, for example, and all conditions are preserved except for the critical Shields number. In Figure 4.12 (a), the upper setting is defined by ourselves (critical Shields number = 0.06) and down is given by FLOW-3D itself. The color bar is the sediment elevation. For the serious numerical experiments,

we can observe clearly that scouring hole of the upper numerical setting will move as time went on. On the contrary, if the critical Shields number is not defined by ourselves, the overfall flow will continually erode the same place and the scour hole does not move with time. This scouring behavior infringes the laboratory experiment in Figure 4.12. From the numerical tests of defining the adequate critical Shields number, a significant note is that the more suitable material parameter we chosen, the more reasonable results we will get.

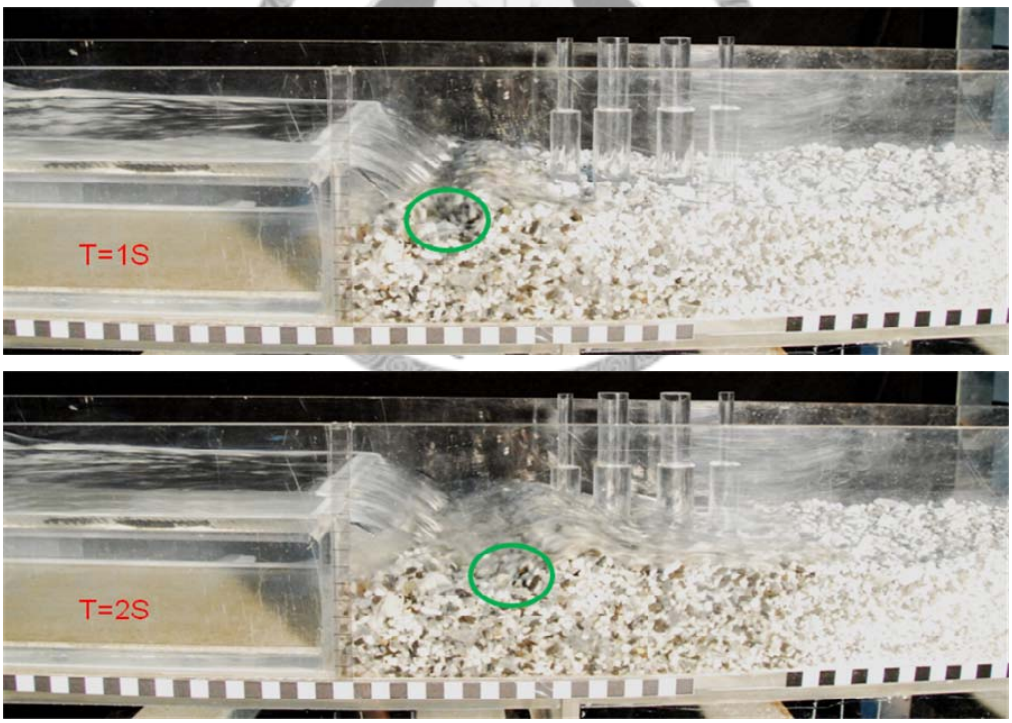

Figure 4.11 The mobile bed case result (photoed by H.N. Hsieh)

Figure 4.12 Test the significance of critical Shields number (a) 0 sec (b) 1 sec (c) 3sec (d) 5sec (e) 7sec

4.3 Mobile bed simulation with ultrasound device

In this section, the mobile bed case with the ultrasound device is simulated. The sensor help the laboratory experiments to scan the real topography getting rid of the disturbance of the fluid-solid mixtures are shown in Table3.3. In Figure 4.13 the packed sediment height was perturbed in light of the sensor. It is placed too close to the position where the overfall flow fallen. Hence its existence absolutely interferes with flow intensity and changes the flow direction when the water dropped. The major scouring place is around the sensor if we placed the ultrasound device in numerical experiment. Because this numerical result has a lot of factors, we are unable to confirm the problem in this case.

Table 4.1 The sediment setting for mobile bed case with ultrasound device

number of sediment species			1	maximum packing fraction			0.52
	diameter	density	critical Shields number	drag coefficient	entrainment coefficient	bed-load coefficient	angle of repose
Sediment	0.29	2.65	0.06	0.5	0.018	8	45

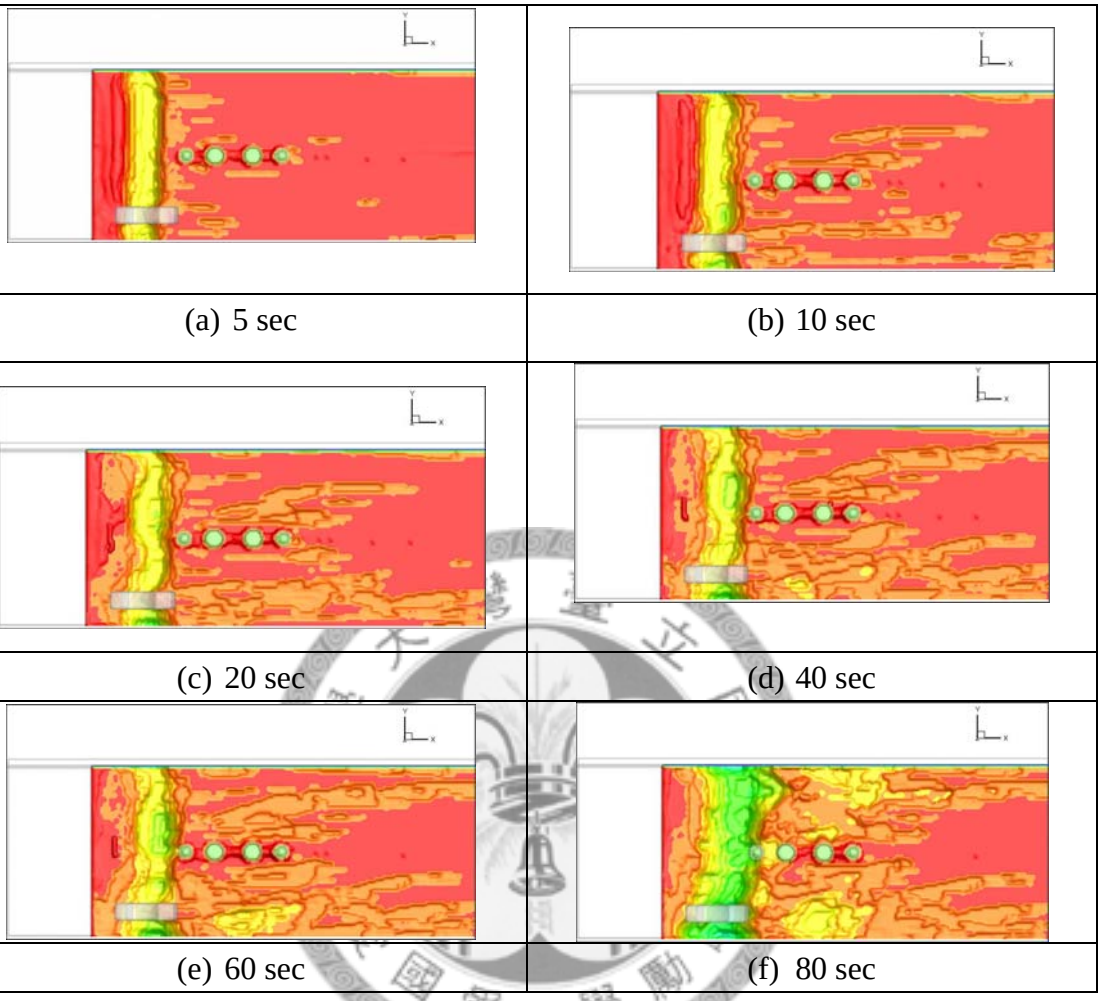

Figure 4.13 Numerical results for mobile bed with ultrasound device (a) 5sec (b) 10sec (c) 20sec (d) 40sec (e) 60sec (f) 80sec

The process of sediment scour is exhibited in Figure 4.13 and then we will discuss the x-velocity, z-velocity in our numerical results. The x-velocity and the z-velocity fields are shown in Figure 4.14 and Figure 4.15, respectively. It can be seen that the x-velocity is influenced by the ultrasound device obviously because the x-velocity has the different values on the both sides of bridge piers. The higher value is centralized on the region of the black line in light of the flow direction which is changed by the ultrasound device. The sediment particles are easily entrained when the maximum x-velocity occurrs in this place. For the z-velocity, the velocity filed is not like the x-velocity which is turbulent in any stage. On the contrary, it is symmetrical at 5sec (see Figure 4.15(a)) but the minimum velocity occurred near the ultrasound device in 10 sec. Because the shape of the ultrasound device, the z-velocity is increased (see Figure 4.15). In addition, we also can find out the contraction scour among the wall of channel and the sensor. Because the sensor is close to the wall, the flow velocity increases due to the contraction scour effect. Hence the scour hole around the ultrasound device is attributed to the combined effects of the contraction scour and the shape of the ultrasound device (see Figure 4.16).

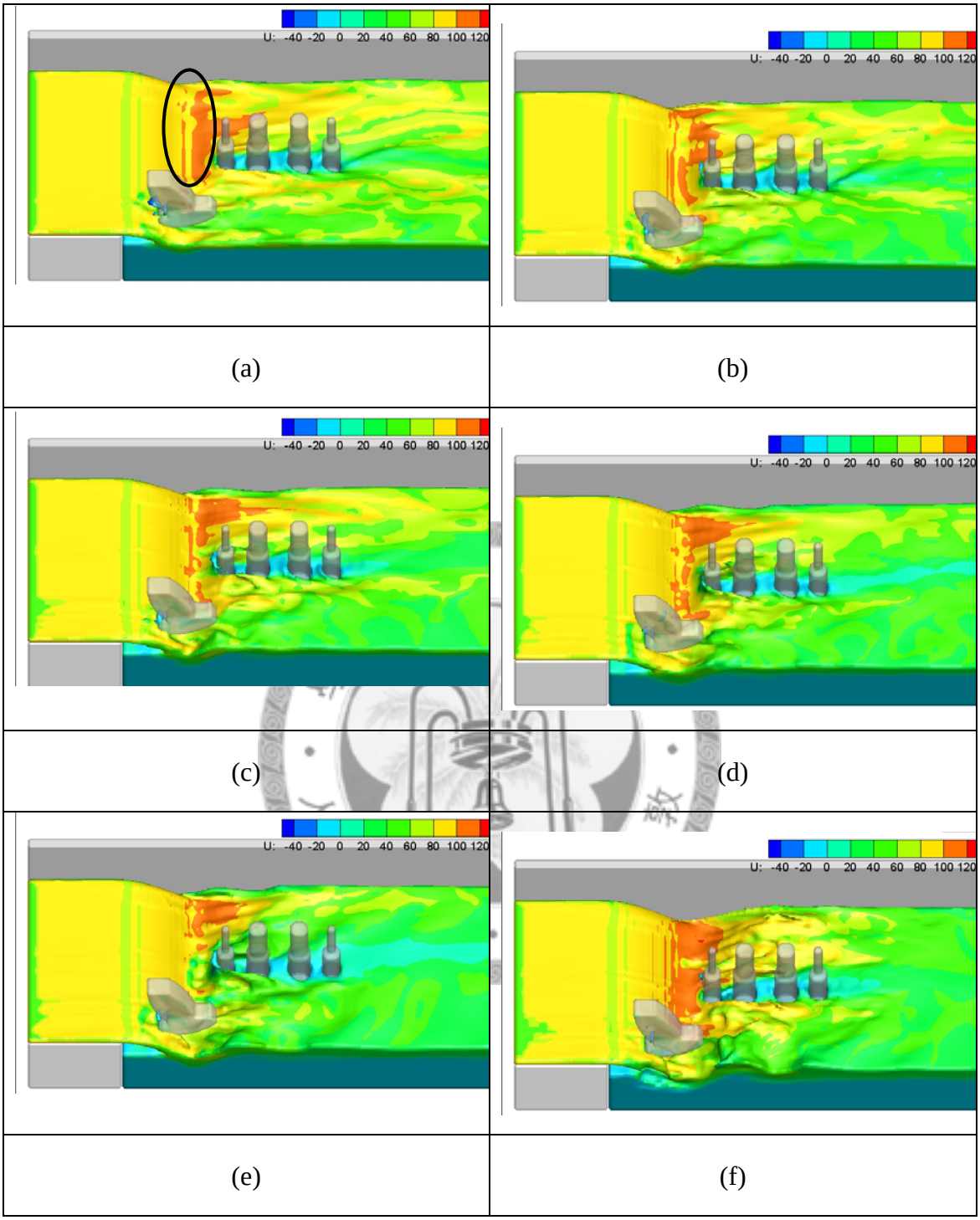

Figure 4.14 The x-velocity field for mobile bed with ultrasound device (a) 5 sec (b) 10sec (c) 20sec (d) 40sec (e) 60sec (f) 80sec

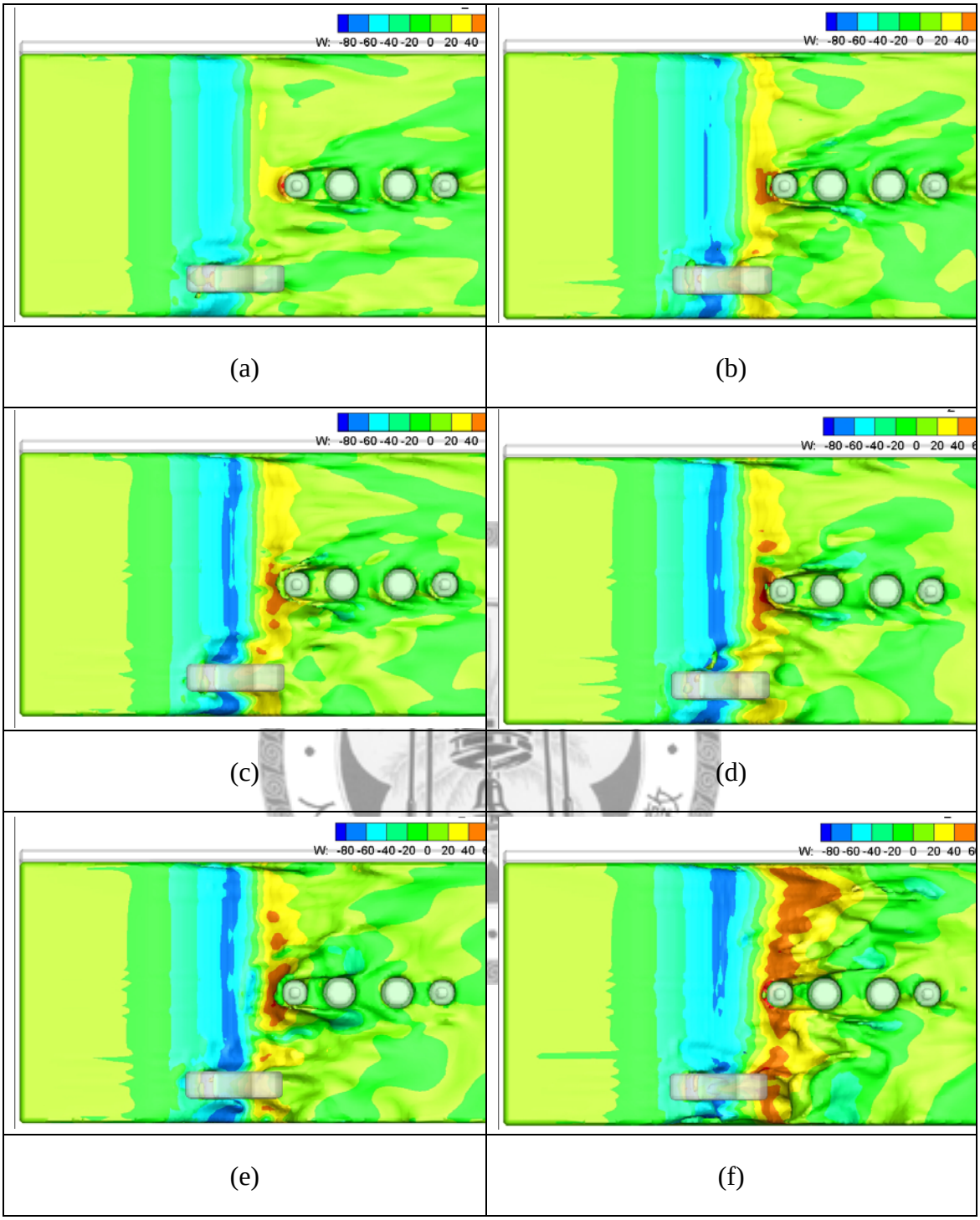

Figure 4.15 The z-velocity field for mobile bed with ultrasound device (a) 5 sec (b) 10sec (c) 20sec (d) 40sec (e) 60sec (f) 80sec

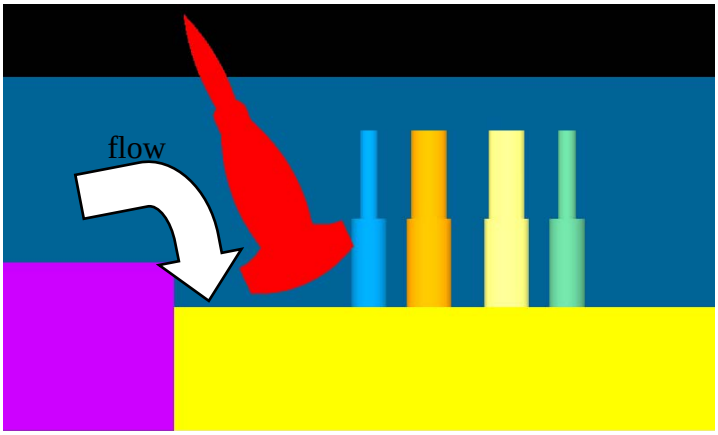

Figure 4.16 The flow condition is influenced by the ultrasound device

In order to distinguish level of the scour process with the different cross-sections, three cross-sections are defined in Figure 4.17. In the beginning (see Figure 4.18(a)), all the scour elevations are very similarly however the cross-section of y= 15 is scoured deeply more than the cross-section of y=5 in Figure 4.18(b). Hence it illustrates that the flow filed is influenced due to the bridge piers and the ultrasound device. The sensor has brought about the variation of x-velocity and the x-velocity increases light of the reason which can be observed in Figure 4.16. At the same time, the particles are easily entrained due to this reason. In addition, the scour elevations are changed rapidly after 5sec and the strong z-vorticities are around the bridge piers (see Figure 4.6(b)). Finally we have mentioned in rigid bed simualtion, there are obvious z-vorticities around the bridge piers. As seen in Figure 4.18 (a) and (b), the sediment is certainly deposited among the bridge piers. The result coincides with the discussion in the rigid bed case.

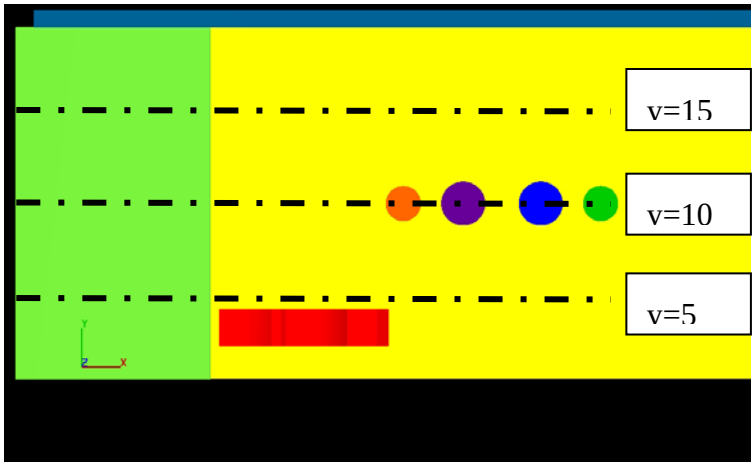

Figure 4.17 The three different cross-sections in mobile bed simulation

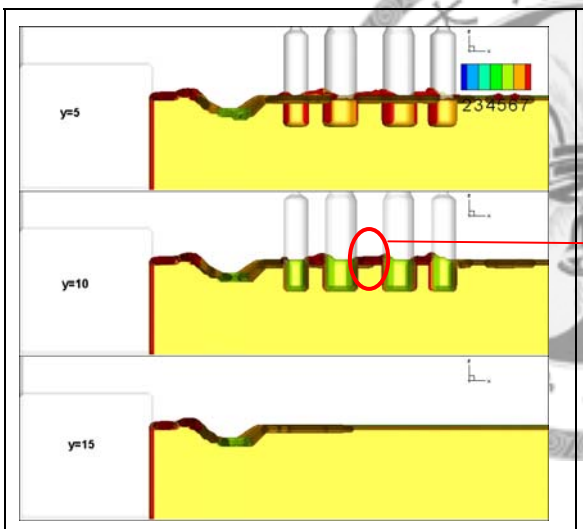

(a)

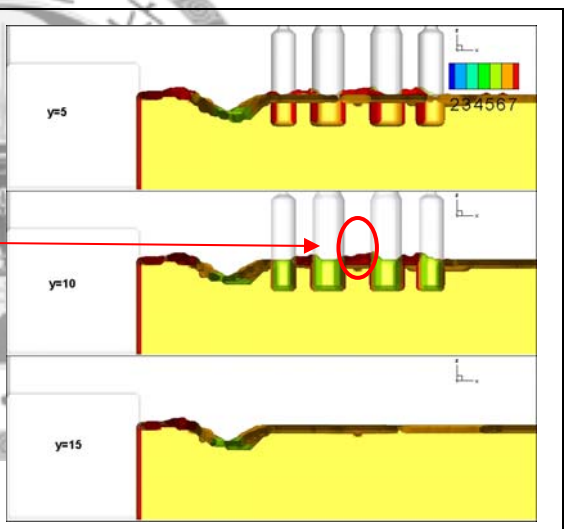

(b)

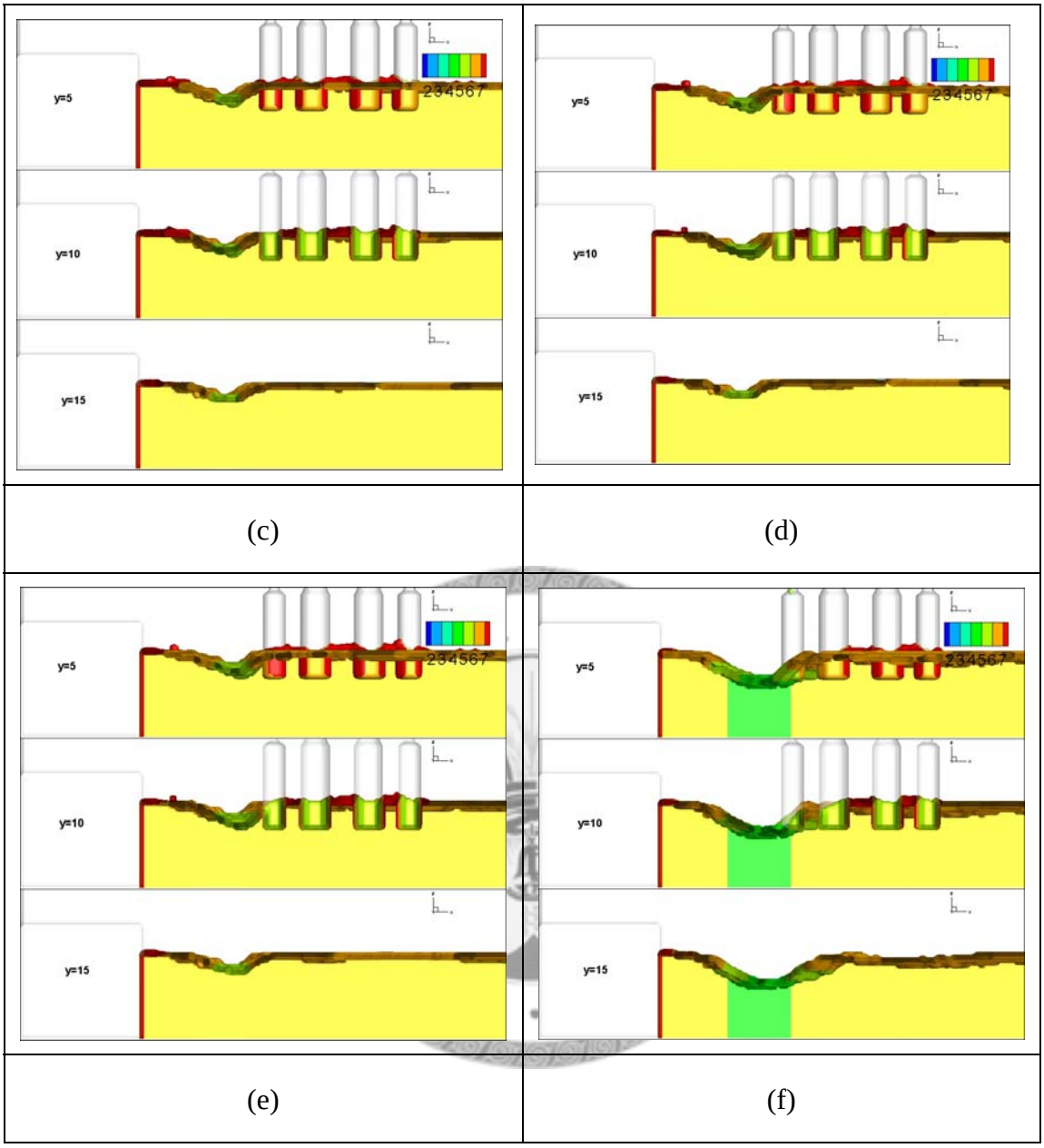

Figure 4.18 The scour elevation in three different cross-sections (a) 5sec (b) 10sec (c) 20sec (d) 40sec (e) 60sec (f) 80sec

4.4 Mobile bed case

In chapter 3.4.3, we know that the sensor would interfere with the flow field. In order to prevent this stuff to affect our result, then we remove the ultrasound device. This is the advantage for numerical experiments, namely we can change any condition quickly and we do not need any tools to measure the experimental data. After we remove the sensor, we can observe clearly the variation of sediment scouring.

For the mobile-bed study, we preserve all the conditions that utilized in the rigid-bed case. This step was primarily to test numerical modeling approaches, and laboratory experiments with small-scale models will be performed. We envision setting up experimental analogues of bedrock-alluvial transitions and local bridge scour configurations, and acquiring measurements using the ultrasound device. For illustration, we present below some results from preliminary experiments and Flow-3D modeling designed to simulate the Hou-Feng Bridge collapse. Figure 4.19 shows the distribution of the mobile-bed and the color contour presented the packed sediment height. From these results, the model shows that the present setting of sediment scour model is quite similar to the small-scale experimental results, and we could obtain some intelligence by means of the sediment erosion in light of abrupt change in the height of the

mobile-bed simulation.

Although we do not have the accurate experimental results, the sediment elevation is still measured by means of the photographs. Figure 4.20 shows the sediment elevations. The black line is the numerical results and the symbol of the circle stands for the experimental results. As can be seen, the numerical results decrease as time went on and this phenomenon has the tendency toward the experimental results. The sediment elevations approach the equilibrium scour depth quickly during our simulation time. When we compare the numerical results to the experimental results, the sediment elevations of numerical simulation are less than 2 cm. We think the errors of numerical results are acceptable.

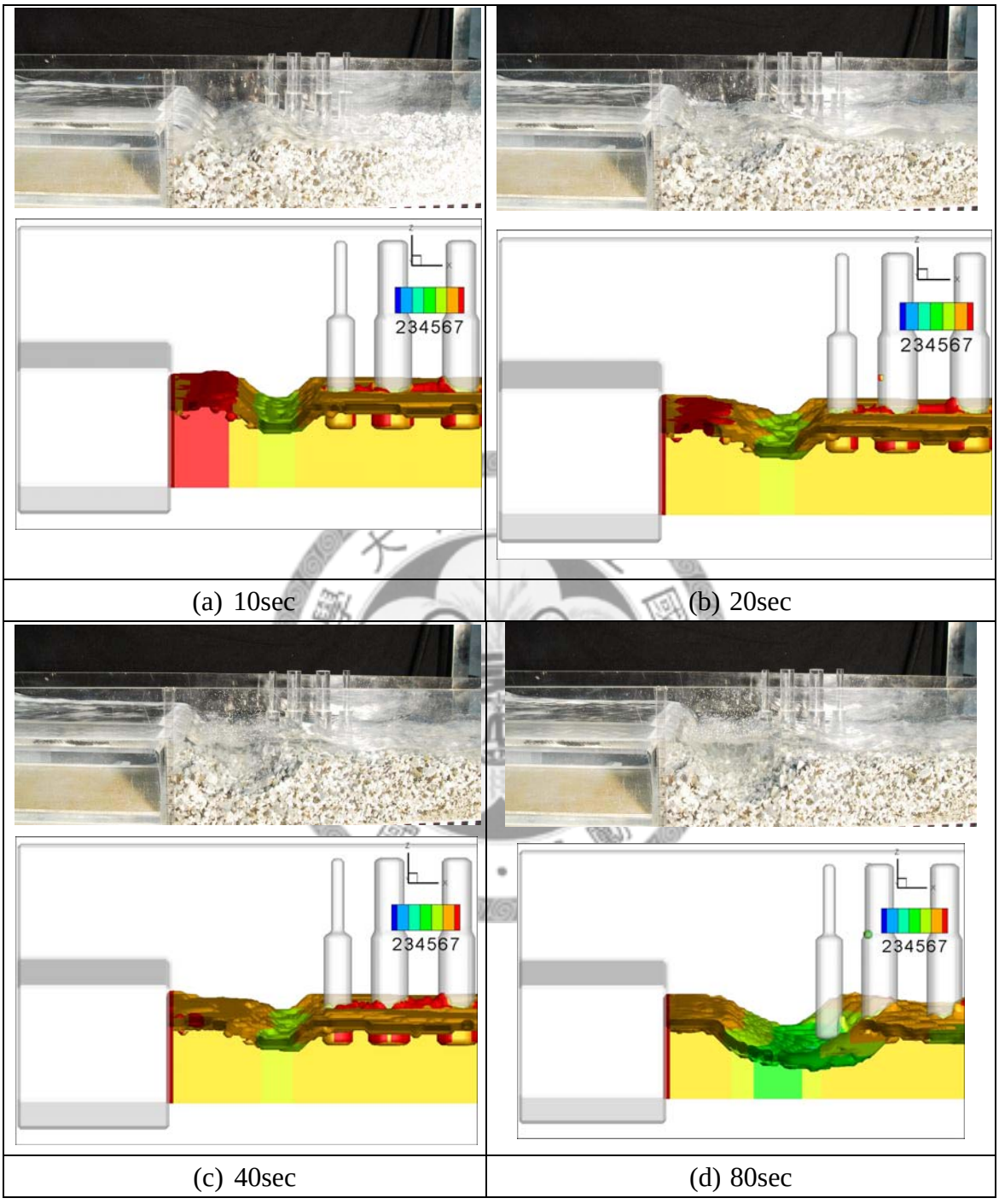

(a) 10sec (b) 20sec

(c) 40sec (d) 80sec

Figure 4.19 Views of a preliminary small-scale experiment and Flow-3D modeling performed to simulate the conditions of the Hou-Feng Bridge collapse. (a)10 sec.; (b)20 sec.; (c)40 sec.; (d)80 sec. (top: experiment; bottom: numerical simulation)

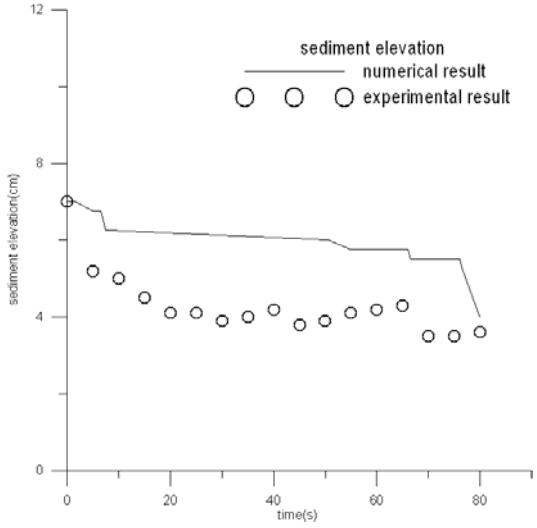

Figure 4.20 The sediment elevation (x=10cm, y=0cm) for the time history

Figure 4.21 illustrates the x-velovity in the mobile bed simulation. The velocities are very symmetric for the mobile bed case. From the Figure 4.21, the angle of attack protects the piers (except for the first one) obviously and the x-velocity in this area is less than 60 cm/s.

Some people have the query about the event of Hou-Feng Bridge and in their opinion, the bridge collapse in light of the structure failure. The phenomenon can be also observed in our numerical simulations (see Figure 4.22). Figure 4.22 shows that the strong current flow along the scour hole and ram into the first piers. The x-velocity is exhibited in Figure 4.23 and it shows the velocities in front of the first pier. The y-axis is x-velocity and x-axis is the time. Three curves present the different location of z-direction. The z=7.5(black line), 8.5(red line) and 9.5(blue line) are chosen and the

cross-section is defined at x=10cm (y=10cm). As seen, the first pier is truly sustained the high velocities and the maximum velocity is occurred at the bottom of the first pier. The velocities are about 60 cm/s and it is the largest in all the numerical results.

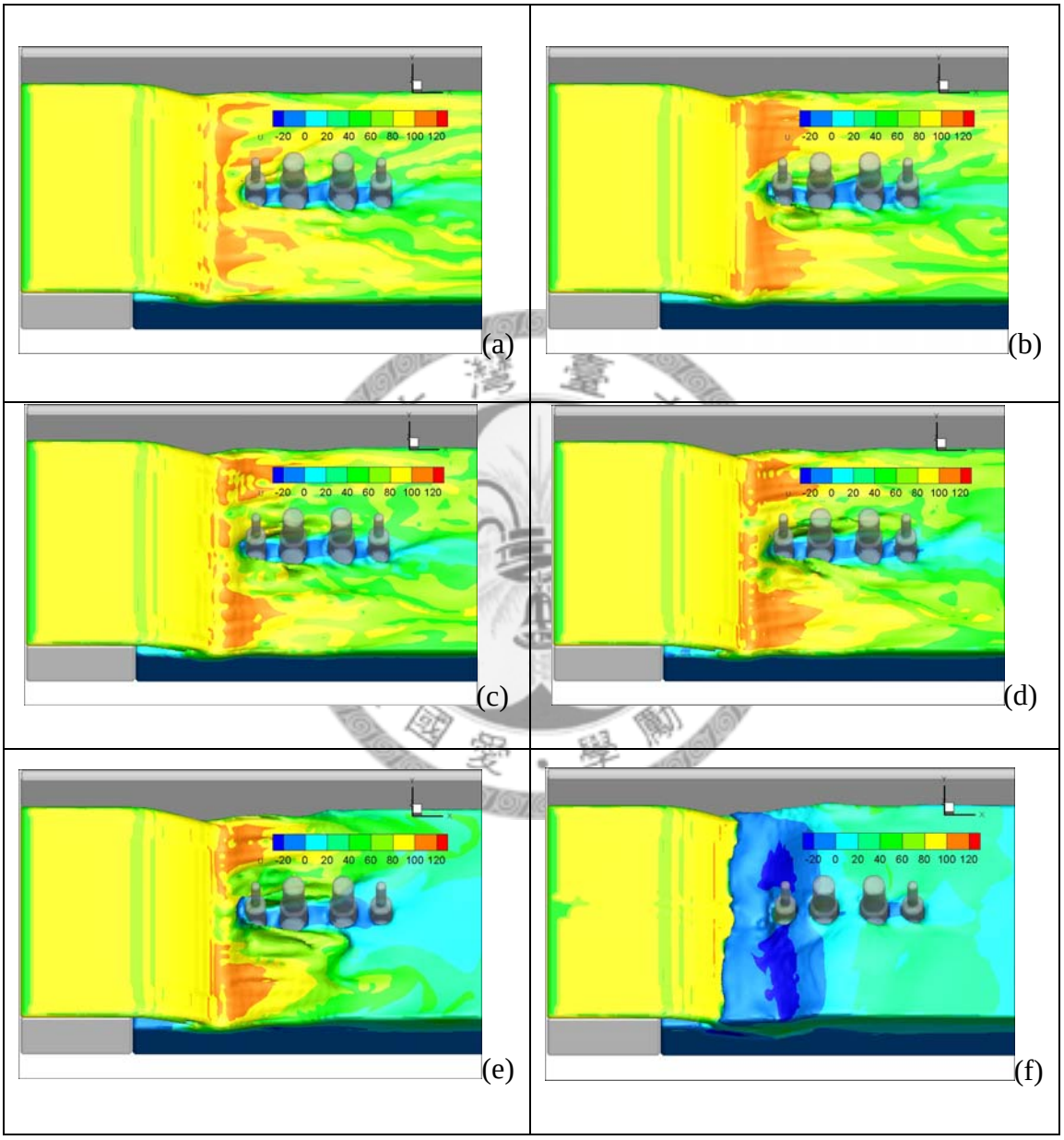

Figure 4.21 The x-velocity field for mobile bed (a) 5 sec (b) 10sec (c) 20sec (d) 40sec (e) 60sec (f) 80sec

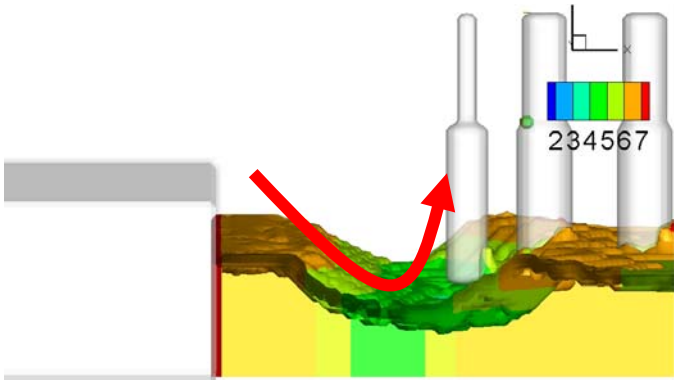

Figure 4.22 The strong current flow along the scour hole and ram in to the first pier

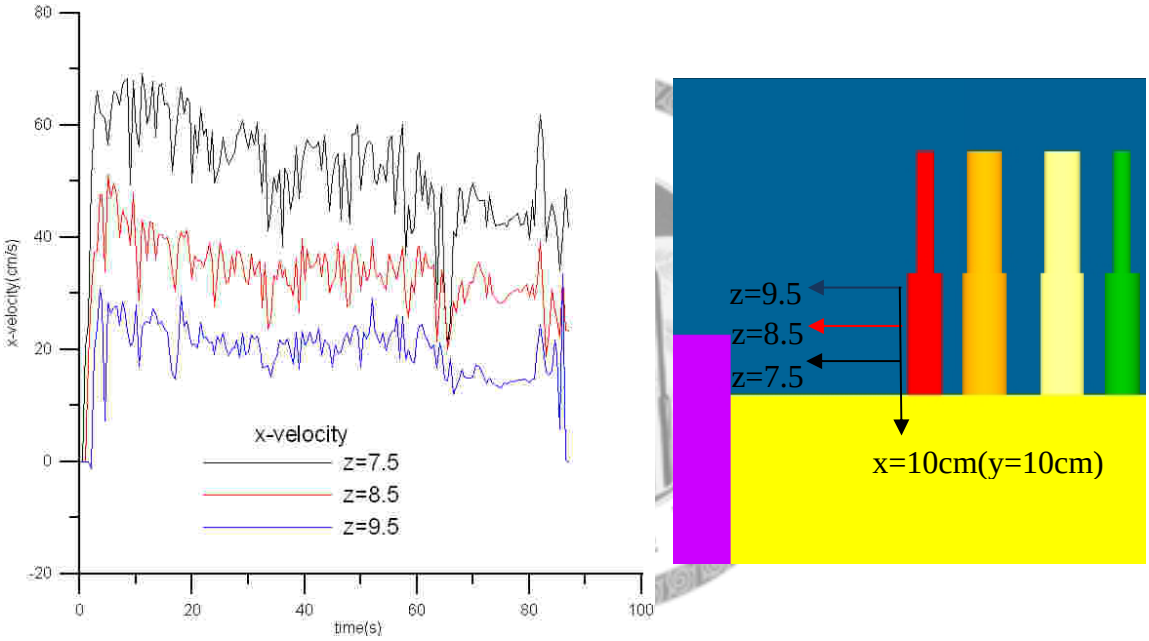

Figure 4.23 The x-velocity in front of the first pier

We already study the influence of the x-velocity in mobile bed simulation. Now we want to know that the relation between the Froude number and the z-velocity. First of all, we have to set the cross-section for discussing as exhibited in Figure 4.24. The results are shown in Figure 4.25 and Figure 4.26, respectively. In the left hand side, the

y-axis and the x-axis are the Froude number and the time. In the right hand side, the y-axis and the x-axis are the z-velocity and the time. In Figure 4.25, it is apparent that the z-velocity is influenced by the Froude number when z is equal to 7 cm and 8 cm. The z-velocity increase like the Froude number does in the initial scour process. The higher location of z-axis, however, does not have the similar trend. In addition, the positive z-velocity does not occurred in the higher location of z-axis (see Figure 4.25(c) (d)). By contrast, the z-velocity has the high relation toward the Froude number when x is located on the upstream of the bridge pier. The results are shown in Figure 4.26. As can be seen, all the z-velocity curves are similar to the Froude number except for the location of z-axis equals to 10 cm. When z-axis exceeds 10 cm all the curve of Froude number has the rapid variation after 60 sec and we can find the similar situation in the curve of z-velocity.

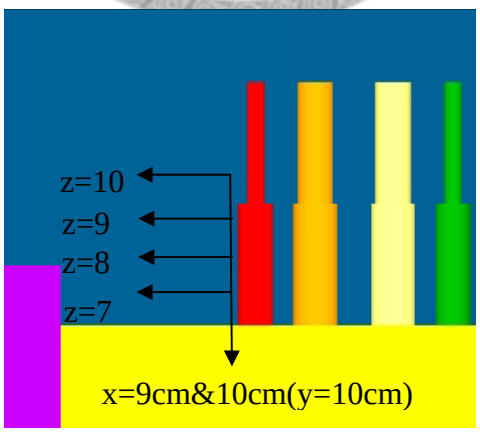

Figure 4.24 Schematic diagram we defined in the numerical simulation

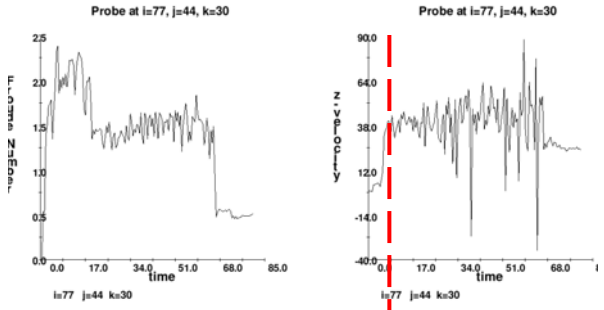

(a)

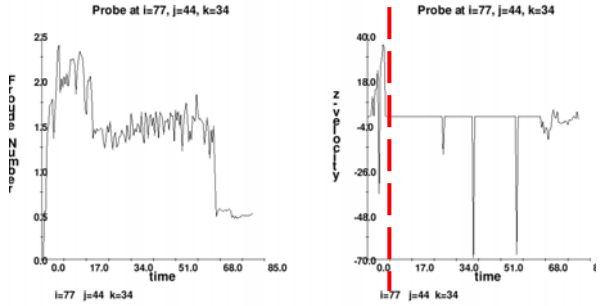

(b)

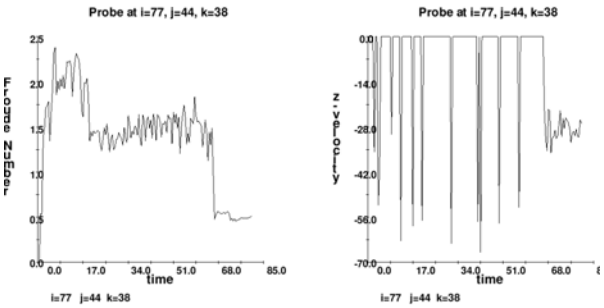

(c)

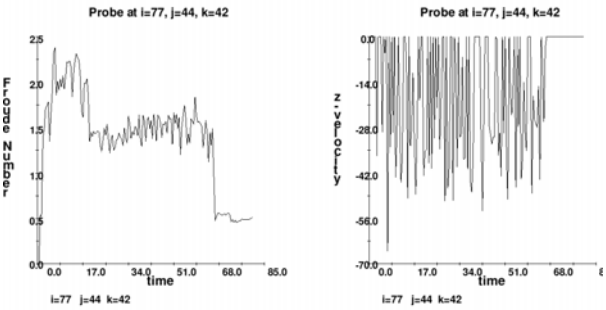

(d)

Figure 4.25 The Froude number and the z-velocity in mobile bed simulation (a) x=9, y=10, z=7 (b) x=9, y=10, z=8 (c) x=9, y=10, z=9 (d) x=9, y=10, z=10

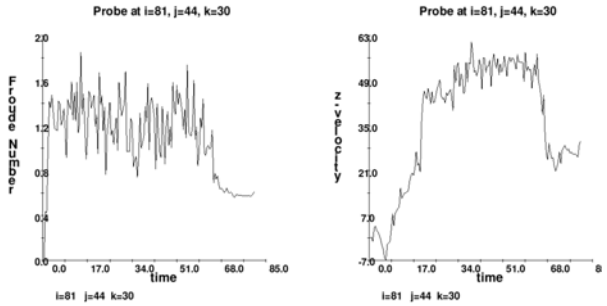

(a)

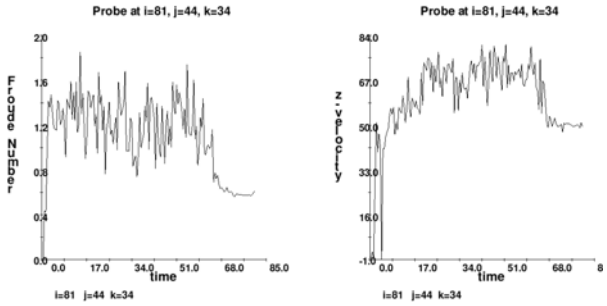

(b)

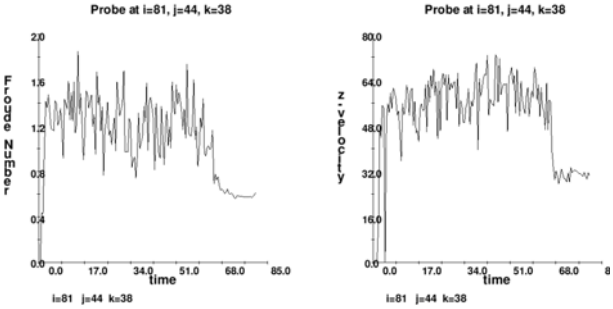

(c)

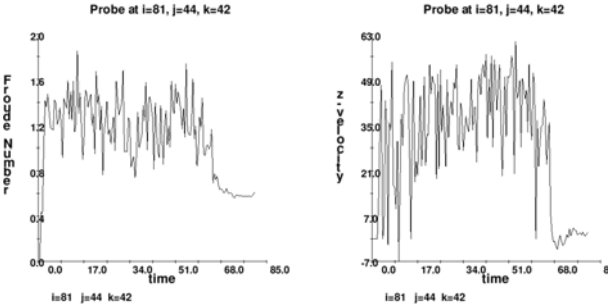

(d)

Figure 4.26 The Froude number and the z-velocity in mobile bed simulation (a) x=10, y=10, z=7 (b) x=10, y=10, z=8 (c) x=10, y=10, z=9 (d) x=10, y=10, z=10

After we realize how the velocities work on the mobile bed simulation, we continue to discuss the path of streamline. First of all, we put 12 points in front of the first pier and the location is shown in Table 4.2. Therefore, the path of the flow around the first pier can be observed by means of the numerical simulation. Figure 4.27 shows a sequence of pictures, illustrating the time evolution of the streamline obtained in the present numerical simulation. The streamlines move along the arc of scour hole and then ram into the bridge pier. Besides, they are separated averagely when they ram into the pier before 80sec and the positive z-velocity does not exist in Figure 4.25 (c) and (d) which can be illustrated here. In Figure 4.27 (b), when the streamlines hit the bridge pier, they rebound about 1 cm from the bridge pier. Hence the z-velocitiy is always negative due to this reason.

In Figure 4.27 (f), the scour hole is apparently conspicuous and the streamlines is difficult to depart from the scour hole in this stage. It illustrates that the flow is going to be trapped in the scour hole in the whole scour process. The scour hole becomes intensive gradually due to the strong vortex effect where the vortices act like ‘cyclones’ or ‘tornadoes’ to pick up the sediment from the surface of the river bed and transport it in the downstream direction. The y-vorticity is exhibited in Figure 4.28 and the high y-vortocity is measured on the upstream of the scour hole (see the red color). In addition,

the same phenomenon can be observed in the laboratory experiments which are shown in Figure 4.29.

Table 4.2 The location points of streamline setting

point number	x	y	z
1	x=9.8cm	y=9.5cm	z=7.5cm
2			z=8cm
3			z=8.5cm
4			z=9cm
5		y=10cm	z=7.5cm
6			z=8cm
7			z=8.5cm
8			z=9cm
9		y=10.5cm	z=7.5cm
10			z=8cm
11			z=8.5cm
12			z=9cm

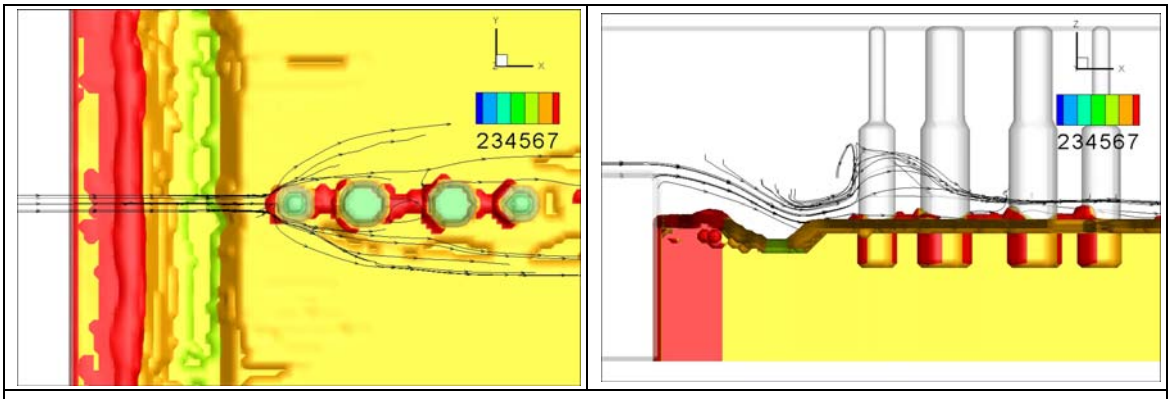

(a) 5 sec

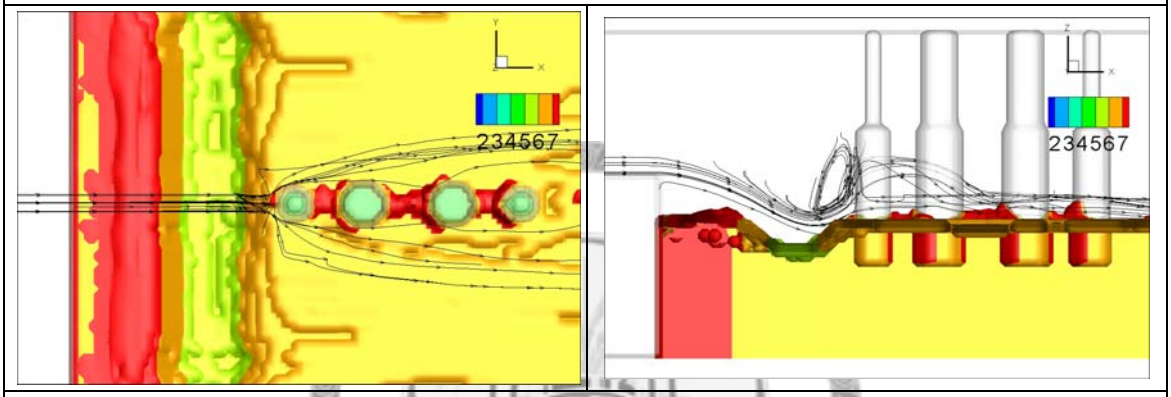

(b) 10 sec

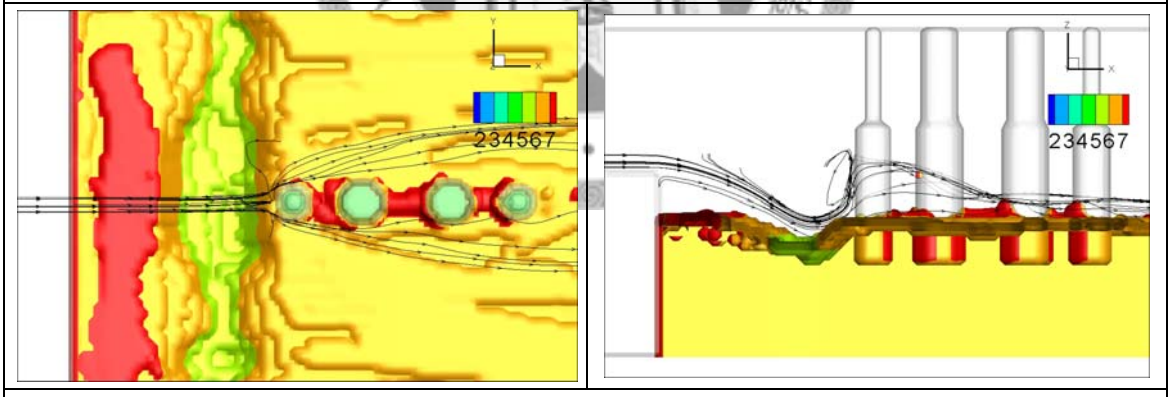

(c) 20 sec

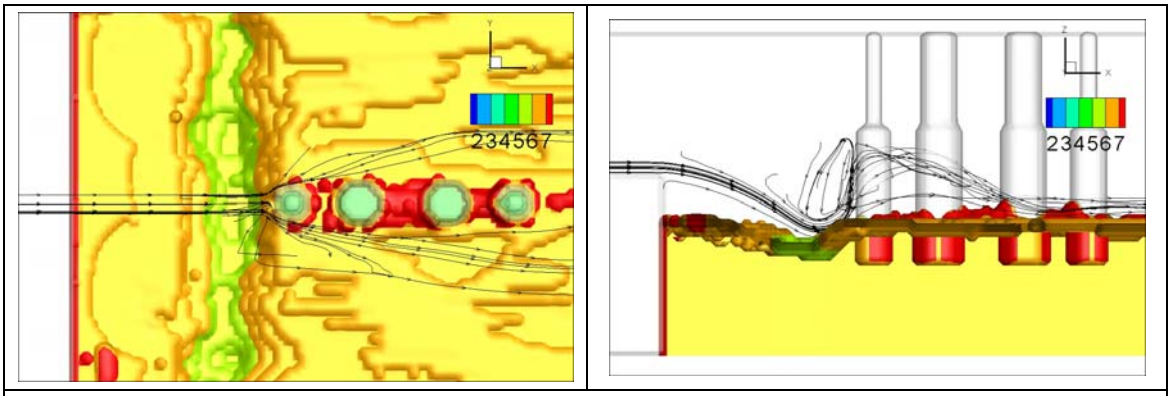

(d) 40 sec

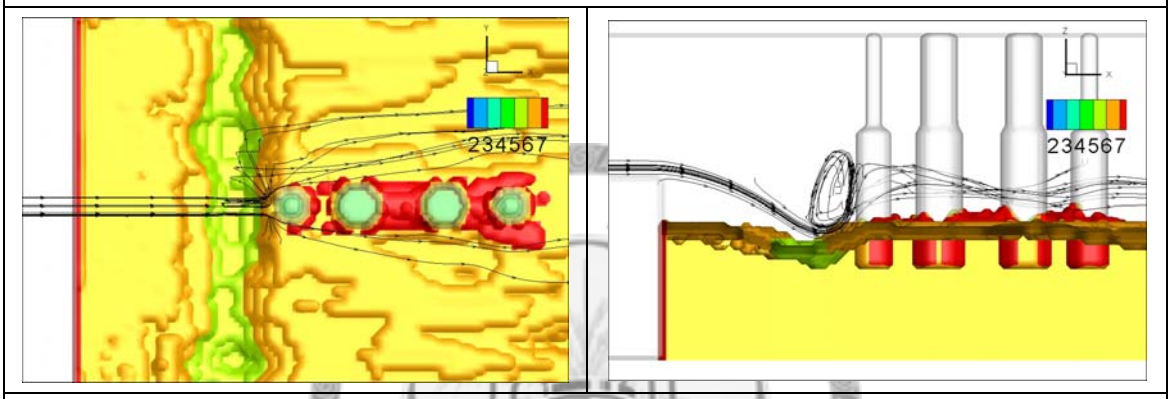

(e) 40 sec

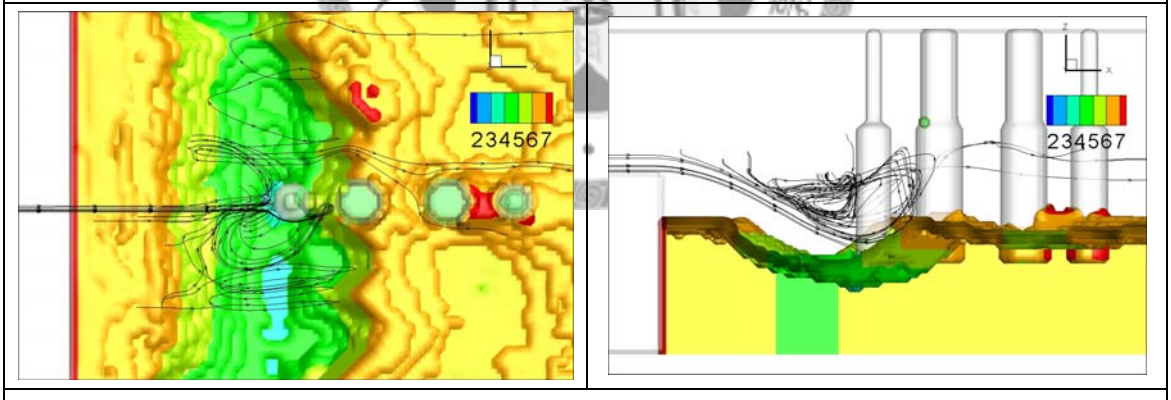

(f) 80 sec

Figure 4.27 The streamline of mobile bed simulation (a) 5 sec (b) 10sec (c) 20sec (d) 40sec (e) 60sec (f) 80sec

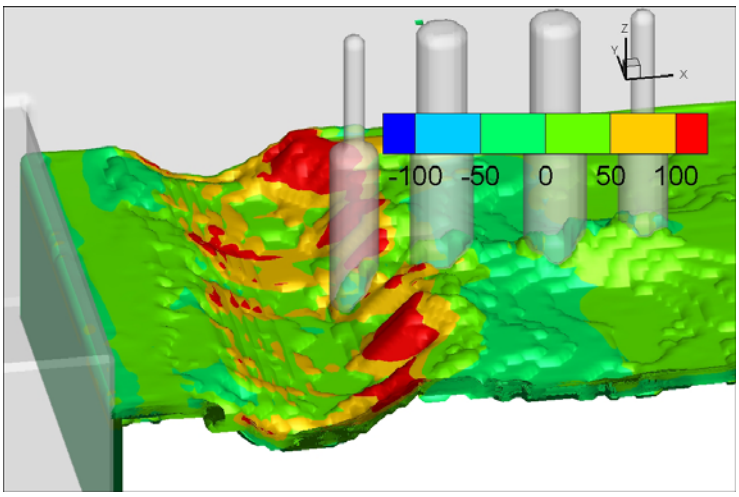

Figure 4.28 The y-vorticity of numerical simulation at 80 sec

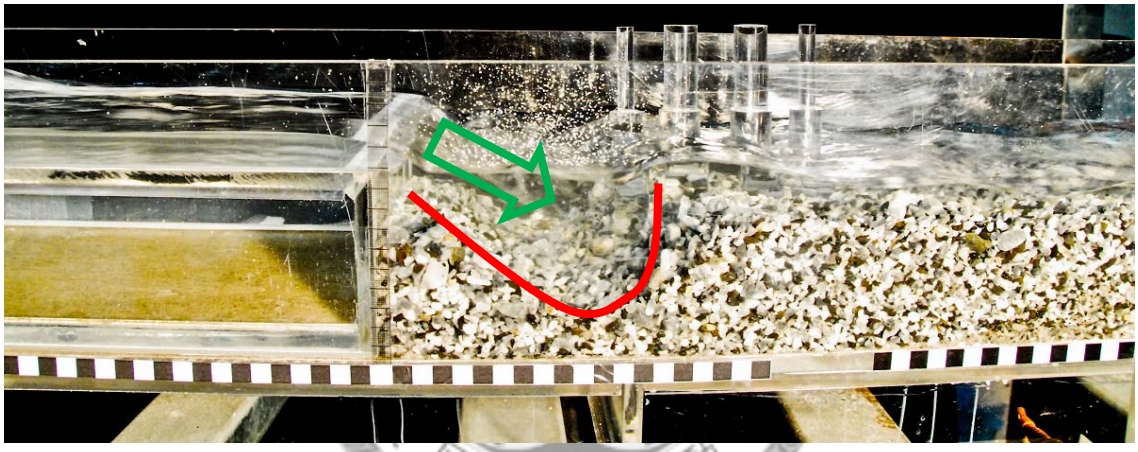

Figure 4.29 The laboratory experiment for mobile bed case (photoed by H.N. Hsieh)

4.5 Remove the first river bed in mobile bed case

About the final numerical experiment, the first river bed is removed in this simulation and it has been mentioned in chapter 3.4. We have two reasons regarding this numerical simulation. First, we try to realize the influence for overfall flow effect because there are some doubts that the bridge collapse is attributed to the overfall flow

effect. Second, the problems become easier because the overfall flow is not considered in this simulation. Hence the flow conditions are not turbulent as it is observed from the numerical simulation in chapter 4.4.

First of all, Figure 4.30 exhibited the time evolution of the scour processes in the numerical simulation and the color bar stands for the sediment elevation. As will be seen, the sediment scour is not very violent as the mobile bed simulation does which has the overfall flow effect. The sediment in front of the first pier is not scoured so quickly as the mobile bed simulation and the sediment is also deposited among the bridge piers. Besides, the consequence of this numerical simulation coincides with the laboratory experiments in terms of the scour shape. As we mentioned in chapter 2.2.2, the bridge local scour can be divided into four parts; namely, the surface roller, the down flow, the horseshoe vortex and the wake vortex. The scour hole around the bridge pier is attributed to these factors. In this stage, the same phenomenon is successful in simulation and one of the results is shown in Figure 4.30 (d). The red line indicates the scour hole around the bridge pier.

Although there are four factors in the local bridge scour, the down flow and the horseshoe vortex are the principle reasons regarding the scour hole generation, especially the down flow. Furthermore the horseshoe vortex is caused due to the down

flow. Hence we focus on the variation of the z-velovity around the bridge pier due to this reason. The z-velocity is exhibited in Figure 4.31 and we can find out two phenomena in the Figures. They are bow wave and down flow respectively. The bow wave is shown in Figure 4.31 (a) (see the red line) and the bow wave means that the fluid depth increases rapidly in front of the bridge pier. On the other hand, the down flow effect is observed in Figure 4.31 (b) (c) (see black line). The negative z-velocity increases under the scour process until it attains the critical velocity.

In order to discuss the z-velocity more carefully, three cross-sections are defined in Figure 4.32. The locations of three cross-sections are x=10 cm, x=10.5 cm and x=11cm, respectively. In Figure 4.33, we can observe that the z-velocity is separated into two parts and the positive part is due to the surface roller effect. At the same time, the minimum of z-velocity occurred near the upstream of the first bridge pier. The same situation can also be observed in Figure 4.34. Hence the horseshoe vortex is generated due to the down flow which cooperates with the current flow. The final scour hole is show in Figure 4.30. The down flow effect is not very obvious when x= 11 cm and the results are shown in Figure 4.31. Nevertheless, we still can observe that the vectors of the z-velocities are toward to the river bed.

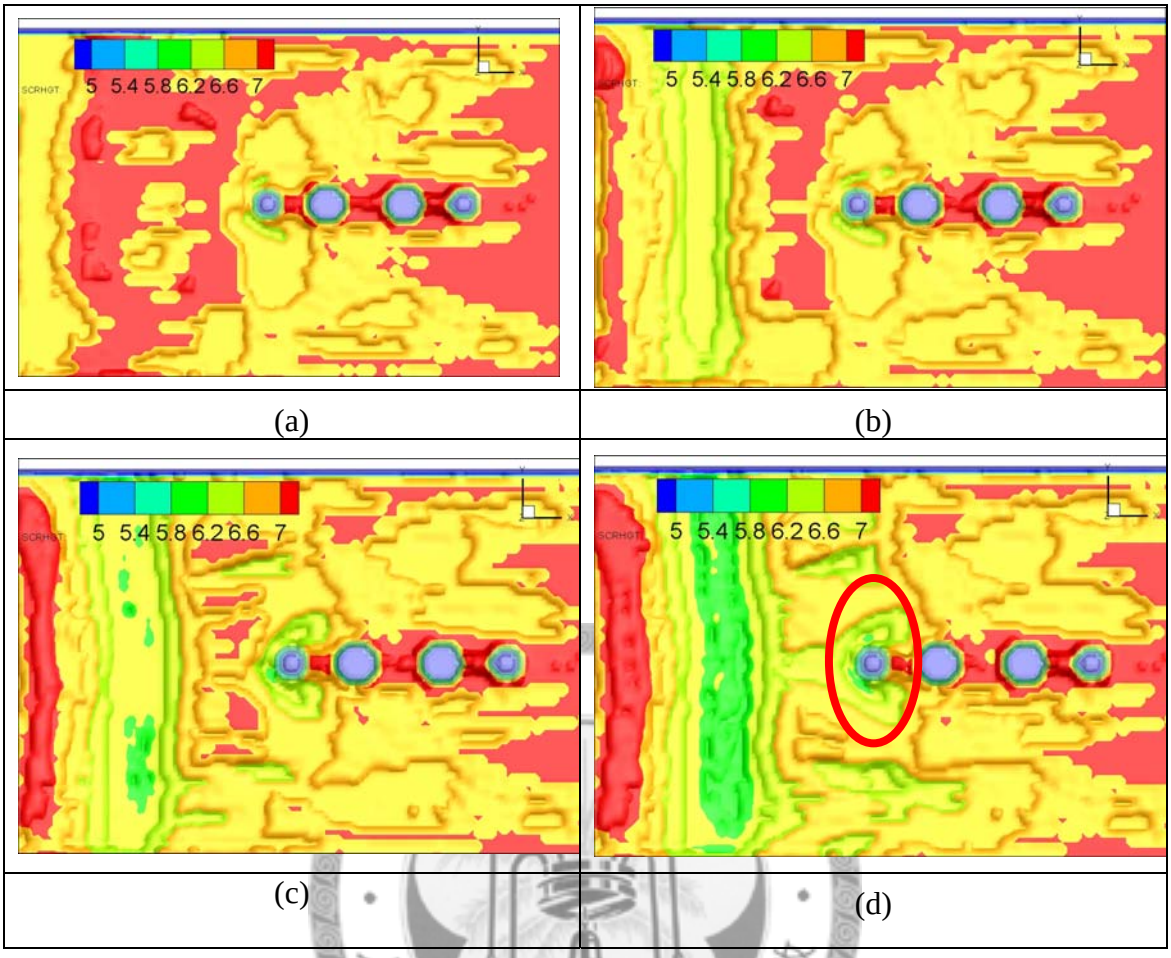

Figure 4.30 The scour process about mobile bed simulation and the first river bed is removed (a) 10 sec (b) 20 sec (c) 40sec (d) 60sec

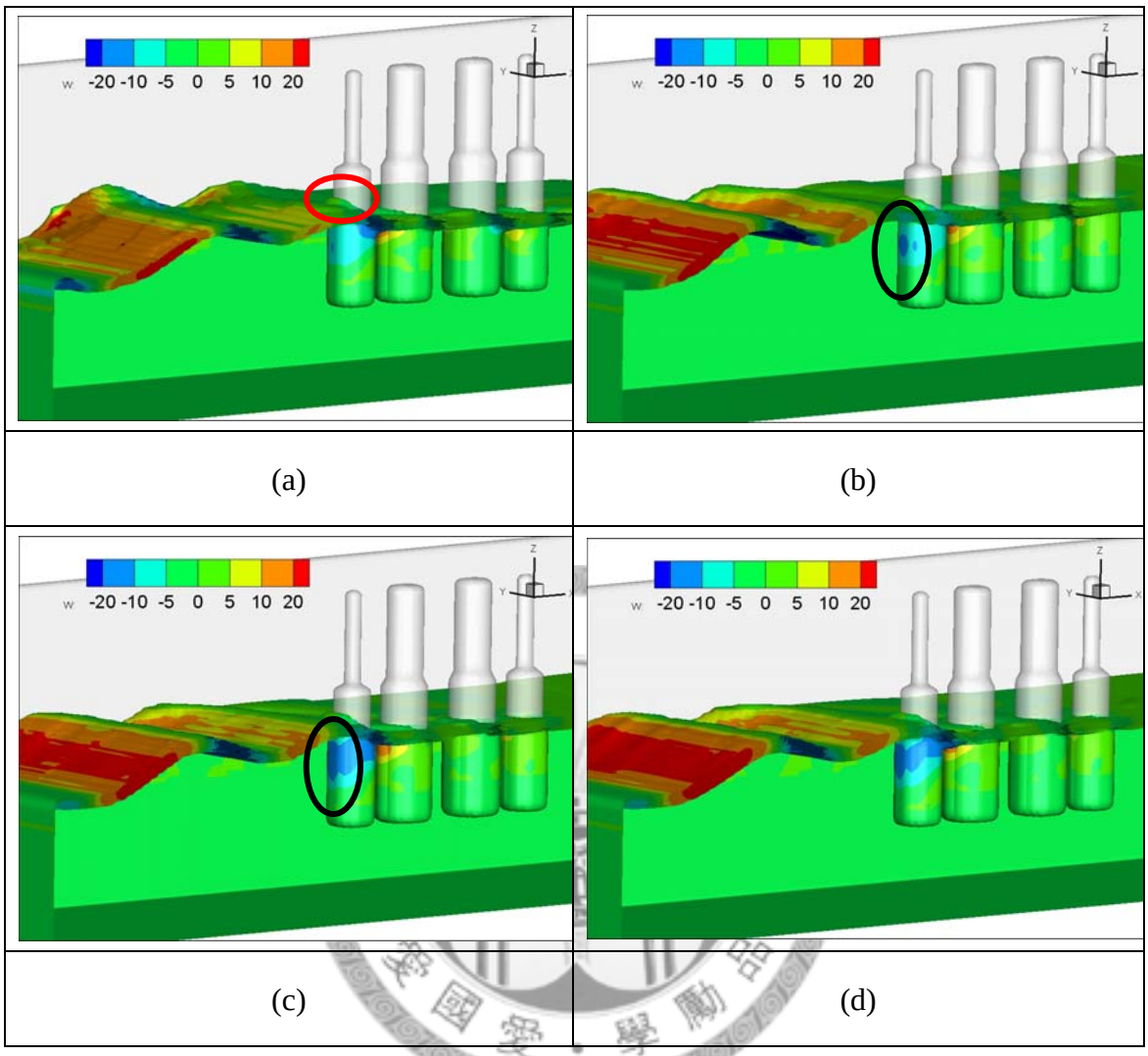

Figure 4.31 The z-velocity in the numerical simulation without the first river bed (a) 10 sec (b) 20 sec (c) 40 sec (d) 60sec

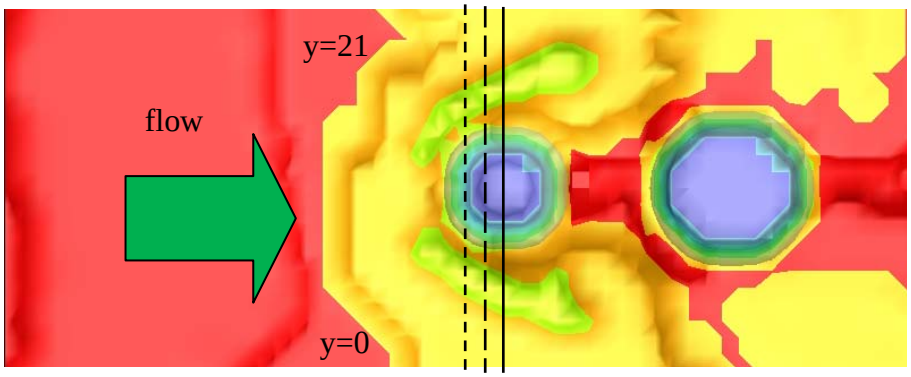

Figure 4.32 Three cross-sections are defined in order to observe the down flow effect

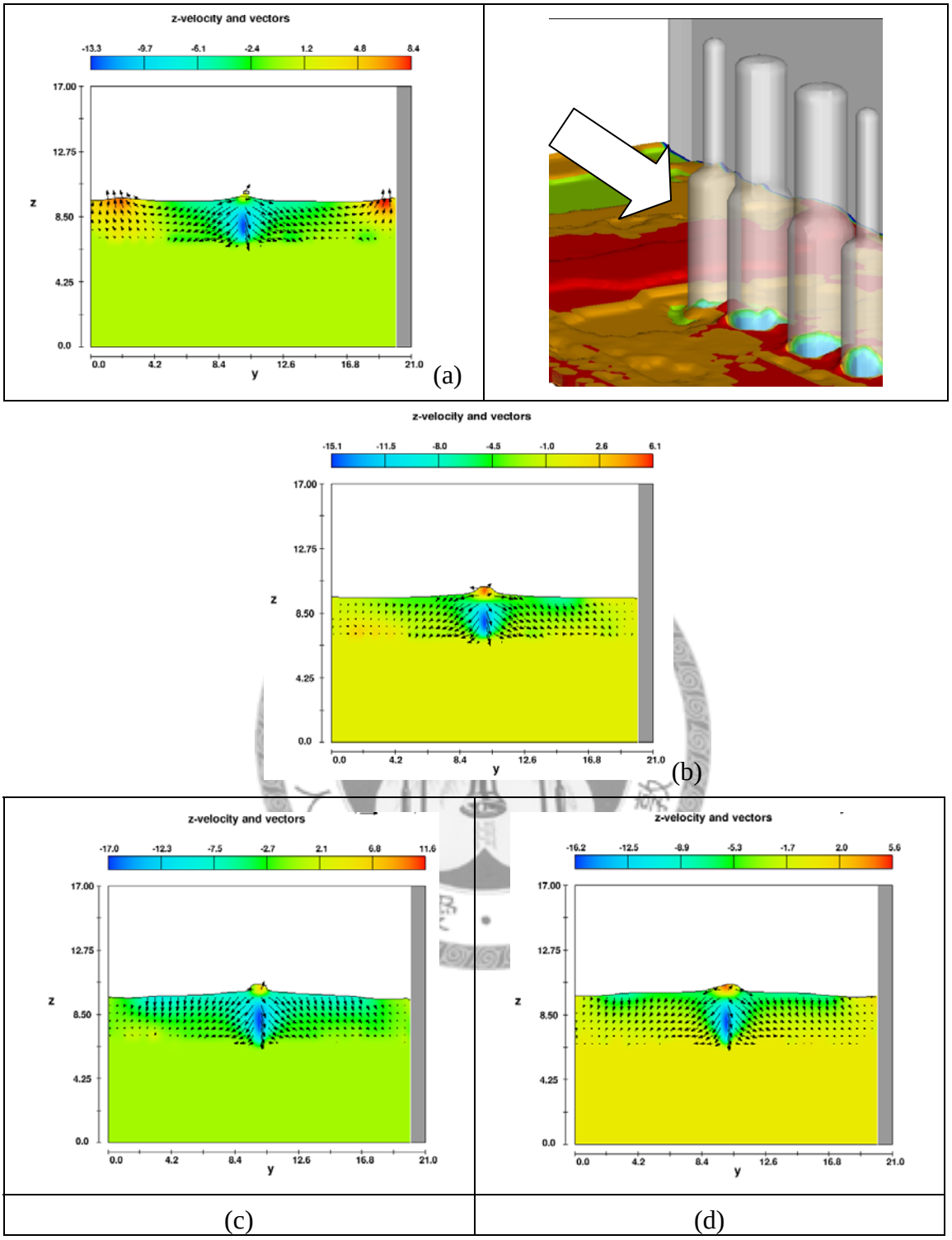

Figure 4.33 The time evolution of z-velocity in front of the bridge pier (x=10 cm) (a) 10sec (b) 20sec (c) 40sec (d) 50sec

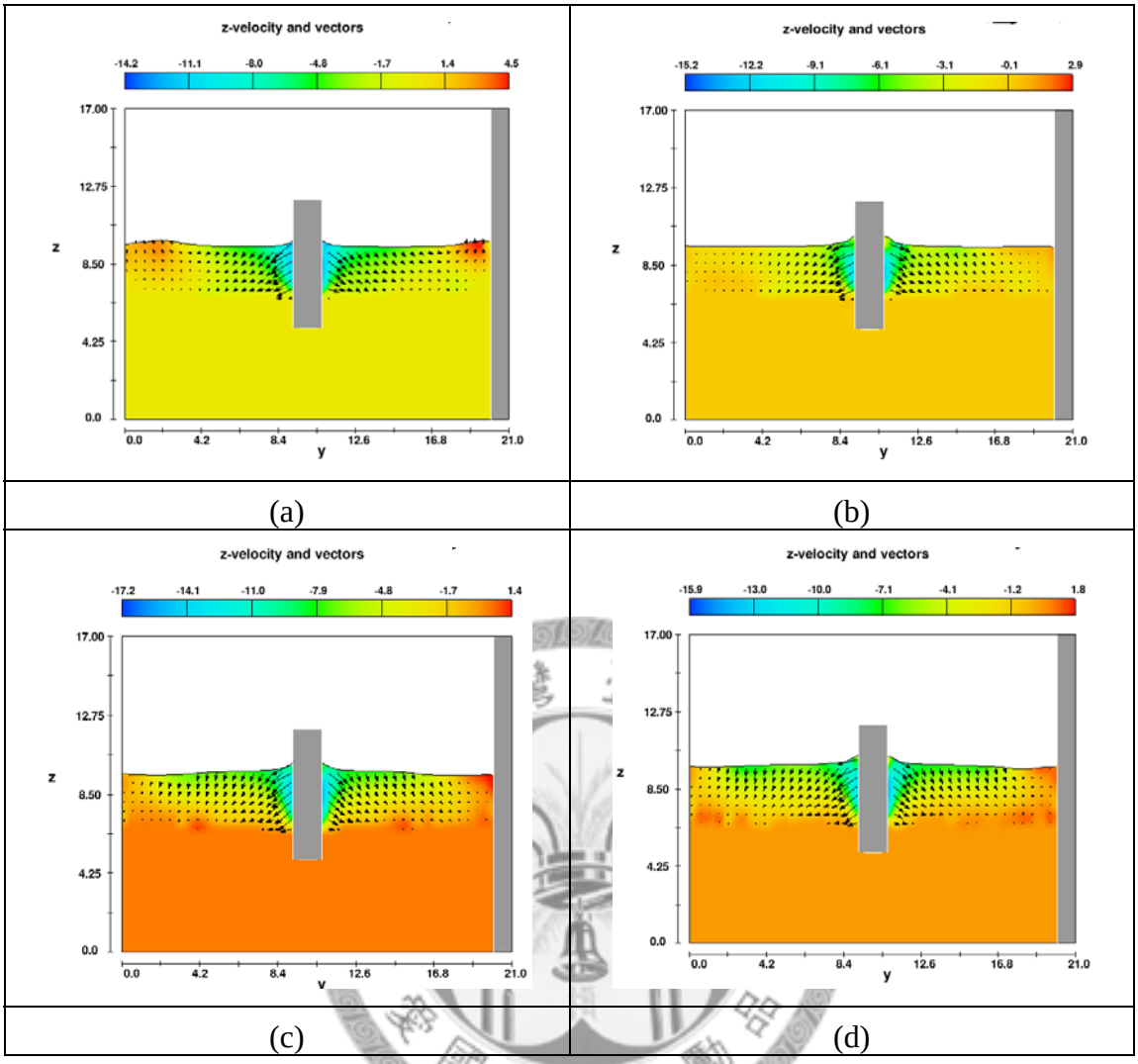

Figure 4.34 The time evolution of z-velocity (x=10.5 cm) (a) 10sec (b) 20sec (c) 40sec (d) 50sec

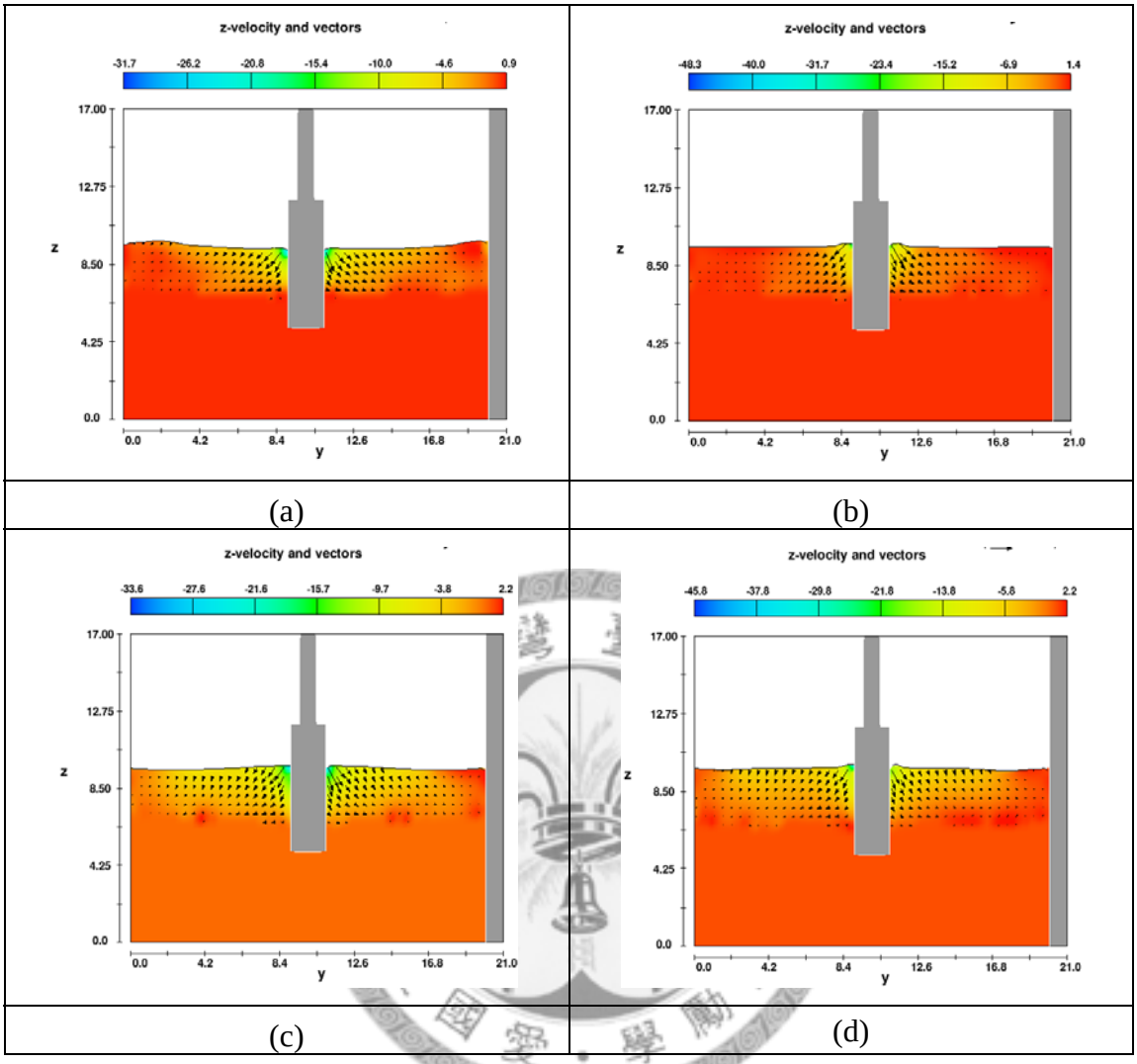

Figure 4.35 Time evolution of z-velocity (x=11 cm) (a)10sec(b)20sec(c)40sec(d)50sec

In the final discussion, we compare the sediment elevation between the mobile bed simulation and mobile bed simulation without drop water. Two positions are chosen in this discussion. Figure 4.36 (a) and (b) are taken at x=10 cm and 9 cm, respectively. The blue line stands for the mobile bed simulation and the red line stands for the numerical simulation without the overfall flow effect. Figure 4.36 (a) illustrates that the sediment elevation of mobile bed simulation which is higher than the same case without overfall

flow. It is because that the scour behavior of mobile bed simulation is mainly located on the place where the water drops. Because this location(x=10) is too close to the first bridge pier, the erosion is not obvious for the mobile bed simulation. On the contrary, the mainly scour area of the mobile bed case without overfall flow is around the bridge pier which is caused by the combined effects of the down flow and the horseshoe vortex. It implies that sediment scour of the overfall flow effect is stronger than the down flow and the horseshoe vortex effect.

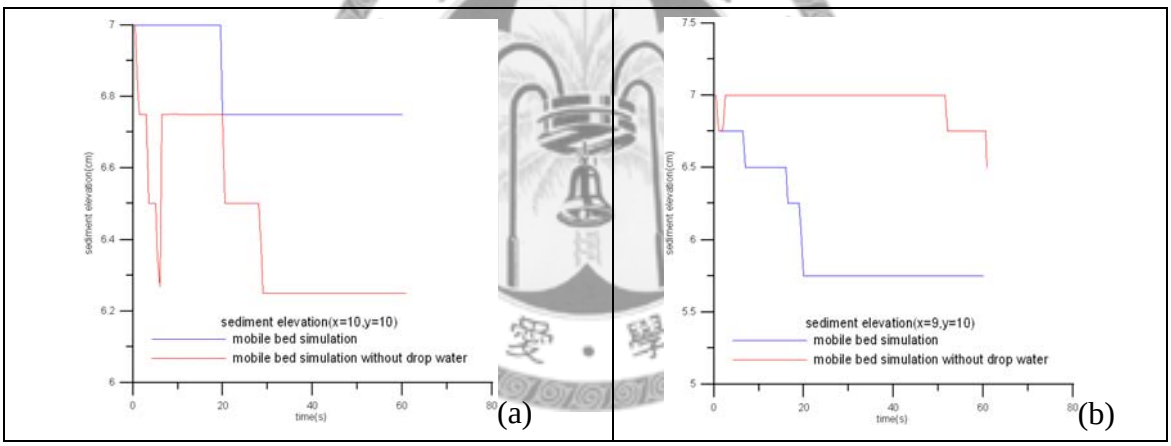

Figure 4.36 The sediment elevation for two different mobile bed simulations (a) x=10 cm (b) x=9 cm

Chapter 5 Experimental setting of gap scour and discussions

5.1 Field site investigation

This study carried out a field investigation at the stepped concrete block grade control structure downstream of Highway No.1 in Ta-Chia River in central Taiwan in November 2009. The Taiwanese Highway Department built this structure in 1999 to restrain general scour or degradation of the riverbed near the bridge. Sediment was then stored upstream of the structure. The width of the structure is 840 m. They constructed the structure using 3-m cubic concrete blocks. The height of the first-row blocks is 5 m. The gap width between the blocks is 50 cm. There are 20 step-drops in the flow direction and the drop height of each step is 50 cm. The constructors connected the blocks by using steel wires. They initially submerged the second 10 steps of the stepped concrete block grade control structure with the original bed material.

Figure 5.1 shows pictures of the stepped concrete block grade control structure. The field investigation showed all steps exposed because of downstream degradation. The major cause of the degradation was the sediment deposition upstream, which raised

the bed elevation upstream. The controller raised the water head, which resulted in high velocity movement downstream. The scour potential also increased on the downstream reach. The study found edge scour at the toe of the structure and a few blocks in the last row tilted or overturned due to extra-added support. Figure 5.1 reveals how the removal of stones in the gaps resulted in the weakening of the lateral supports and tilting of the blocks. The stones in the gaps provided lateral support. The blocks sank due to the excessive gap scour around them. Figure 5.1(a) shows the titling blocks and Figure 5.1(b) provides a closer view of the gap scour. The scour depth in some of these areas was more than 3 m, more than the height of most of the concrete blocks. The gap widths increased because of the movement of individual concrete blocks. This further enhanced stones mobility, causing the steel wires to break. The tilting and sinking of the blocks compromised the structure in terms of energy dissipation. Titling and sinking of the blocks eventually spreads in all directions. The high velocity of the water in this area flushes out most fine bed material. Figure 5.1(c) shows the formation of a scour hole at the upstream end of the structure. A scour hole will have a profound effect on the stability of the first row of blocks. This is a serious problem for the preservation of the overall stability of the bridge structure.

(a)

(b)

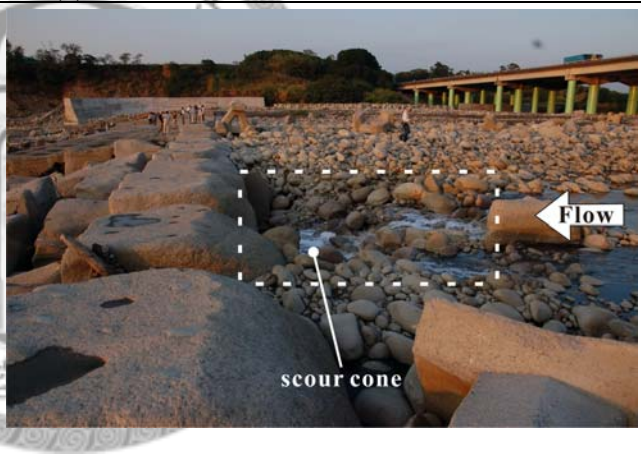

(c)

Figure 5.1. Failure of stepped concrete block grade control structure located downstream of Highway No.1 in Ta-Chia River in central Taiwan (November 2009): (a) blocks tilting and sinking; (b) deeper scour depth than block height; and (c) a scour hole upstream of the sinking area

5.2 Experimental setting

Sumer et al. [34] discussed how the vortices were developed in the gaps formed within the gravel have contributed to the entrainment of the fine sediment particles. Such a mode of entrainment is unlikely to take place in the present condition in which the main flow passes through the gap (Tsorng et al. [35]). Evidence from both field and laboratory observations reveal that the stones in the lateral gaps, gaps that are perpendicular to the main flow direction, were stable.

Conventional design of stepped concrete block grade control structures considers the stability of concrete blocks by block weight under a specific flow condition, usually at high designed discharges (Lagasse et al. [36], Wu [37], Guo and Chang [38]). They ignored failures due to gap scour. Recent experiences in Taiwan have exposed the fallacy of that design philosophy. A better understanding of the mechanism and the development of a design methodology that takes into consideration gap scour is necessary. We used a physical model to study gap scour for design modification and a proposal for cost-effective gap scour countermeasures.

It was necessary to determine the general block geometry and stone dimension to match the real flow and scour characteristics. Most of the stepped concrete block grade

control structures in Taiwan consist of five steps with an individual step drop-height of 50 cm. The projection area of the block is 2 x 2 m^2 and the gap width is 50 cm. The average median stone size used to fill the gap is about 20 cm. We fixed the upstream and downstream beds of the structure since this study only considered the scour between the blocks. A rectangular flume was used that is 30 cm in width, 60 cm in height, and 1500 cm in length located at the Hydrotech Research Institute, National Taiwan University to carry out the experiments. At least six blocks in each row were determined in order to display the global scour patterns and avoid boundary effect. A 1/50 scaled model was built in the flume using scaled blocks with an area = 4 x 4 cm^2. The block heights were at least 25 cm to measure the equilibrium scour depth in the gaps. The scaled gap width and drop height of each step was 1 cm. A uniform sand with median grain size = 3.56 mm was used to fill the gaps. Figure 5.2 shows the model design of the experiments. The researchers simulated the slope of 0.01 in the model tests since the longitudinal bed slope of rivers in Taiwan generally ranges from 0.01 to 0.001. The study adopted a clear-water condition without sediment influx from upstream. The bed elevation in the gaps was the same as the ambient block surfaces before the tests. We performed two sets of experiments, the “all-gaps-opened” and “only-lateral-gaps-opened” conditions.

The scour depth variations were monitored in both cases to ensure the equilibrium scour condition. The scour hole approached its equilibrium stage in approximately 15 minutes. The measurement of the bed elevation in both the longitudinal and lateral gaps continued for 40 minutes. The average bed elevation in the wise stream direction was the mean value of all the measured data in the transverse direction at the same streamwise positions. This study tested the scour depth variation for five different unit discharges, which varied from 0.008 to 0.051 m^2/s. Table 5.1 summarizes the test conditions of all the experiments conducted in this study.

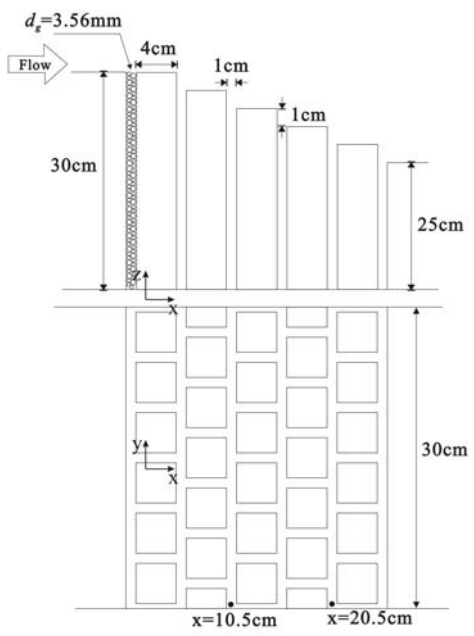

Figure 5.2 Sketch of scaled physical model and dimensions (side and top view)

Table 5.1 Experimental conditions and measured data: q – unit discharge; d_{50} – diameter of stone in the gaps; S_b – flume slope，S_{rm} – slope of structure; y_{bm} –lowest bed elevation; x_s – the corresponding position of y_{bm}; y_{bo} –original bed elevation at x_s; e –maximum scour depth

Run	**q [m^2/s]**	**d_{50} [mm]**	**S_b**	**S_{rm}**	**y_{bm} [cm]**	**x_s [cm]**	**y_{bo} [cm]**	**e [cm]**
GS1	0.0089	3.56	0.01	0.20	21.98	15.50	27.00	5.02
GS2	0.0188				21.65	12.00	28.00	6.35
GS3	0.0314				22.31	15.50	27.00	4.69
GS4	0.0433				22.91	15.50	27.00	4.09
GS5	0.0505				23.45	15.50	27.00	3.55
GSP1	0.0089	3.56	0.01	0.20	28.75	5.50	29.00	0.25
GSP2	0.0188				29.92	0.50	30.00	0.08
GSP3	0.0314				25.79	20.50	26.00	0.21
GSP4	0.0433				25.84	20.50	26.00	0.16
GSP5	0.0505				28.80	5.50	29.00	0.20

5.3 Scour of “all-gaps-opened” conditions

Figure 5.1 shows the average measured bed profiles for Tests GS1 – GS5. Table 5.1 contains the measured data, which include the lowest bed elevation, their corresponding position, and the maximum scour depth. Figure 5.1 shows that the average bed profiles for all five tests were similar. The bed elevation decreased from the first-row of blocks reaching the minimum level near the third-row of blocks. The minimum level was approximately 15 cm downstream from the leading edge of the

bridge structure and coinciding with the lateral gap behind the third-row of blocks. The bed elevation increased beyond this location.

The measured data show that the maximum scour depth for all the tests was e = 6.35 cm, which is for Test GS2, with unit flow rate, q = 0.0188 m^2/s. The scour depth in the gap of a stepped concrete block grade control structure was not directly proportional to the approach discharge. The scour depth increased as the discharge increased initially. It then decreased with a further increment of the approach flow rate. Serious gap scour occurs at a low or moderate rate of flow. The design of a stepped concrete block grade control structure should be re-examined in light of this finding. Furthermore, the gap scour depth at the first to third-row of blocks could potentially exceed 4 cm, which was deeper than the height of the adjacent cubic blocks. The gaps can potentially be completely entrained leaving no lateral support for the concrete blocks. The height of the concrete blocks used in Taiwan is insufficient. Field investigation supported this conclusion, as shown in Figure 5.1(a).

The experimental results show that the design of stepped concrete block grade control structures should consider the stability of a single concrete block under a designed flow condition and the extent of the gap scour depth(see Figure 5.3). The designed height of a block must be more than the estimated scour depth and the block

height should be dependent on its location.

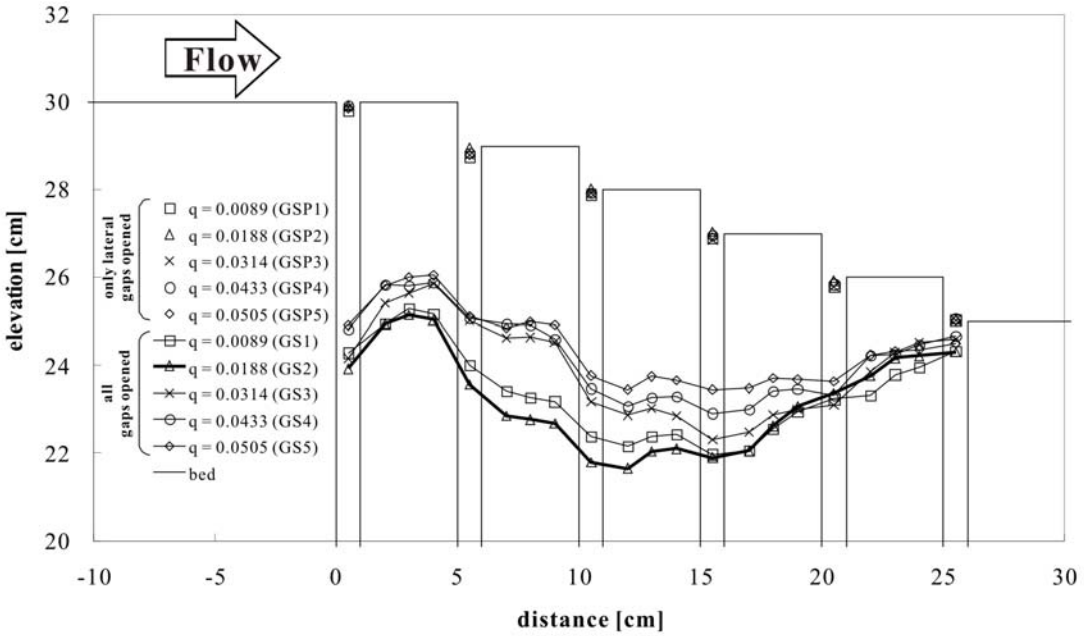

Figure 5.3 Mean bed form profiles in the gaps

5.4 Numerical setting for gap scour

The numerical setting for gap scour at a steeped concrete block grade control structure is introduced in this chapter. First of all, we have the two different numerical simulations. All of the numerical simulations are illustrated respectively later and those problems are more difficult than the local bridge scour. The gap width is only 1 cm and we have to simulate the sediment scour here. Hence we must use the more grid points for the numerical simulations. In addition, the same problem in these simulations we meet is we have to use trial and error to test the suitable parameters for every case. From these reasons, we do not add the sediment condition at the gap scour in the beginning stage and the numerical simulation can be simplified such as we dispose the bridge scour setting in chapter 3. After the rigid bed case is done, the sediment conditions are considered in the gap scour simulation.

The experimental setting is introduced before and we know that a lot of flow rates are tested. The three different discharges are chosen in our numerical simulation. They are $1980\,cm^3/s$, $4110\ cm^3/s$ and $15150\,cm^3/s$ respectively. These values are based on the maximum, median and minimum flow rate.

5.4.1 Numerical simulation 1: the scour depth is fixed in the geometry

In this stage, we build the geometry by Flow-3D which is exhibited in Figure 5.4. We can find out the gap width is so small, and it must increase the degree of difficulty in the numerical simulation. The mesh is similarly disposed in this simulation. In Figure 5.5(b), the mesh is refined surrounding the steeped concrete block grade control structure. In addition, the laboratory experiments are already done so we can use those data to observe some physical phenomenon. The numerical settings are shown clearly in Figure 5.7. This scour elevation is measured when the laboratory experiment are quasi-steady, that is to say, the sediment elevation is not changed radically. These numerical simulations are set for this stage in light of that we want to know the flow condition on the sediment surface. Hence the mechanism of the gap scour can be observed in the numerical simulation 1. We have mentioned that there are three types of flow rate. In Figure 5.6(a), the flow rate is set for 1980 cm^3/s , Figure 5.7(b) is 4110 cm^3/s and Figure 5.6(c) is 15150 cm^3/s . Finally, the physical condition is set such as the numerical simulation 1 and is shown in Table 5.2.

Table 5.2 The condition and parameter setting of rigid bed case in FLOW-3D

simulation time	60 s
simulation units	CGS
gravity vector	X: 9.8095
	Y: 0
	Z: -980.951
turbulent model	RNG model
total number of cells	about 4,000,000 points
boundary condition	x-min: volume flow rate
	x-max: out flow
	y-min: wall
	y-max: wall
	z-min: wall
	z-max: wall
pressure solver options	implicit
momentum advection	second order monotonicity preserving
Fluid flow solver options	Solve momentum and continuity equations

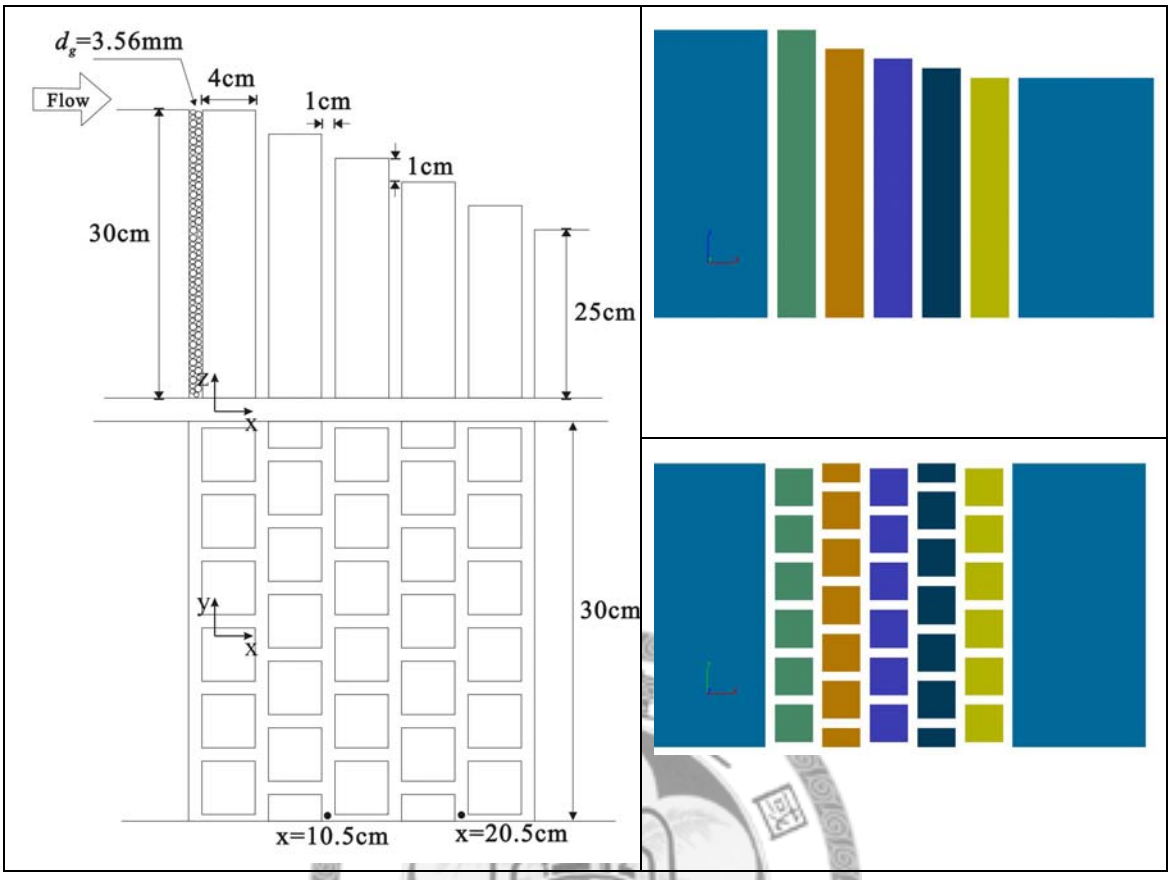

Figure 5.4 Physical model and the geometry we build by Flow-3D

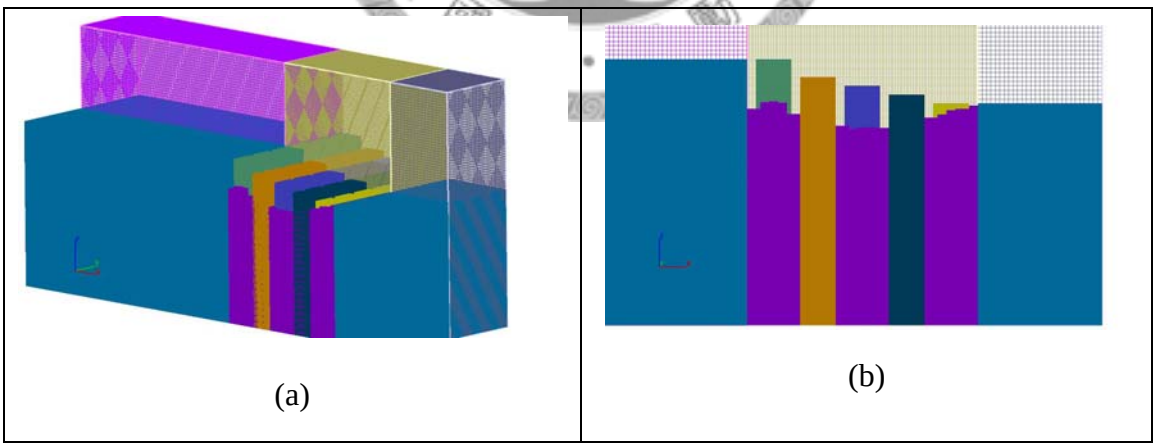

Figure 5.5 The geometry we build by Flow-3D with the different view

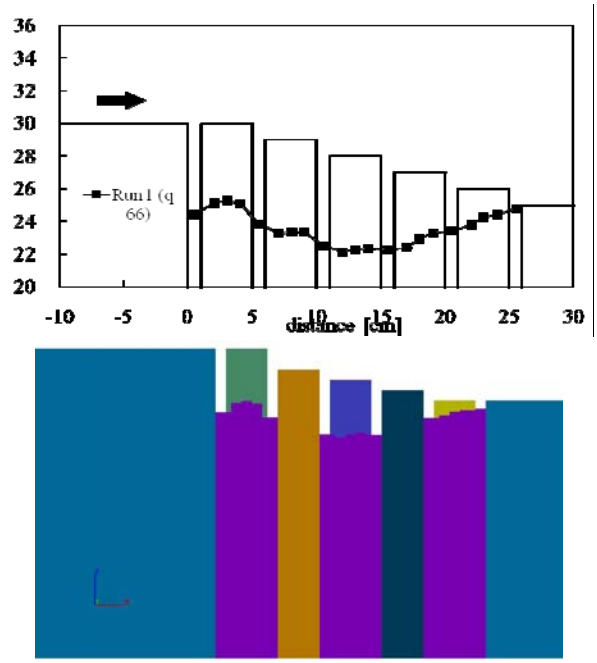
36
34
32
30
28
26
24
22
20
Run1 (q
66)
-10
-5
0
5
10
15
20
25
30
distance [cm]

(a)

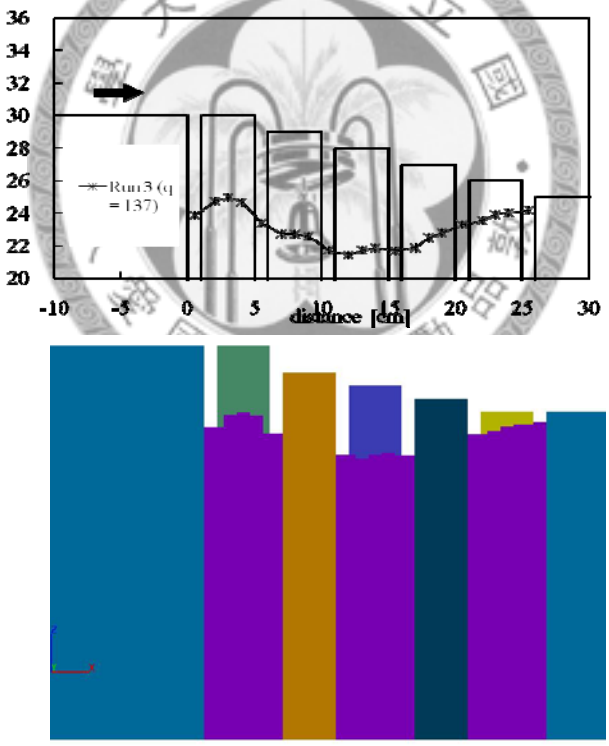
36
34
32
30
28
26
24
22
20
Run3 (q
=137)
-10
-5
0
5
10
15
20
25
30
distance [cm]

(b)

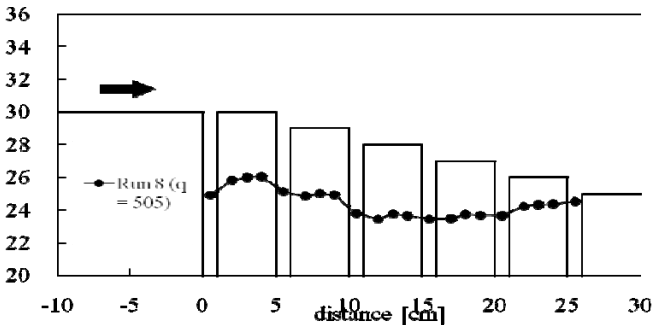

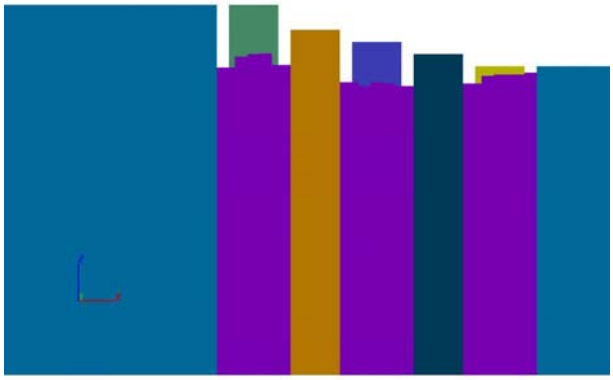

(c)

Figure 5.6 The scour elevation are given in our geometry (a)Q is 1980 cm^3/s (b)Q is 4110 cm^3/s (c)Q is 15150 cm^3/s

5.4.2 Numerical simulation 2: gap scour at a steeped concrete block grade control structure

This is our final numerical simulation for gap scour cases. All the numerical settings are followed by the laboratory experimental condition. We can observe the whole procedure of the gap scour in our numerical simulation. The geometry we build is shown in Figure 5.7. In Figure 5.7(a), the figure is the vertical view for the numerical

geometry, and the purple part represents the sediment. In Figure 5.7(b), we can see the whole geometry, and the mesh is refined surrounding the stepped concrete block grade control structure (see Figure 5.7(c)). The red line is shown in Figure 5.7(b) which illustrates the upstream channel and the laboratory experimental setting does not tell us the accurate channel length. Hence the channel length is set for 50 cm by ourselves, and this length is enough to make the flow condition develop into the fully developed flow. In addition, the physical condition is shown in Table 5.3 and the sediment conditions are shown in Table 5.4. From Table 5.3, we can see that the simulation time is 600 sec and we use about 4 million mesh points in order to obtain the correct numerical results.

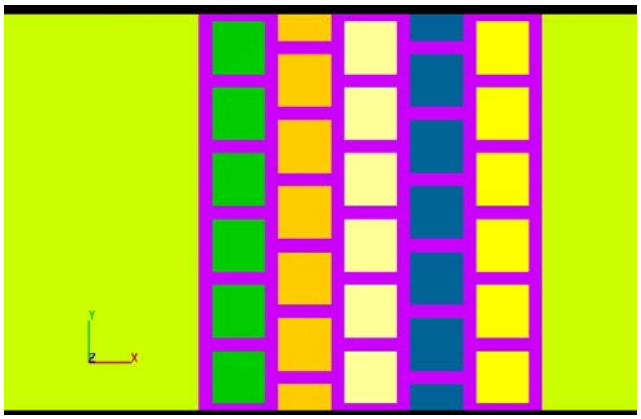

(a)

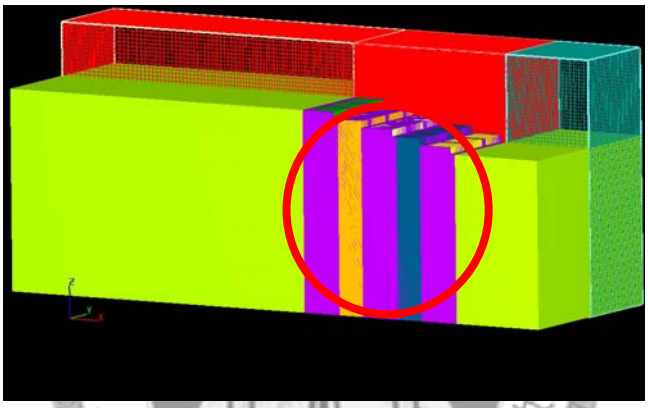

(b)

(c)

Figure 5.7 The geometry for gap scour with the mobile bed condition.

Table 5.3 The condition and parameter setting of mbile bed case in FLOW-3D

simulation time	600 s
simulation units	CGS
gravity vector	X: 9.8095
	Y: 0
	Z: -980.951
turbulent model	RNG model
total number of cells	about 14,750,000 points
boundary condition	x-min: volume flow rate
	x-max: out flow
	y-min: wall
	y-max: wall
	z-min: wall
	z-max: symmetry
pressure solver options	implicit
momentum advection	second order monotonicity preserving
Fluid flow solver options	Solve momentum and continuity equations

Table 5.4 The sediment setting for gap scour with the mobile bed condition

number of sediment species			1	maximum packing fraction			0.52
	diameter	density	critical Shields number	drag coefficient	entrainment coefficient	bed-load coefficient	angle of repose
sediment	0.359	2.65	0.06	0.5	0.018	8	45

5.5 Results and discussions

The results of clear-water simulation with Flow-3D software would be compared to the small-scale experiments in this section. The discussions in this thesis are divided into two parts: (i) the gap scour and the scour depth by the given geometry, (ii) the gap scour with the sediment conditions. For the rigid-bed (i), three types flow rate are used in the numerical simulations. The fluid depth, y-vorticity and z-velocity are discussed in the later section. As we mentioned, this numerical simulation is used to simplify our numerical experiments. Hence we can realize the characteristics of the flow when the river bed approaches the equilibrium scour depth. For the mobile bed simulation, it is still a hard work for us and we illustrate the problem when we meet.

5.5.1 The gap scour with the given scour depth

First of all, the numerical and experimental free surface elevations are exhibited in Figure 5.8. The symbol of cross is the experimental result and the circle is the numerical result. Figure 5.8 (a), (b) and (c) stands for the different flow rate which are Q=1980cm^3 /s, Q=4110cm^3 /s and Q=15150cm^3 /s respectively. The numerical results are chosen at 60 sec because flow fields is reaching the quasi-steady. The result reveals that we obtain the fine results when the flow rate increases but it can not imply that we have the bad results when the flow rate is low. After all, every curve of the numerical result still has the trend to approach the experimental results and the comparison is favorable. It is used to confirm whether our numerical simulation is reasonable or not and it can be validated against the experimental data.

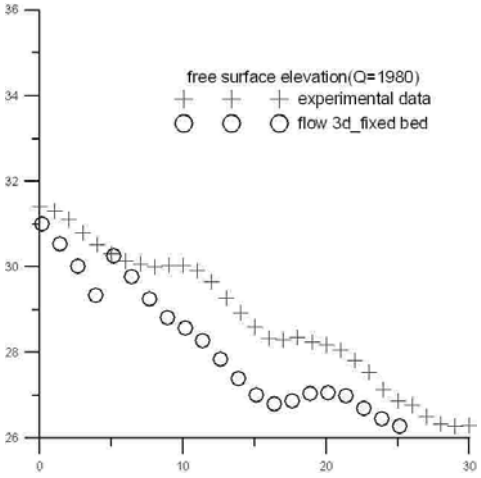

(a)

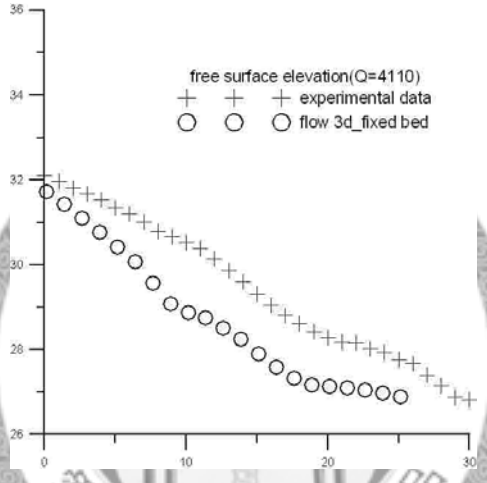

(b)

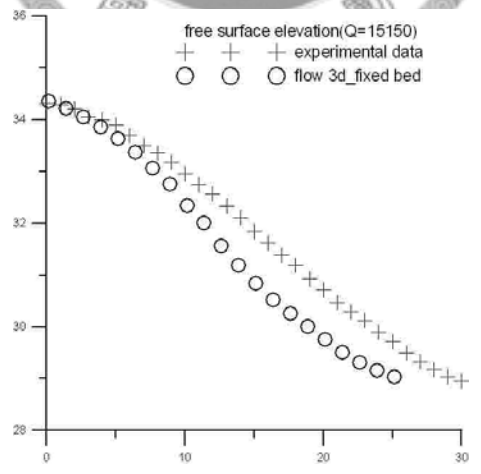

(c)

Figure 5.8 The free surface elevation with the different flow rate (a) $Q=1980\,{cm^3}/{s}$ (b)$Q=4110\,{cm^3}/{s}$ (c)$Q=15150\,{cm^3}/{s}$.

The z-velocity and the y-vorticity for the different flow rates are exhibited in Figure 5.9 and Figure 5.10 respectively. For the z-velocity, we can observe that the high velocity is always existent, no matter in which flow rate is. The scour depth of laboratory experiments are exhibited before and the place of the maximum scour depth coincide with the phenomenon in our simulations. At the same time, the velocities also increase when we increase the flow rate in the red line region (see Figure 5.9(a)). In addition, the obvious z-velocity and the y-vorticity occurred between the first stepped concrete block grade control structure and the river bed. The phenomena also correspond to the laboratory experiments. Furthermore, from the y-vorticity, the anticlockwise vorticity is generated in the same place and is exhibited in Figure 5.10(c). The results illustrate the shape of the scour elevation in the gap between the river bed and the first stepped concrete block grade control structure. It indicates that the positive z-velocity is always existent in the upstream wall (the black dash line). The wall close to the river bed (the black line) has the opposite effect so it has the negative z-velocity.

Finally, the y-vorticity reveals that there are a lot of strong vorticities generated in the edge of the stepped concrete block grade control structure. Above all, as the flow rate increases, the trend is more obvious (see the purple line) which are shown in Figure 5.10. The failure of the stepped concrete block grade control structure in the engineering

constraction case can be illustrated in light of the reason we discussed.

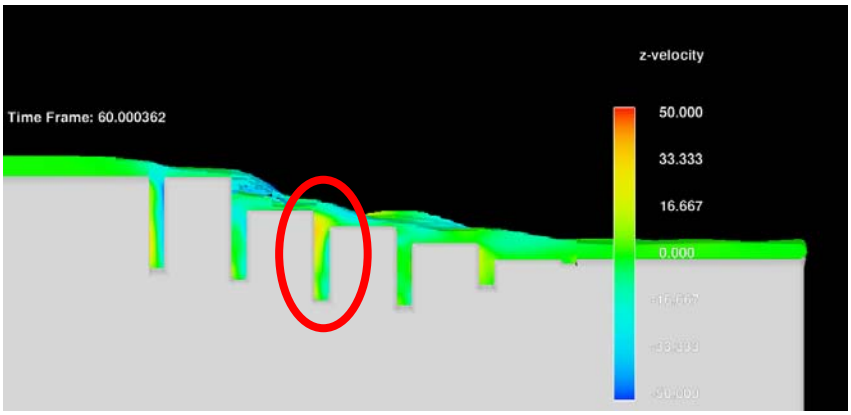

(a)

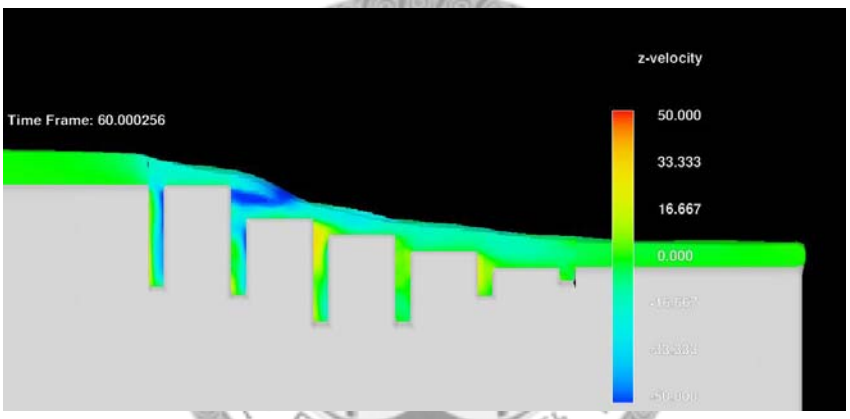

(b)

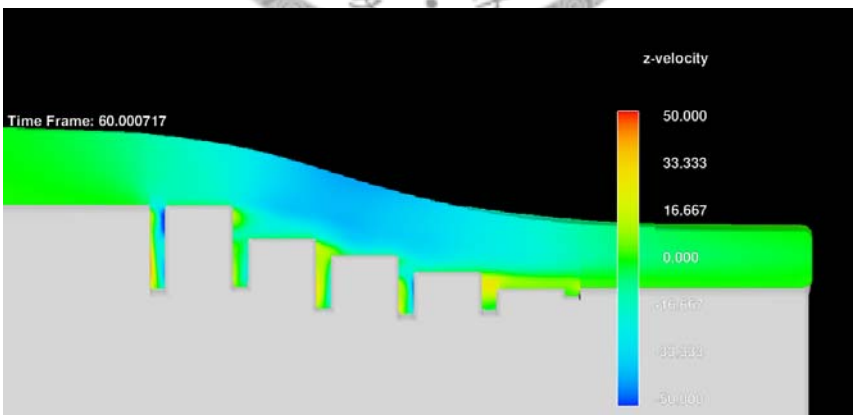

(c)

Figure 5.9 The z-velocity for the different flow rate (a) Q=1980 cm^3/s (b)Q=4110 cm^3/s (c)Q=15150 cm^3/s .

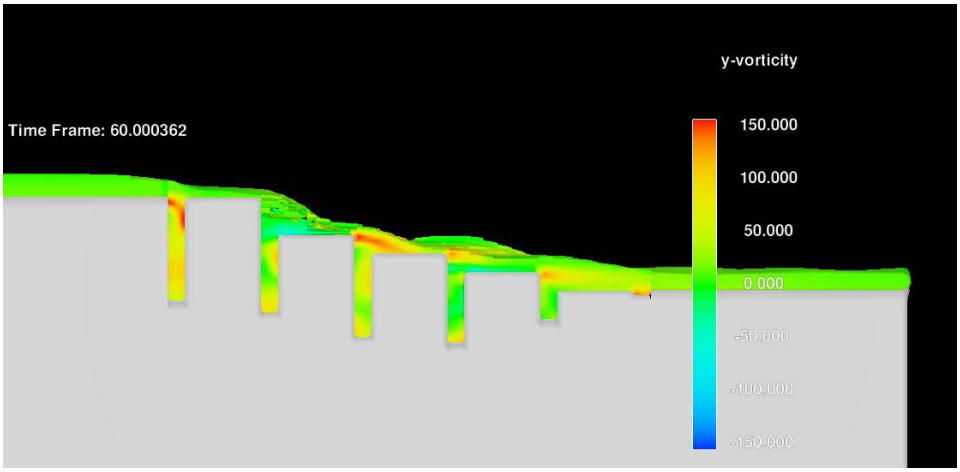

(a)

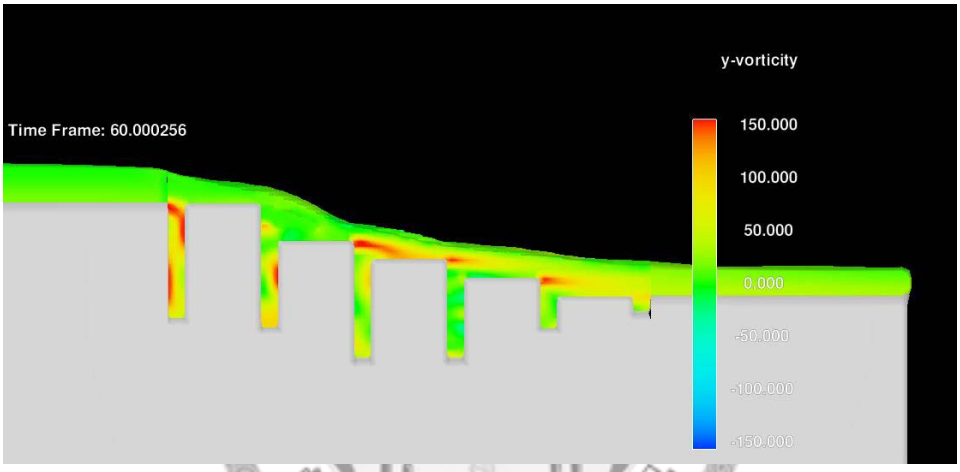

(b)

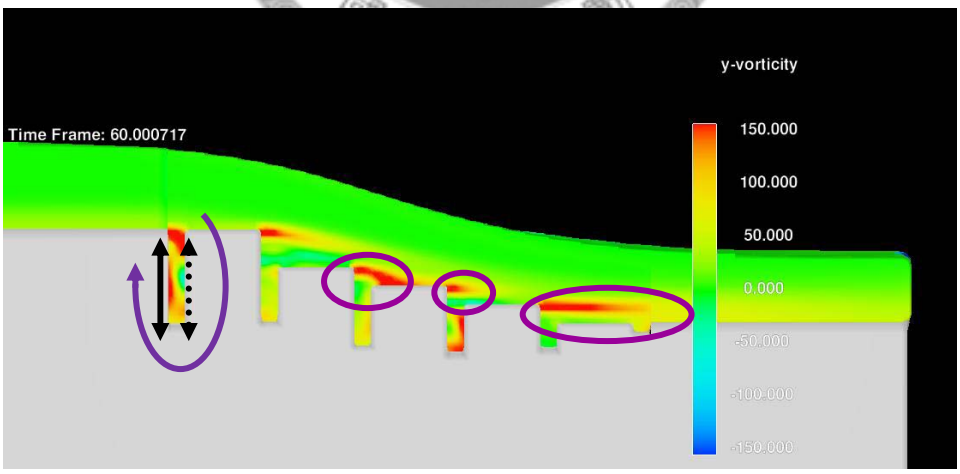

(c)

Figure 5.10 The y-vorticity for the different flow rate (a) Q=1980 cm^3/s (b)Q=4110 cm^3/s (c)Q=15150 cm^3/s .

5.5.2 The gap scour with the mobile bed condition

First of all, we want to illustrate the difficulty in the gap scour with the mobile bed condition. The sediment elevation with the different mesh points is shown in Figure 5.11. For Figure 5.11 (a), the mesh points are used about 3,000,000 points in the numerical simulation. Hence every simulation second needs to take about 2 hours in the computation process. Unfortunately, the figure reveals that the mesh points are not enough for the gap scour problem. Due to this reason, the more mesh points are added in the numerical simulations. The results are exhibited in the Figure 5.11(b) and it is more reasonable than the Figure 5.11(a) obviously. The expense is that we have to use more time to simulate the case. In Figure 5.11(b), we have to spend about 3 hours for every simulation second. It is the big challenge even by using computation station or for researchers.

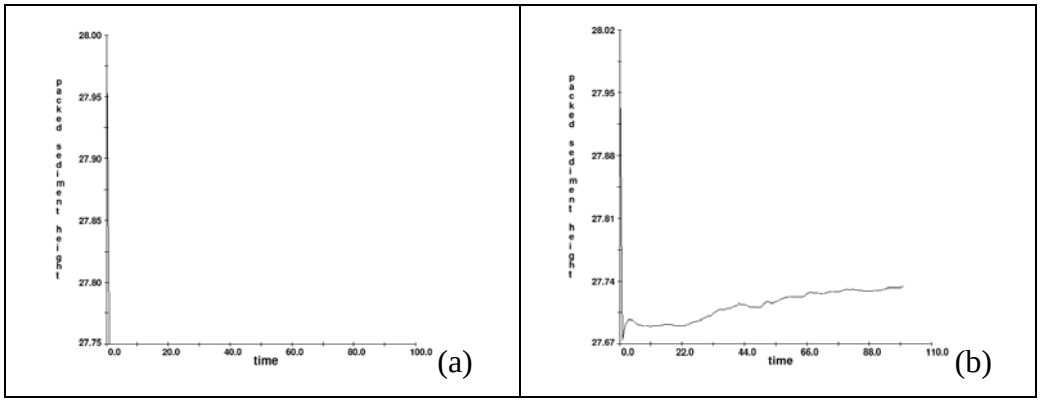

Figure 5.11 The sediment elevation with the different mesh points. (a) use about 3,000,000 points(b) use about 4,000,000points

The sediment elevation is exhibited in Figure 5.12. The left hand side and the right hand side are the numerical result and the laboratory experimental result respectively. The experimental result approaches the equilibrium scour depth and the numerical result is chosen at the 100 sec. Although we may doubt that the numerical results do not approach the equilibrium, the sediment elevation is already reaching the quasi-steady at the 100 sec.. From Figure 5.12, the curve of the numerical result does not fit the experimental result. It implies that our sediment is not easy to retrain during the scour process.

In writer's opinion, the more mesh points are necessary. In the present work, the cell size is 0.16cm*0.16cm*0.16cm but we once try to use the 0.125cm*0.125cm*0.125cm. The consequence reveals that every simulayion second needs to take about 8 hours. Due to this reason, we give up increasing the mesh points. How to improve the numerical results and its accuracy is our future work.

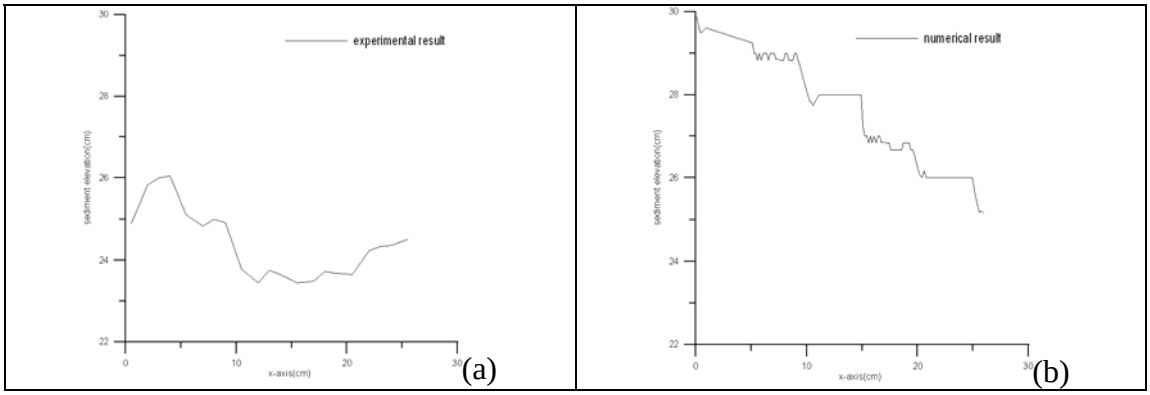

Figure 5.12 The sediment elevation for the numerical and experimental results. (a) the experimental result (b) the numerical result

Chapter 6 Conclusion and recommendation

6.1 Conclusion

1. The local bridge scour problem:

For the rigid bed simulation, the numerical results coincide with the laboratory experiment. In addition, we are successful in predicting the trend toward the sediment scour. We can find out that the sediment is deposited among the bridge piers in light of the z-vorticity and the strong velocity occurs in front of the first pier. As we discussed before, the ultrasound device is necessary in order to measure the sediment scour. Unfortunately, the shape of sensor and its location at the channel apparently affect the flow condition in the laboratory experiments. Due to this reason, the sediment elevation is bound to interfere with the sensor. After we remove the sensor, we obtain the fine results which correspond to the laboratory results. Hence the ultrasound device has to be changed place in the laboratory experiment.

The numerical results of the mobile bed simulation coincide with the laboratory photography. We can find that the overfall flow not only scours the river bed but also

generates the strong velocity on the upstream of the first pier. Furthermore, the mainly scour type are different between the mobile bed simulation and the same case without the overfall flow effect. The mainly scout type in mobile bed simulation is overfall flow scour. On the contrary, the mainly scour types are the down flow and the horseshoe vortex when we remove the first river bed. Finally, from the example of Hou-Feng bridge, the pipeline located at the upstream of the bridge is one of the main causes of piers collapsed. Even though we have the acceptable numerical results, we believe that we should use more mesh points in order to obtain the more fine results of flow and sediment for bridge structures.

2. The gap scour problem:

We are also successful in simulating the gap scour when the scour depth is given. The high velocities always occur between the river bed and the first stepped concrete block grade control structure. It coincides with the laboratory experiment. In addition, there are strong vortices near the edge of the stepped concrete block grade control structure. The stepped concrete block grade control structure failure happened at this place in the engineering constraction case.

6.2 Recommendation

1. We suggest that we have to make good use of the multi-block mesh systwm. In order to retrench the computation resource, the mesh points are not used on the solid body or use the lower mesh points. Although the mesh points are not computed in the program, it still saves the numerical results in the memory.
2. In our numerical simulation in the mobile bed simulation, it reveals that the critical Shields number is necessary to be defined. The suggestion numbers are 0.01 to 0.06.
3. The work statio
4. n is necessary when we want to simulate the sediment scour problem. It is because that the sediment scour problems have to use large computational storage during the numerical simulation. The problem has been discussed and exhibited in the chapter 5.

5. When the sediment condition is added in the numerical simulation, it obviously enhances the difficulty of simulation. The cell size in the numerical setting is suggested to be smaller than 0.166.

References

[1] H.N. Hsieh, “Acoustical scour monitoring applied to scale model of HouFeng Bridge”, master's thesis in Department of Civil Engineering College of Engineering, NTU, 2010.

[2] Rouse, H. “Discharge characteristics of the free overfall.” Civil Engineering (N.Y.), 1936.

[3] Beltaos, S. “Oblique impingement of plane turbulent jets”, J. Hydr. Div., pp. 1177-1192,1976.

[4] Beltaos, S., and N. Rajaratnum. “Plane turbulent impinging jets”. J. Hydr. Res., 1973.

[5] Robinson, K. M. “Predicting stress and pressure at an overfall”, Res, 11:29-59, 1992.

[6] Fogle, A. W., J. C. McBurnie, B. J. Barfield, and K. M. Robinson. “Modeling free jet trajectory at an overfall and resulting shear stress distribution in the plunge pool”, Trans. ASAE, 36(5): 1309-1318. 1993.

[7] Stein, O. R., P. Y. Julien, and C. V. Alonso. “Mechanics of jet scour downstream of a headcut”. J. Hydr. Res., 31:6, 723-738, 1993.

[8] Jia, Y., T. Kitamura, and S. S. Y. Wang. “Simulation of scour process in plunging pool of loose bed material”. ASCE J. Hydraulic Eng, 127(3): 219–229, 2001.

[9] G. J. Hanson, K. M. Robinson and K. R. Cook. “Scour below an overfall: part II. prediction”, Trans. ASAE, Vol. 45(4): 957–964, 2002

[10] Chabert, J. and EngeldInger, P., “Etude des Affouillements Authur des Piles des Ponts”, Laboratoire National d'Hydraulique, 1956.

[11] Laursen, E. M., “Scour at Bridge Crossings”, Trans. A.S.C.E., Voil. 127, Pt. 1, pp.

166-180, 1962.

[12] Jain, S. C. and Fischer, E. E., “Scour around bridge piers at high Froude numbers”, Report Number F.H.W.A.-R.D.-79-104, Federal Highway Administration, Washington D.C, 1979.

[13] Chee, R. K. W., “Live-Bed Scour at bridge sites”, M.E. Thesis, Auckland University, Auckland, New Zealand, 1982.

[14] Ettema, R., “Scour at bridge piers”, Ph.D. Thesis, Auckland University, Auckland, New Zealand. Report No. 124, 1980.

[15] Y.M. Chiew And B.W. Melville, “Local scour around bridge piers”, J.Hydr. Res., Vol.25, No.1, pp15-26, 1987.

[16] Flow-3D user manual version 9.4, 2009.

[17] Melville, B. W., and Coleman, S. E. “Bridge scour”. Water Resources Publications, Colorado, USA, 550pp, 2000.

[18] Laursen, E. M., “Analysis of relief bridge scour”, J. Hydr. Div., Vol. 89, No. 3, pp. 93-118, 1963.

[19] Melville, B. W. and Chiew, Y. M., “Time scale for local scour at bridge piers,” J. Hydr. Engrg., ASCE, Vol.125, No.1, pp. 59~65, 1999.

[20] Shen, H. W., Schneider, V. R., and Karaki, S. S, “Mechanics of local scour”. U.S. Department of Commerce, National Bureau of Standards, Institute for Applied Technology, Washington, D.C, 1966.

[21] Maza, J. A,‘‘Socavacion en cauces naturales.’’ A. J. Miguel Rodriguez, translator, *Rep. No. 114*, School of Engineering, University of Auckland, Auckland, New Zealand, 1968.

[22] Ettema, R, ‘‘Scour at bridge piers.’’ Rep. No. 216, School of Engrg., University of Auckland, Auckland, New Zealand, 1980.

[23] Chiew, Y. M, ‘‘Local scour at bridge piers.’’ *Rep. No. 355*, Dept. of Civ. Engrg., University of Auckland, Auckland, New Zealand, 1984.

[24] Raudkivi, A. J. and Ettema, R., “Clear-water acour at cylindrical piers " , J. Hydr. Engrg., ASCE, Vol.109, No.3, p.338-349, 1983

[25] Raudkivi, A. J., Ettema, R., “Effect of sediment gradation on clear water scour " , J. Hydr. Div. ASCE, Vol.103, No.NY10, p.1209-1213, 1977

[26] Guo, J., Hunter Rouse and Shields diagram, Proc 1th IAHR-APD Congress, Singapore, Vol. 2, 1069-1098, 2002.

[27] Kleinhans, M.G., Sort out sand & gravel: sediment transport and deposition in sand-gravel bed rivers, Ph.D. Thesis, Universitaat Utrecht 2002.

[28] Soulsby, R., Dynamics of Marine Sands, Ch 9: Bedload transport, Thomas Telford Publications, London, 1997.

[29] Mastbergen, D.R. and J.H. Von den Berg, Breaching in fine sands and the generation of sustained turbidity currents in submarine canyons, Sedimentology

[30] Raudkivi, A.J. and Ettema, R.,"Stability of armour layers in rivers." J. Hydr. Div., pp. 1047-1057, 1982.

[31] Raudkivi, A.J. and Ettema, R., "Scour at cylindrical bridge piers in armored beds." J. Hydr. Engrg. vol. 111, no. 4, 1985.

[32] Worman, A., "Riprap protection without filter layers." J. Hydr. Engrg. pp. 1615-1630, 1989.

[33] Worman, A., "Incipient motion during static armoring." J. Hydr. Engrg. pp. 496-501, 1992.

[34] Sumer, B.M., Cokgor, S. and Fredsoe, J., "Suction removal of sediment from between armor blocks." J. Hydr. Engrg. pp. 293-30, 2001.

[35] Tsorng, S.J., Yang, Z.S., and Lai, J.S., "Measurements of flow field between blocks in various geometries." 18th Conference of Hydraulic Engineering, PingTung, Taiwan, H-11., 2009.

[36] Lagasse P.F., Byars M.S., Zevenbergen L.W. and Clopper, P. E., "Bridge Scour and Stream Instability Countermeasures." Federal Highway Administration, 1997.

[37] Wu, C.S., "Design of stepped concrete block grade control structure", Master Thesis, Hydraulics & Ocean Engineering, NCKU, Tainan, Taiwan., 2004.

[38] Guo, Y.H. and Chang, Y.Z., "Failure mechanisms of flexible grade control and protections. "Hydraulics. (16): 201-210, 2006.

[39] Chang, C.C., " Experimental study on the reciprocal effect of overfall flow scour and bridge scour", Master Thesis, Hydraulics & Ocean Engineering, NCKU, Tainan, Taiwan., 2002.

個人簡歷

姓名:陳峰琨 Chen Feng-kun

生日:1986 年 01 月 11 號

學歷:

國立台南第一高級中學

國立暨南國際大學土木工程學系 學士

國立台灣大學土木工程學研究所水利工程組 碩士

Conference paper

Chen F.K. , Lin Y.C. , Wu C.S. , Young D.L., “Research of Local Bridge Scour in Alluvial River”, The 34th National Conference on Theoretical and Applied Mechanics, Yunlin, Taiwan, November 19-20, 2010